A Thermodynamic Model of Magnetic Hysteresis in Active Magnetic Regenerative Refrigeration (AMRR) Cycles

by

William D. Brey

A thesis submitted in partial fulfillment of

the requirements for the degree of

Master of Science

(Mechanical Engineering)

at the

UNIVERSITY OF WISCONSIN – MADISON

2012

This page intentionally left blank.

APPROVED BY

_____

PROFESSOR GREGORY F. NELLIS

_____

PROFESSOR SANFORD A. KLEIN

DATE:_____

This page intentionally left blank.

ABSTRACT

Active magnetic regenerative refrigeration (AMRR) has recently become an attractive alternative to vapor compression refrigeration due to its potential environmental benefits through the use of working materials with low ozone depletion potential (ODP). Several prototype machines have been constructed that achieve refrigeration at modest efficiencies with commercially available permanent magnets. Additionally, numerical modeling and experiment have shown that the efficiency of an AMRR device can be increased through layering with a tunable magnetic refrigerant. However, current numerical modeling is limited to second order magnetic transition (SOMT) materials that exhibit modest adiabatic temperature changes and no magnetic hysteresis. Since the discovery of the giant magnetocalotic effect (GMCE) in first order magnetic transition (FOMT) materials, there is increasing interest to investigate the performance of an AMRR cycle that uses these materials. Near the Curie temperature, FOMT materials yield large adiabatic temperature changes relative to SOMT materials, but also exhibit magnetic hysteresis in a changing magnetic field.

Currently there is no known numerical model that can accurately capture the effects of magnetic hysteresis on the performance of an AMRR cycle. This thesis quantifies the effects of magnetic hysteresis on the performance of AMRR cycles which use FOMT materials. Thermodynamically, magnetic hysteresis is treated as a source of entropy generation that is proportional to the area swept by a hysteresis loop for one refrigeration cycle. The one-dimensional numerical model presented by Engelbrecht (2008), is modified to include entropy generation from magnetic hysteresis in the regenerator energy equations

AMRR system performance losses due to magnetic hysteresis are shown to be directly proportional to regenerator volume. Thus at large refrigeration capacity to volume ratios, AMRR cycles operating with layered FOMT materials significantly outperform the same cycle with layered SOMT type refrigerant under the same operating conditions.

ACKNOWLEDGEMENTS

The work described in this thesis could not have been accomplished without the help and guidance of many people. First, I would like to give thanks to my advisers Sandy Klein and Greg Nellis for allowing me the pleasure of working under them as a graduate assistant. Greg and Sandy's fastidiousness and efficiency in problem-solving pushed me to approach my work in much the same fashion, which I believe significantly furthered my development as an engineer. Thanks to Doug Reindl for serving as the third member for my defense committee and helping me with my job search.

I am grateful to have worked with such great peers in the Solar Energy Lab, who made the office relaxed and entertaining place to work. I would like to thank Greg for sharing the window seat in 1337 with me for my entire time in the SEL and always providing a fresh set of heat transfer jokes. I give thanks the then-seasoned SEL-ers Mandy, Will, and Ty who welcomed me into the SEL through sarcastic humor and regular soccer games in the office. I would also like to recognize the Brad K., Brad M., Nevzat, Russell, Rogelio and Eric for keeping the relaxed tradition of office 1337 going. It has also been a great pleasure to meet and work with John, Mike Cheadle Amir, Bryant, Dan, Sönke, Diego, Rodrigo, Kendra, Mike Zhang, Mark, Doug Gavic and Weinje. I would also like extend my special gratitude to SEL alumnus Harrison Skye for introducing me to Sandy and Doug during my initial visit to the UW Graduate School.

I would like to thank my father Rob and my sister Daisy for all the support that they have given me throughout my graduate study and life in general. I would like to thank my late mother Ann for teaching me the importance of hard work, but also the importance of relaxing and sharing a laugh with someone.

Lastly, I would like to acknowledge the U.S. Department of Energy for their financial assistance to this project.

TABLE OF CONTENTS

LIST OF FIGURES

LIST OF TABLES

NOMENCLATURE

A_c	cross-sectional area (m^2)
a_s	volume specific surface area (m^2/m^3)
AR	aspect ratio (-)
B_J	Brillouin function
C	Curie constant (K)
C_c	adiabatic temperature change scaling factor (-)
C_h	hysteresis scaling factor (-)
C_M	isothermal entropy change scaling factor (-)
C_W	Curie-Weiss constant
COP	coefficient of performance (-)
$c_{\mu_0 H}$	constant field specific heat capacity (J/kg-K)
d_h	hydraulic diameter (m)
d_p	particle diameter (m)
f	friction factor (-)
G	Gibbs free energy (J)
g_L	Landé g-factor (-)
H	applied magnetic field (A/m)
h	mass specific enthalpy (J/kg)
J	total molecular angular momentum number (-)
K	compressibility (m^2/N)
k	thermal conductivity (W/m-K)
k_B	Boltzmann constant (J/K)
L	regenerator length (m)
M	volume specific magnetic moment (A/m)
M_{an}	anhystretic magnetization (A/m)
M_{irr}	irreversible magnetization (A/m)
m	mass of magnetic refrigerant material (kg)
$\dot{m}$	mass flow rate (kg/s)
N	number of magnetic spins
N_L	number of layers in regenerator bed
Nt	number of time steps
Nx	number of spatial steps
Nu	Nusslet number (-)
P	pressure (Pa)
Pr	Prandtl number (-)
Q	heat transfer (J)
q	mass specific heat transfer (J/kg)
Re	Reynolds number (-)
S	entropy (J/K)
s	specific entropy (J/kg-K)
T	temperature (K)

t	time (s)
U	internal energy (J)
u	mass specific internal energy (J/kg)
V	volume (m^3)
v	mass specific volume (m^3/kg)
W	work (J)
w	mass specific work (J/kg)
x	regenerator axial position (m)

Greek

α	domain coupling constant (-)
ΔM	maximum irreversible magnetization (A/m)
Δs_M	mass specific isothermal entropy change (J/kg-K)
ΔT_{ad}	adiabatic temperature change (K)
$\Delta \mu_0 H$	change in magnetic field (T)
ε	bed porosity (-)
η	efficiency (-)
μ	viscosity (N-s/m^2) or magnetic permeability (T-m/A)
μ_0	permeability of a vacuum (T-m/A)
μ_B	Bohr magneton (J/T)
$\mu_0 H$	applied field (Tesla)
ρ	density (kg/m^3)
σ	dimensionless magnetization (-)
τ	cycle duration (s)
ω	dimensionless change in volume (-)

Subscripts

ad	adiabatic
amp	amplitude
an	anhysteretic
C	cold
Curie	Curie temperature
eff	effective
f	fluid or final
gen	generation
H	hot
i	spatial step index
irr	irreversible
j	temporal step index
mag	magnetic

max	maximum
mid	midpoint
min	minimum
motor	motor
r	regenerator material
ref	reference or refrigeration
s	saturation

Chapter 1 INTRODUCTION

1.1 The Magnetocaloric Effect

The magnetocaloric effect is a phenomenon by which a magnetic material experiences a decrease in internal entropy when it is exposed to an externally applied magnetic field. In ferromagnetic materials near the ordering temperature (the Curie temperature) or paramagnetic solids near absolute zero, the applied magnetic field causes the magnetic spin domains to align in a manner that decreases the internal disorder of the material, resulting in a decrease in the magnetic portion of the entropy in the system [1]. Under adiabatic conditions with no entropy generation, the total entropy of the material must remain constant. Therefore, the decrease in the magnetic entropy must result in an increase in the thermal entropy and an adiabatic temperature rise (ΔT_{ad}) is induced that is characteristic of a particular magnetocaloric material.

The thermodynamic relation for the internal energy (U) of a closed system can be expressed as:

$$dU = \delta Q - \delta W \tag{1-1}$$

where kinetic and potential energy effects have been neglected. The δQ term represents the differential heat flow *into* the system and the δW term represents the differential work done *by* the system. Because Eq. (1-1) holds true for all thermodynamic systems in (quasi-) equilibrium, an isothermal magnetization process can be compared to the isothermal compression of a gas. When a magnetocaloric material is magnetized isothermally, the magnetic portion of the entropy and therefore the overall entropy is decreased. Analogously, when a gas is compressed isothermally, the spatial component of the entropy is reduced, reducing the overall entropy of the system. This analogy is depicted in Figure 1-1.

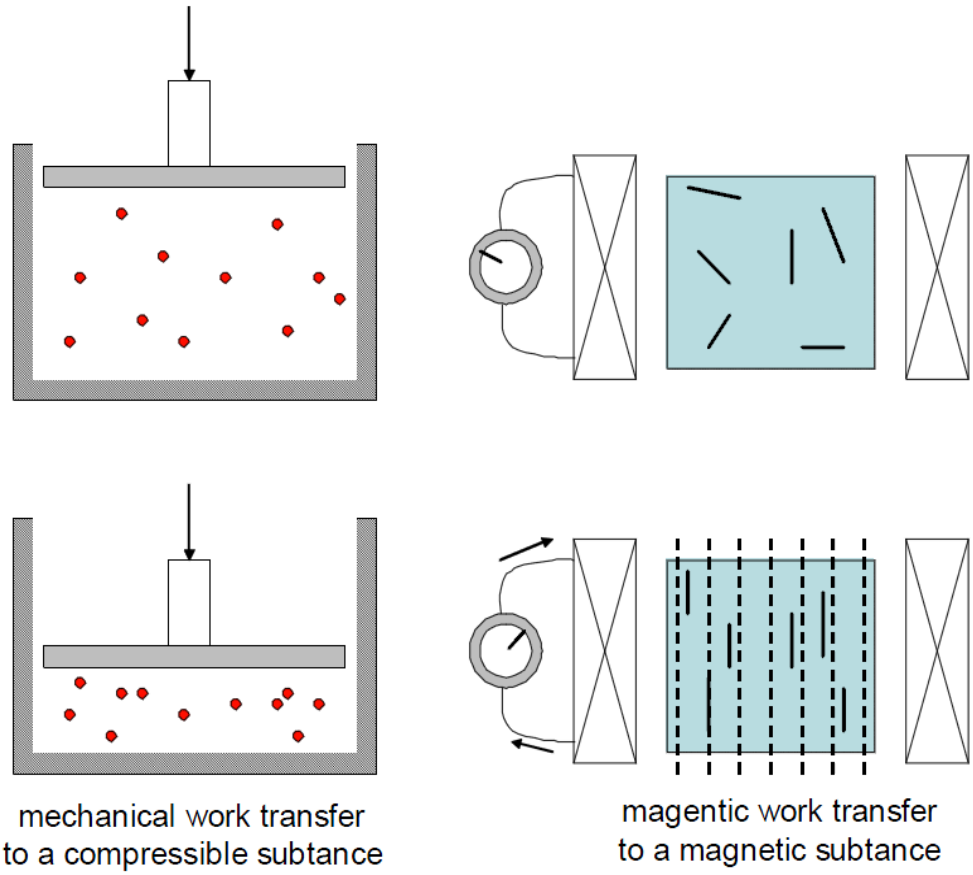

Figure 1-1. Analogy between mechanical work and magnetic work to reduce entropy

For expansion or compression of a gas, the differential work done *by* the system is represented by:

$$\delta W = P\,dV \tag{1-2}$$

where P is the pressure of the gas and dV is the differential volume of the gas. Similarly, the work term for magnetic work done *by* the system can be represented as:

$$\delta W = -\mu_0 H\, d\left(V\,M\right) \tag{1-3}$$

where $\mu_0 H$ is the applied magnetic field, V is the volume of the magnetic material, and M is the volume magnetization of the magnetic material. By comparing Eq. (1-2) and (1-3), it is clear that the applied field is analogous to the applied pressure and that the magnetization of the material is analogous to the

(inverse of) volume. Substituting Eq. (1-3) into Eq. (1-1) allows the internal energy of a magnetocaloric material to be expressed as:

$$dU = \delta Q + \mu_0 H \, d(V M) \tag{1-4}$$

The heat input term in Eq. (1-4), δQ , will be discussed in Chapter 3.

The magnetocaloric effect for a given material is typically reported in the literature in terms of either an isothermal entropy change or an adiabatic (isentropic, assuming no irreversible losses) temperature change. These two quantities describe the difference in entropy or temperature, respectively, between two lines of constant applied magnetic field on a temperature-specific entropy diagram. A temperature-specific entropy diagram for gadolinium is shown in Figure 1-2. Figure 1-3 (a) shows a temperature-specific entropy diagram for a typical ferromagnetic material and Figure 1-3 (b) shows the corresponding adiabatic temperature change and isothermal entropy change as a function of temperature near the Curie temperature of the material. Figure 1-2 shows that for all temperatures, the entropy of gadolinium decreases as the magnetic field is increased, and this effect is most dramatic near the Curie temperature of 293 K. Note that both figures report the volume specific entropy instead of the mass specific entropy. In the design of a magnetic refrigerator, volume is the important metric that must be minimized, not mass. However, the specific isothermal entropy change is most commonly reported in the literature on a mass basis, and will thus be written on a mass basis in the subsequent sections of this thesis as well. Most magnetocaloric materials can be assumed to be incompressible over the temperature range near the Curie temperature.

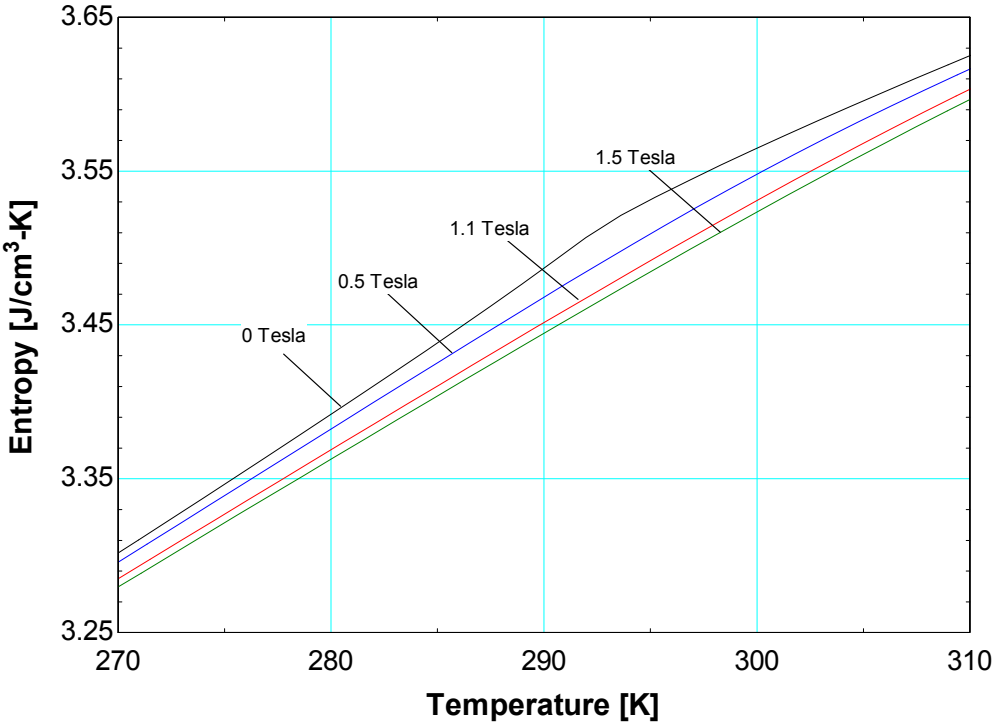

Figure 1-2. Temperature-volume specific entropy diagram for gadolinium for different applied magnetic fields near the Curie temperature (293 K)

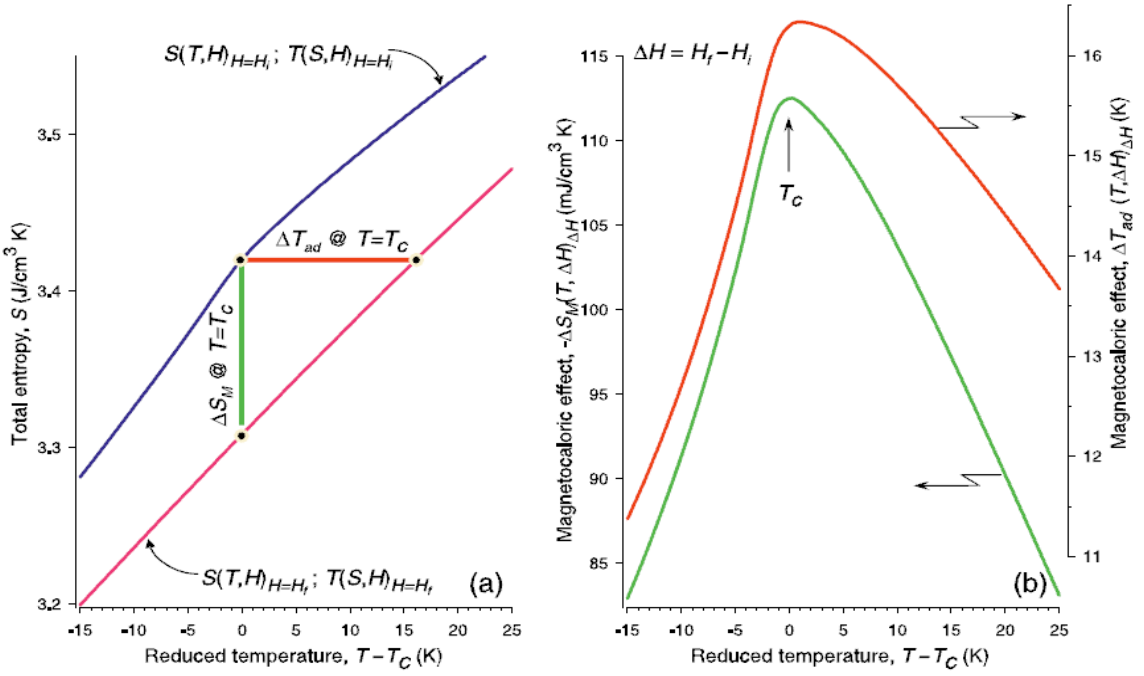

Figure 1-3. (a) Temperature-volume specific entropy diagram of a typical ferromagnetic material. (b) Negative magnetic isothermal entropy change and adiabatic temperature change as a function of temperature near the Curie temperature [1]

1.2 Magnetic Refrigeration

Since the discovery of the magnetocaloric effect by Emil Warburg in 1881, there has been an interest in exploiting the effect for the movement of heat in the form of a refrigeration cycle. More recently, the discovery of the giant magnetocaloric effect (GMCE) in $Gd_5(Si_xGe_{1-x})_4$ type materials in 1996 has stimulated research interest in room temperature magnetic refrigeration applications [2]. Several magnetic refrigeration cycles have been developed, most notably the adiabatic demagnetization refrigeration (ADR) cycle and the active magnetic regenerative refrigeration cycle (AMRR).

1.2.1 Adiabatic Demagnetization Refrigeration (ADR) Cycle

The adiabatic demagnetization refrigeration cycle (ADR) is the magnetic equivalent of a Carnot cycle for vapor compression systems. The cycle was first proposed by Debye (1926) and Giauque (1927) as a means of achieving temperatures below the boiling point of helium [3, 4]. The cycle was subsequently demonstrated by Giauque and MacDougall (1933) and successfully achieved sub-Kelvin temperatures [5]. Figure 1-4 depicts the ideal ADR cycle on a temperature-specific entropy diagram for pure gadolinium with lines of constant magnetic field shown.

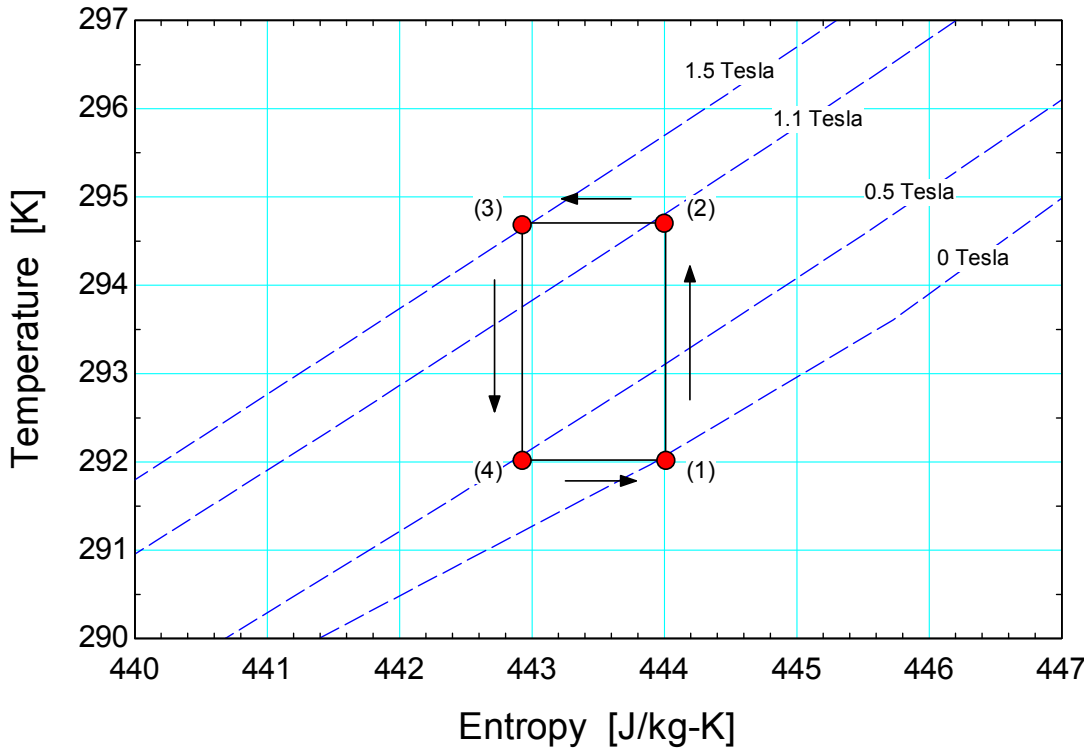

Figure 1-4. Adiabatic demagnetization refrigeration (ADR) or magnetic Carnot cycle for gadolinium.

The ideal ADR cycle shown in Figure 1-4 consists of four distinct processes that are summarized below:

1. Process 1 → 2: Adiabatic magnetization
2. Process 2 → 3: Isothermal heat rejection
3. Process 3 → 4: Adiabatic demagnetization
4. Process 4 → 1: Isothermal heat addition

In practice, it is difficult to reject heat isothermally, since the magnetic field must also be modulated properly in order to achieve this condition; this requires complex heat switches that limit heat flux rates. Also, the temperature lift of an ADR cycle is limited to the adiabatic temperature change of the material. The ADR cycle has therefore been limited to cryogenic sub-Kelvin refrigeration applications using paramagnetic salts as refrigerants.

1.2.2 Active Magnetic Regenerative Refrigeration (AMRR) Cycle

The active magnetic refrigeration (AMR) cycle is similar to the ADR cycle, but heat addition and rejection occurs at a constant magnetic field rather than at constant temperature. Isothermal heat rejection and addition is impractical to implement since the applied magnetic field must be modulated to match the temperature with the heat rejection rate. The AMR cycle is the magnetic equivalent of the Brayton cycle for a compressible fluid and is shown on a temperature-entropy diagram in Figure 1-5.

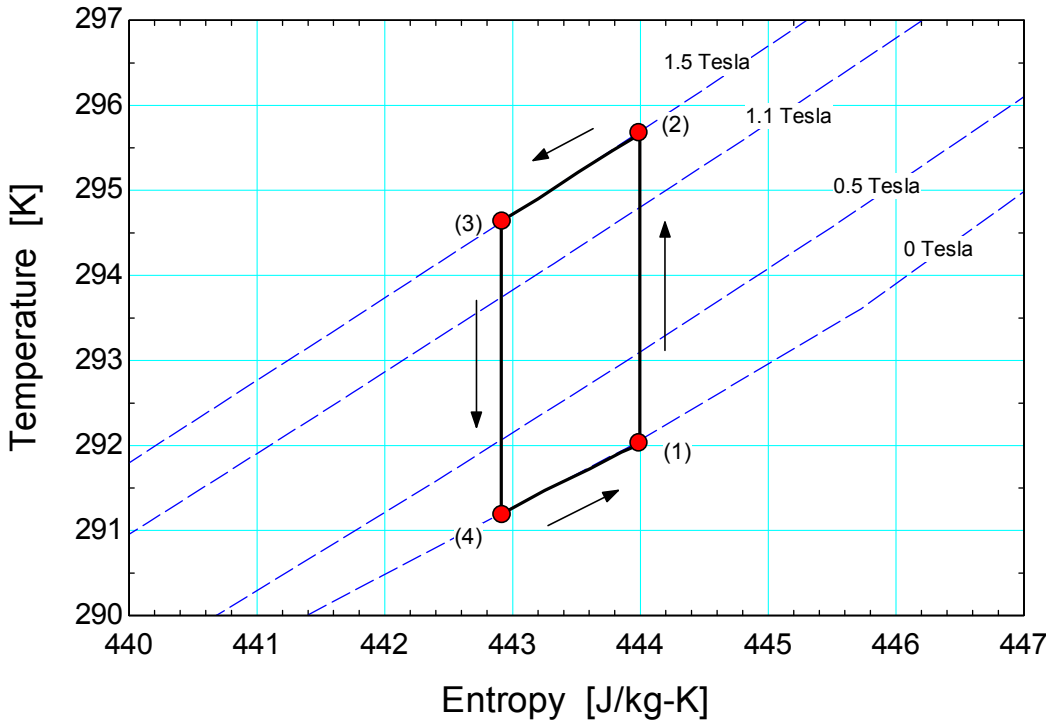

Figure 1-5. Temperature – Entropy diagram for an ideal Active Magnetic Refrigeration (AMR) cycle for gadolinium.

The ideal AMR cycle shown in Figure 1-5 consists of four distinct processes which are summarized as follows:

1. Process 1 → 2: Adiabatic magnetization
2. Process 2 → 3: Isofield heat rejection
3. Process 3 → 4: Adiabatic demagnetization

4. Process 4 → 1: Isofield heat addition

The achievable temperature span for a single AMR cycle near room temperature is limited to the adiabatic temperature change by the strength of the applied magnetic field change. Currently, the strongest permanent magnets (neodymium-based) can achieve fields near 1.5 Tesla, which does not take into account geometric limitations and demagnetization effects [6]. From Figure 1-5, the adiabatic temperature change for gadolinium near the Curie temperature for a field change from 0 to 1.5 Tesla is approximately $\Delta T_{ad} = 3.5$ K. This limited operating temperature range is not useful for most refrigeration applications. The solution to this problem is to arrange a porous matrix magnetocaloric material in a regenerator bed with a heat transfer fluid flowing through it. Each infinitesimal segment of the regenerator bed undergoes a unique thermodynamic refrigeration cycle and thermally interacts with an adjacent cycle through the flowing heat transfer fluid. In this arrangement, a much larger temperature span can be achieved. This cycle is called the active magnetic regenerative refrigeration (AMRR) cycle.

Practical AMRR cycles utilize either a porous matrix of packed magnetocaloric spheres housed in a regenerator bed or a parallel plate regenerator consisting of stacked parallel plates of magnetocaloric material. Brown (1976) first demonstrated a regenerative magnetic heat pump operating near room temperature with gadolinium as the refrigerant under a high magnetic field that varied between 0 to 7 Tesla. The regenerator was a vertical column with a stationary fluid and a moving regenerator of gadolinium plates, oscillating between the hot and cold reservoirs of the column [7]. More recently, Zimm et al. (2006) constructed a rotary regenerator that consists of six packed sphere regenerator beds of gadolinium operating with stationary permanent magnets. This system uses variable speed pumps with rotary valves to control the heat transfer fluid (water) flow [8]. Yu et al. (2010) provide a comprehensive review of AMRR prototype systems that have been built before the year 2010 [9].

The AMRR cycle consists of four processes that are similar to the AMR cycle. For an AMRR cycle operating at steady state, the first process is an adiabatic magnetization of the magnetocaloric matrix in thermal contact with the entrained fluid, resulting in a temperature rise across the bed. In this instance,

heat transfer occurs between the entrained fluid and the regenerator material, but the regenerator housing is assumed to be adiabatic. The second is an isofield heat rejection by the regenerator matrix and entrained fluid through a cold-to-hot flow of heat transfer fluid. In this process, the magnetic field is held constant while the heat transfer fluid flow is activated and flowing from the cold heat exchanger to the hot heat exchanger. As the third process begins, the fluid flow is halted, and the magnetic field begins to decrease. The third process is an adiabatic demagnetization of the regenerator material and entrained heat transfer fluid, resulting in a temperature decrease along the length of the bed. Once the bed is completely demagnetized (i.e., the field reaches zero Tesla) the fourth process begins in which a hot-to-cold fluid flow is activated and an isofield heat addition to the regenerator material and the entrained fluid occurs. A hot-to-cold fluid flow indicates that the heat transfer fluid is flowing from the hot heat exchanger to the cold heat exchanger (the opposite direction of process 2). At the end of the fourth process, the fluid flow is terminated and the cycle restarts.

Figure 1-6 shows the temperature-specific entropy diagram of the regenerator material in an AMRR cycle with a bed using a single material, a porous matrix of $Gd_{0.96}Er_{0.04}$, and water as the heat transfer fluid. The minimum and maximum applied field strengths are 0 and 3 Tesla, respectively. The temperature of the cold reservoir is 299 K and the temperature of the hot reservoir is 310 K. The Curie temperature is specified to be $T_{Curie} = 304.5$ K. Shown on the diagram are refrigeration cycles occurring at dimensionless regenerator positions of x/L = 0, 0.25, 0.5, 0.75 and 1. State points are only shown for the steady state AMRR cycle occurring at x/L = 0.5 for clarity, but occur simultaneously on each independent cycle curve. In this sense, they are not state "points" but spatially-dependent state "lines" that are projected on a two-dimensional temperature-entropy diagram. A three-dimensional projection of the temperature-specific entropy-length diagram is shown in Figure 1-7. This diagram shows a visualization of a three-dimensional 'tube' of temperature as a function of specific entropy through the spatial dimension of the AMRR cycle. The state points (or projections of state lines) shown in Figure 1-6 correspond to the AMRR processes as follows:

1. Process 1 → 2: Adiabatic magnetization transformation with entrained fluid
2. Process 2 → 3: Isofield heat rejection to heat transfer fluid
3. Process 3 → 4: Adiabatic demagnetization transformation with entrained fluid
4. Process 4 → 1: Isofield heat addition to heat transfer fluid

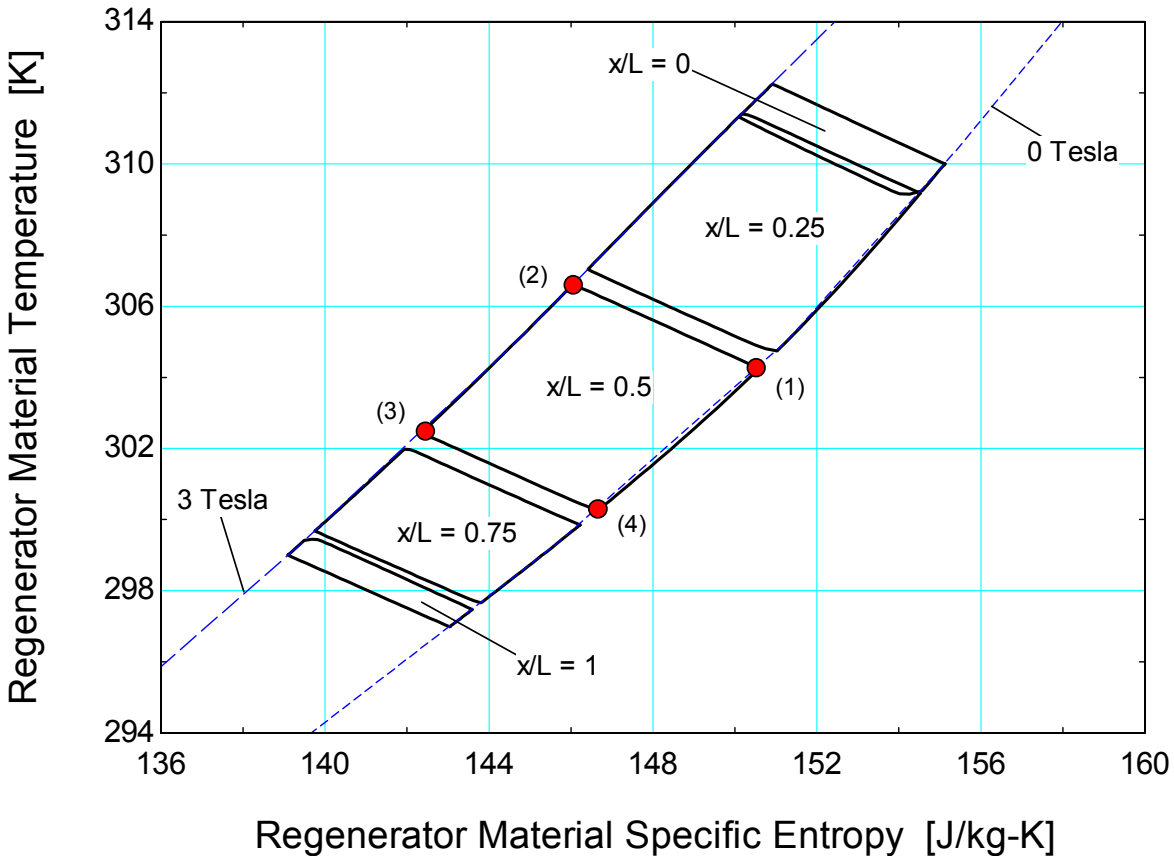

Figure 1-6. Temperature-Entropy diagram of the Active Magnetic Regenerative Refrigeration (AMRR) Cycle for a bed composed of $Gd_{0.94}Er_{0.6}$. State points are shown for the cycle occurring at x/L = 0.5.

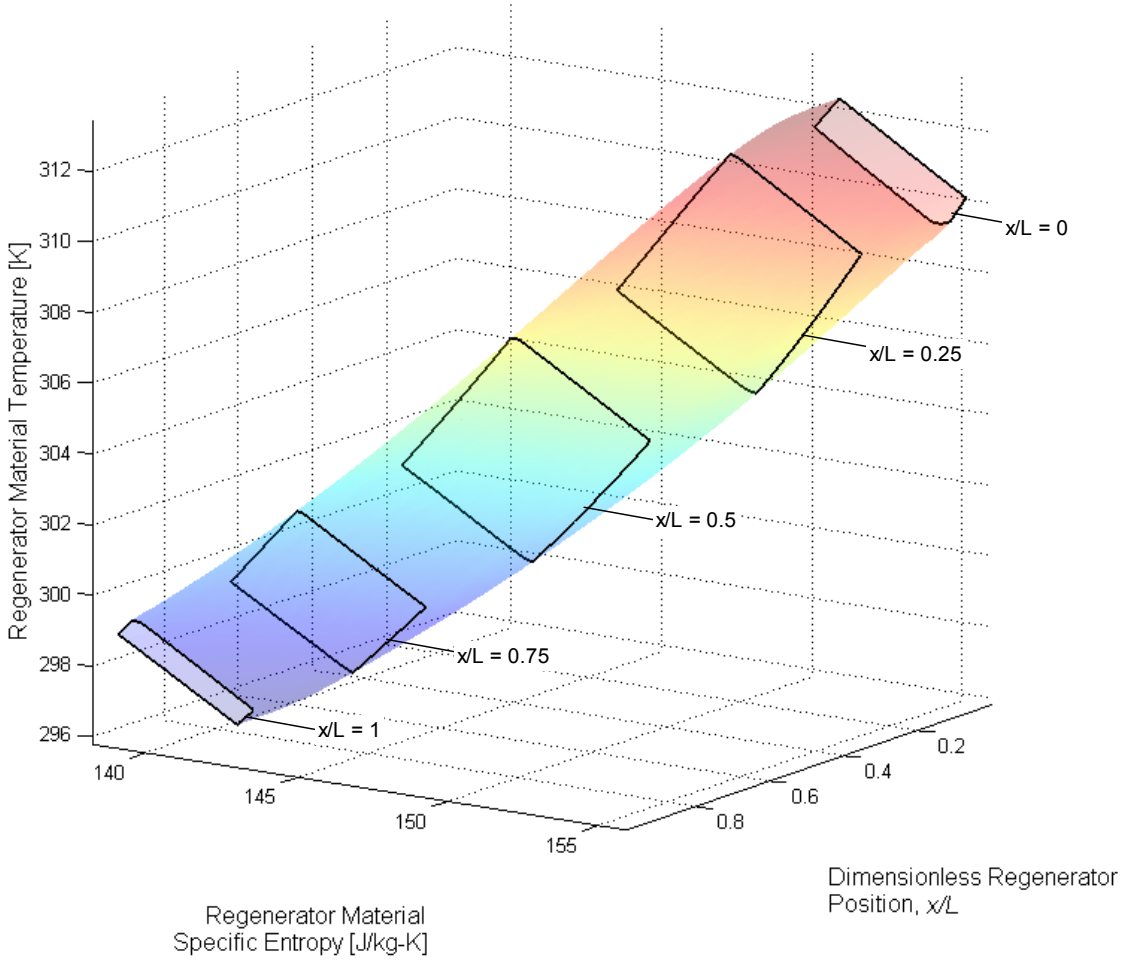

Figure 1-7. Three-dimensional projection of the Temperature-Entropy-Length diagram for AMRR cycle shown in Figure 1-6.

For an AMRR cycle operating with a single refrigerant material, the operating temperature can deviate significantly from the Curie temperature, where the magnetocaloric effect is largest. Thus, a regenerator bed that contains several materials with Curie temperatures near the spatially local operating temperature range would improve cycle performance. This type of arrangement is termed a 'layered' regenerator bed. Figure 1-8 shows the temperature-entropy diagram of the regenerator material in an AMRR cycle with an infinitely layered bed using a porous matrix of gadolinium-erbium alloy and water as the heat transfer fluid. The Curie temperature of the gadolinium-erbium alloy is controlled by altering the composition. For this study, the properties of $Gd_{0.96}Er_{0.04}$ are modulated by adjusting the Curie temperature in order to simulate an infinitely layered bed. The Curie temperature is modulated so that it

varies linearly between the hot and cold reservoir temperatures. The minimum and maximum applied field strengths are 0 and 3 Tesla, respectively. The temperatures of the cold and hot reservoirs are 299 K and 310 K, respectively. Isomagnetic field lines are shown only for the AMRR cycle occurring at x/L = 0.5 for clarity, however each spatial cycle operates with its own refrigerant material composition with separate magnetic properties. By direct comparison of Figure 1-8 and Figure 1-6, there is an increased total area of cycle operation below the cold reservoir temperature (299 K) for the layered bed than the single layered bed; this corresponds to an increased refrigeration capacity for the same operating conditions. Figure 1-9 is a three dimensional surface plot of the temperature-entropy-length diagram for the AMRR cycle with a layered regenerator material shown in Figure 1-8. The total enclosed volume of the temperature-entropy-length 'tube' below the cold reservoir temperature isotherm is the refrigeration capacity.

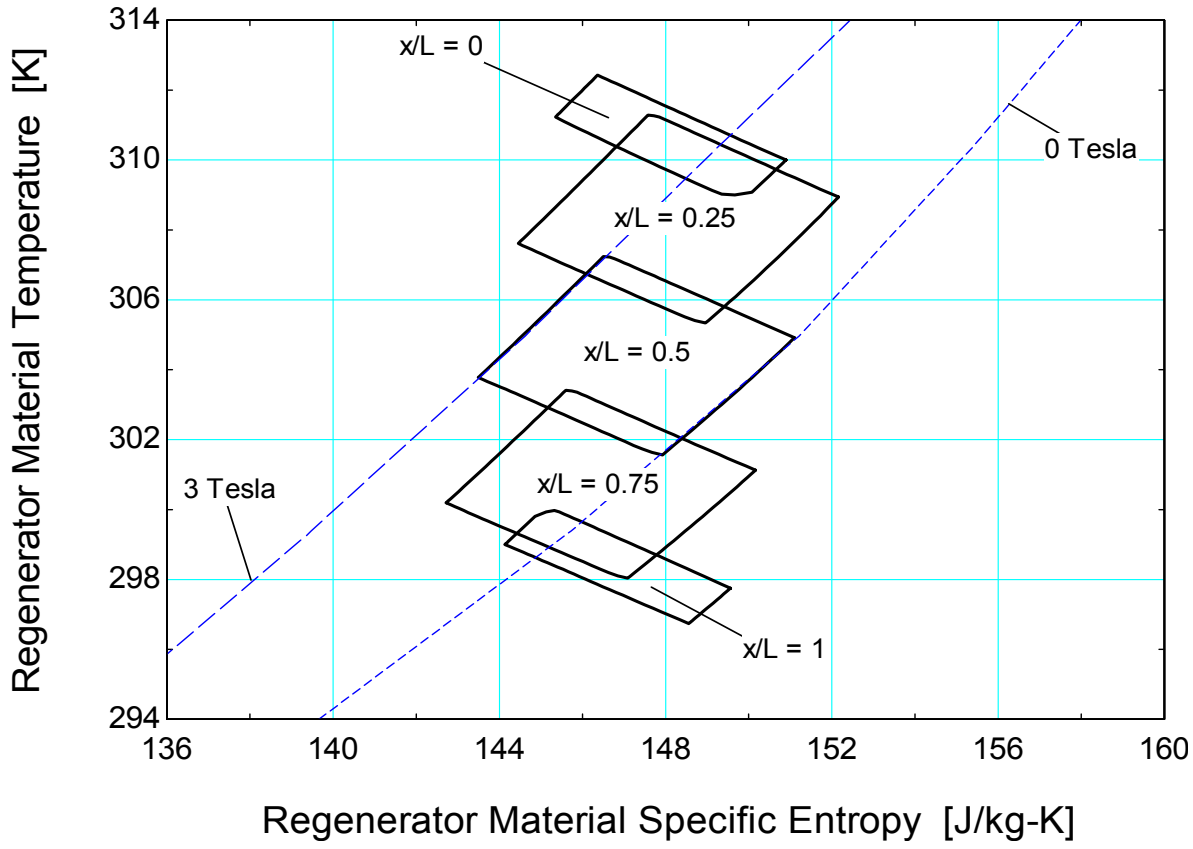

Figure 1-8. Temperature-Entropy diagram of the Active Magnetic Regenerative Refrigeration (AMRR) Cycle for gadolinium-erbium with an infinitely layered bed. Isofield lines for cycle occurring at x/L = 0.5 are shown.

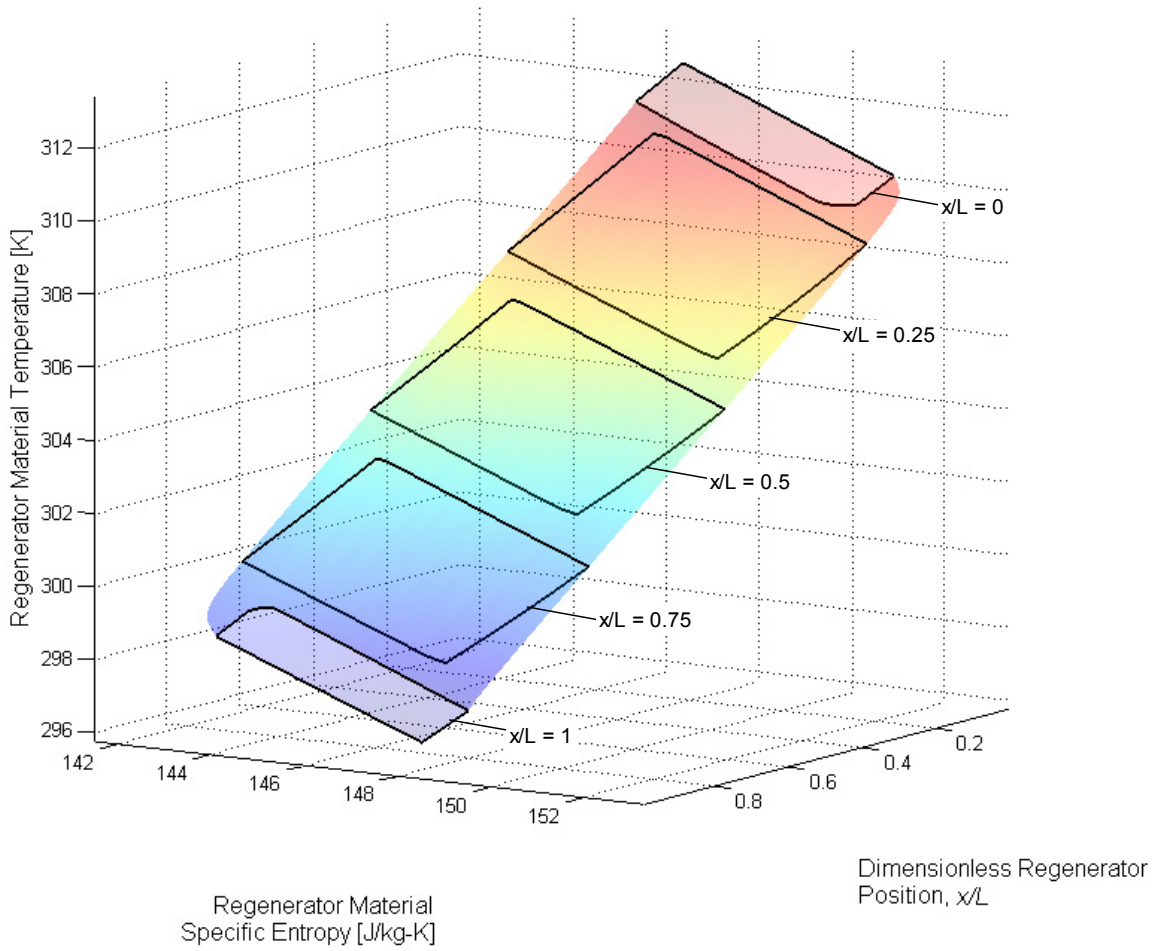

Figure 1-9. Three-dimensional projection of the Temperature-Entropy-Length diagram for AMRR cycle shown in Figure 1-8.

1.3 Magnetic Hysteresis

Magnetic hysteresis is a phenomenon exhibited in ferromagnetic materials when they are exposed to variable magnetic fields. These materials tend to retain a magnetization, even after an applied magnetic field is removed. This effect can be explained by the ability of microscopic magnetic domains to become 'caught' in a magnetized state caused by impedance from neighboring domains, resulting a remnant magnetization even at zero applied magnetic field [10]. Ferromagnetic materials are subdivided into 'hard' and 'soft' magnets. The term 'soft' magnet used to describe a material where a low applied coercive field is required for magnetization but the material does not tend to remain magnetized when the

field is removed. A 'hard' magnetic material is a material that requires a high applied coercive field for magnetization and retains its magnetization long after the applied field is removed. Thus, permanent magnets are 'hard' magnetic materials, and only exhibit significant hysteresis under very high magnetic fields [10].

Hysteresis is a causal process, where the present output is dependent on the present state as well as past input history. An example of a single cycle hysteresis loop, with arrows showing loop direction, is shown in Figure 1-10.

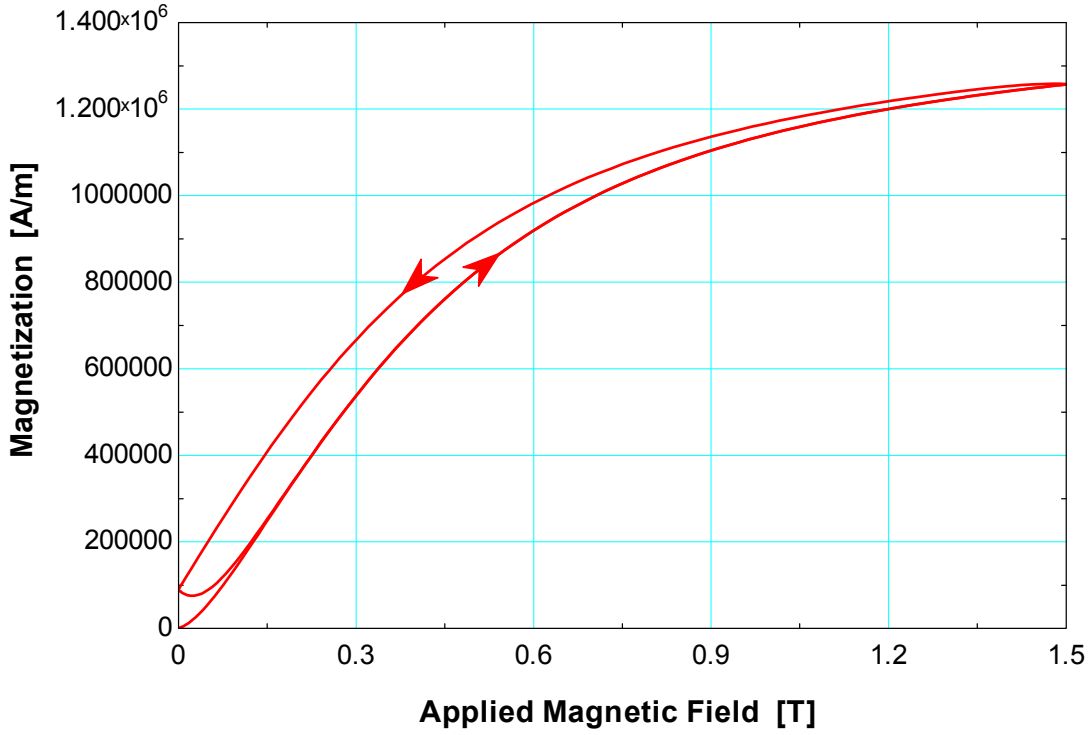

Figure 1-10. Example of a hysteresis loop with an applied magnetic field which cycles between 0 and 1.5 Tesla.

When the ferromagnetic material is first exposed to the applied magnetic field, it has zero magnetization and follows a path known as the anhysteric magnetization curve to the maximum applied field. When the applied field is ramped down again, remnant magnetization within the material causes it to follow a downward magnetization path and ultimately reach a nonzero magnetization when the applied

field reaches zero. When the magnetic field is ramped up again, it follows a path that begins from the non-zero remnant magnetization at zero applied field and eventually smoothly coincides with the anhysteric curve as shown in Figure 1-10. When plotted against time, the magnetization has higher field strength than the applied field due to the effective field within the material that takes contributions from both the applied field and magnetization of the internal domains. This relation is shown in Figure 1-11. There are several variables that influence the shape of the hysteresis curve: the applied field, saturation (or spontaneous) magnetization, material coercivity, susceptibility, and remanence.

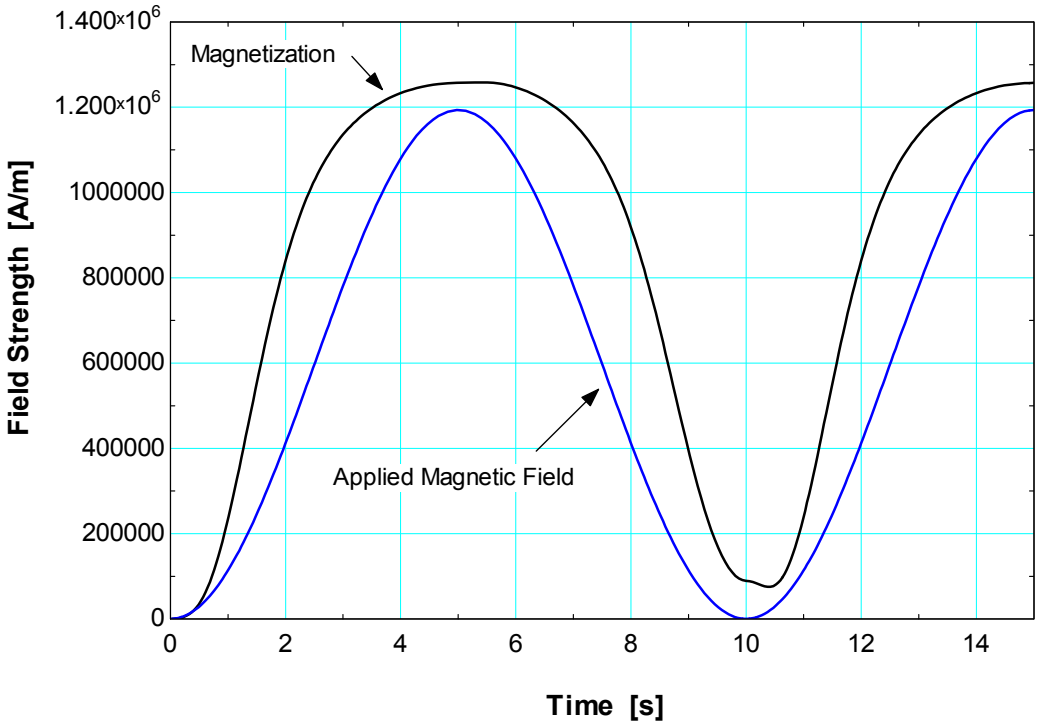

Figure 1-11. Magnetization and Applied Field as a function of time for hysteresis loop in Figure 1-10

The influence of the applied field on a hysteresis curve determines how large the loop spans on an *M-H* curve. The saturation magnetization is the upper limit of the magnetization that the hysteresis loop will approach asymptotically as the applied field approaches infinity. Remanence is defined as the magnetization that remains in a material after it has been exposed to a magnetic field and then removed from it. The coercivity is the applied field that is required to bring a material's magnetization to zero.

The magnetic susceptibility of a material determines the slope of the magnetization versus applied field curve.

The Jiles-Atherton and Preisach models are two common mathematical models for magnetic hysteresis. The Jiles-Atherton model is a deterministic model that empirically defines a hysteresis loop based on five macroscopic characteristic parameters that are based on the properties that characterize a hysteresis loop: saturation magnetization, remanence, coercivity, and anhysteretic magnetic susceptibility [11, 12]. The Preisach model of magnetic hysteresis is a probabilistic mathematical model of hysteresis that attempts to quantify hysteresis in terms of the microscopic magnetic domains rather than the macroscopic volume average magnetization [13].

LoBue et al. (2005) use the Preisach model to show the irreversibilities of magnetic hysteresis and its qualitative negative effects on the performance of AMRR systems. Ultimately, hysteresis results in a generation of entropy internal to the magnetocaloric material. Therefore, one approach for including hysteresis in an AMRR model is to treat it as a source of entropy generation that is physically linked to the hysteretic characteristics of the material as well as the operating conditions of the cycle; this is the approach used for the work in this thesis.

1.4 Magnetocaloric Materials

One of the most significant limitations on the performance of magnetic refrigeration systems is the magnetocaloric material (refrigerant) properties. These materials are generally characterized by an adiabatic temperature change due to magnetization (ΔT_{ad}), an isothermal specific entropy change due to magnetization (Δs_M), or both. The effect of varying these parameters on the performance of magnetic coolers is not well understood, but is generally accepted that increasing each independently improves system performance.

There exist two main groups of magnetocaloric materials: first order magnetic transition (FOMT) and second order magnetic transition (SOMT) type materials. In SOMT materials, the partial derivative

of the Gibbs free energy with respect to any intensive state variable (T or $\mu_o H$ for example) is continuous during the phase transition from a ferromagnetic to paramagnetic state. In these materials, the magnetocaloric effect is a consequence of a reduction in the heat capacity when exposed to a magnetic field [1]. Additionally, SOMT materials exhibit negligible magnetic hysteresis.

In FOMT materials, the partial derivative of the Gibbs free energy with respect to either temperature or applied field is discontinuous at the Curie temperature. The magnetocaloric effect in FOMT materials is a result of a shift in the Curie temperature in an applied magnetic field [1]. Furthermore, FOMT materials exhibit significant magnetic hysteresis. As a consequence of the nature of the first order phase transition, the magnetocaloric effect can be much larger in magnitude in FOMT than in SOMT materials, but generally occurs over a smaller range of temperatures. Furthermore, FOMT materials can exhibit considerable lag time between the application or removal of a magnetic field and the magnetization induced within the material (a phenomenon related to the physical mechanisms behind rate-dependent magnetic hysteresis) [10]. Slow magnetic phase transitions may cause inefficiencies in AMRR systems with small cycle times running with FOMT type materials.

Gschneidner and Pecharsky (2000) provide a detailed explanation of the complex relationship between the adiabatic temperature change and isothermal entropy change [14]. The adiabatic temperature change is dependent on variation of specific entropy with temperature as well as magnetic field in a variable applied field. In contrast, the isothermal entropy change is only dependent on the magnetic portion of the entropy contribution in a variable applied field. The authors also discuss in depth the physical mechanisms by which the two quantitative characteristics of the magnetocaloric effect arise in both FOMT and SOMT type ferromagnetic materials (as well as paramagnetic and antiferromagnetic materials).

The magnitude of magnetic hysteresis for a material is typically reported either as the measured temperature difference in the material after a single magnetization-demagnetization cycle or as a calculated exergy loss per cycle for a specified applied field change. This thesis will discuss another way

to quantitatively characterize magnetic hysteresis in terms of a magnetization loss or gain, which is based on the Jiles-Altherton model of magnetic hysteresis [12]. This method of characterizing magnetic hysteresis is the focus of Chapter 2.

1.4.1 Gadolinium and Gadolinium Alloys

Gadolinium is a rare earth element that exhibits a significant magnetocaloric effect near its Curie temperature (293 K). Pure gadolinium exhibits a second order magnetic transition from the ferromagnetic to paramagnetic phase when it is heated above its Curie temperature. Due to the nature of the SOMT, pure gadolinium shows negligible hysteresis when it is subjected to a variable applied magnetic field near its Curie temperature. Dan'kov et al. (1998) report the adiabatic temperature change of pure gadolinium to be near $\Delta T_{ad} = 5.5$ K and the isothermal entropy change to be approximately $\Delta s_M = -5.5 \frac{\text{J}}{\text{kg-K}}$ for an applied field change from 0 to 2 Tesla [15]. These measurements can vary slightly based on the measurement technique, applied magnetic field alignment with the crystalline structure, and gadolinium purity. The thermal conductivity of gadolinium is approximately $k = 10 \frac{\text{W}}{\text{m-K}}$ near 293 K, but increases nearly linearly to $12 \frac{\text{W}}{\text{m-K}}$ at 350 K [16].

The Curie temperature of gadolinium can be tuned through alloying with other rare earth lanthanides, while preserving the second order nature of the phase transition. $Gd_{1-x}R_x$ compounds (where R = Tb, Ho, Dy, or Er) have been shown to shift the Curie temperature of gadolinium to lower temperatures with a slight decrease in the magnitude of the magnetocaloric effect [17, 18]. Since the magnetocaloric properties of these materials are tunable, these materials are attractive for use in a layered regenerator bed.

1.4.2 $La(Fe_{1-x}Si_x)_{13}H_y$ Compounds

The lanthanum-iron-silicon hydrides are a promising material for use in active magnetic refrigerators since they exhibit a large magnetocaloric effect (MCE) near room temperature. These materials exhibit a first-order itinerant-electron metamagnetic phase transition between the ferromagnetic and paramagnetic phases, during which the material exhibits magnetic hysteresis [19]. The Curie temperature can be tuned

between approximately 200 K to 336 K by adjusting the concentration of hydrogen in the compound (y), depending on the concentration of iron and silicon (x) [20].

Figure 1-12 is the Curie temperature (T_{Curie}) and critical temperature (T_0) as a function of hydrogen concentration in $La(Fe_{1-x}Si_x)_{13}H_y$ with x = 0.12 [19]. The Curie temperature (T_{Curie}) is the temperature at which the phase transition from a ferromagnetic to paramagnetic phase begins when heated, and the material enters the metamagnetic phase transition region. The critical temperature (T_0) is the temperature at which the metamagnetic transition phase ends and the material becomes fully paramagnetic during heating, meaning magnetic hysteresis effects have also disappeared. As the figure shows, T_{Curie} is almost exactly a linear function of hydrogen concentration, and T_0 also correlates nearly linearly with hydrogen concentration. This linear dependence indicates that the material's Curie point can be tuned to a wide range of temperatures, which makes for ideal usage in a layered active magnetic refrigerator.

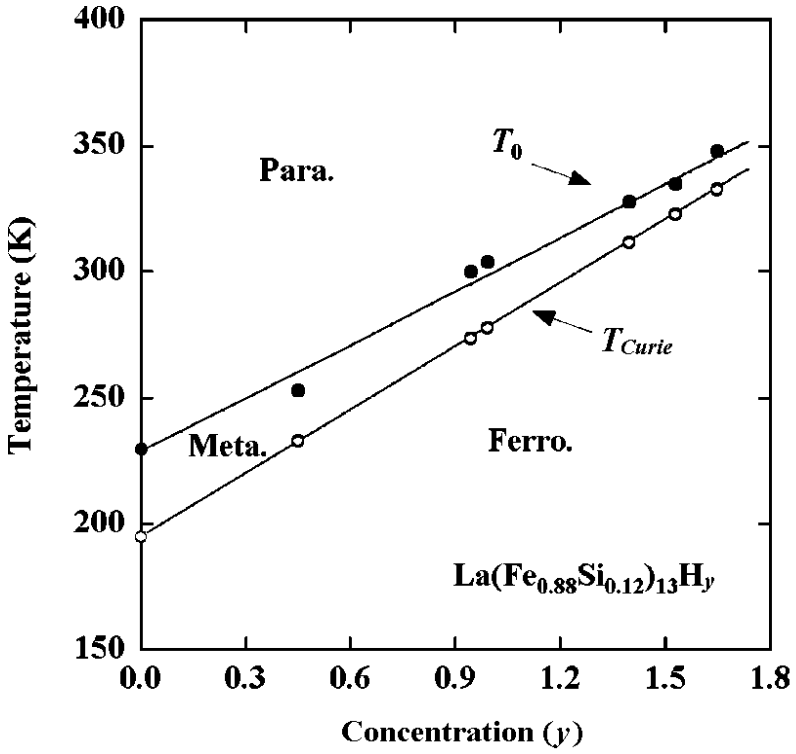

Figure 1-12. Curie temperature (T_{Curie}) and critical temperature (T_0) as a function of hydrogen concentration in $La(Fe_{1-x}Si_x)_{13}H_y$ with x = 0.12 [19].

Fujieda et al. (2002) report an isothermal entropy change of $\Delta s_M = -24 \frac{\text{J}}{\text{kg-K}}$ and an adiabatic temperature change of $\Delta T_{ad} = 6.9$ K for $La(Fe_{0.89}Si_{0.11})_{13}H_{1.3}$ for an applied field change from 0 to 2 Tesla. The particular composition with x = 0.11 and y = 1.3 has a Curie temperature of approximately 291 K, which can be approximately inferred from Figure 1-12. These materials tend to be less expensive to manufacture than pure gadolinium, but require precise and tedious processing to modulate the silicon and hydrogen compositions. Zhao et al. (2009) demonstrated that hysteresis losses may be reduced with the partial substitution of praseodymium for lanthanum with only a slight decrease in the magnetocaloric effect. $La_{0.5}Pr_{0.5}(Fe_{0.88}Si_{0.12})_{13}H_{1.6}$ exhibited a magnetocaloric effect of $\Delta s_M = -17.7 \frac{\text{J}}{\text{kg-K}}$ at a Curie temperature of approximately $T_{Curie} = 320$ K with a hysteresis loss per cycle of $2.3 \frac{\text{J}}{\text{kg}}$ [21].

1.4.3 $Gd_5(Si_{1-x}Ge_x)_4$ Compounds

1n 1997, Pecharsky and Gschneidner announced the discovery of the giant magnetocaloric effect (GMCE) in $Gd_5(Si_{1-x}Ge_x)_4$ type compounds [22]. The gadolinium-germanium-silicon family of magnetocaloric materials is of the FOMT type, and exhibit large isothermal entropy and adiabatic temperature changes for relatively modest applied field changes. For the composition type where x = 0.5, the adiabatic temperature and isothermal entropy change have been reported to be as large as $\Delta T_{ad} = 7$ K and $\Delta s_M = -27 \frac{\text{J}}{\text{kg-K}}$, respectively, for an optimally prepared material under an applied field change from 0 to 2 Tesla [23]. The Curie temperatures of these materials are tunable by varying the germanium content (x) of the alloy, and scale approximately linearly for $0.2 < x < 0.5$ [24]. These materials also exhibit significant magnetic hysteresis by nature of the FOMT, which is dependent on the specific composition of the material.

1.5 Research Objectives

The primary goal of this research is to develop a thermodynamic model of magnetic hysteresis for applications in magnetic cooling systems and evaluate the effect of hysteresis on their performance. Currently there is no known numerical model that can accurately capture the effects of magnetic

hysteresis on the performance of an AMRR cycle, but the effect has been simulated through the use of scaling factors applied to the efficiency of the system calculated without hysteresis [25]. This thesis will quantify the effects of magnetic hysteresis on the performance of AMRR cycles which use FOMT materials. Thermodynamically, magnetic hysteresis is treated as a source of entropy generation that is proportional to the area swept by a hysteresis loop for one refrigeration cycle.

The one-dimensional, numerical model presented by Engelbrecht (2008) [26], is modified to include entropy generation from magnetic hysteresis in the regenerator energy equations. This model accepts inputs such as the regenerator geometry, magnetic refrigerant material, and heat transfer fluid and calculates the steady-state temperature distribution for the complete AMRR cycle as a function of time and space through an iterative successive substitution technique that subject to a specified convergence tolerance. The final fluid and regenerator material temperature distributions are used to quantify the performance of the cycle.

The modified model is used to optimize the performance an AMRR cycle that uses FOMT materials and compare it to the performance of an AMRR cycle that uses SOMT materials. The effect of model input parameters such as regenerator volume, mass flow rate profile, regenerator aspect ratio, and bed layering geometry on the performance of the cycle is studied.

REFERENCES

1. Gschneidner, K.A., V.K. Pecharsky, and A.O. Tsokol, *Recent developments in magnetocaloric materials.* Reports on Progress in Physics, 2005. **68**(6): p. 1479.

2. Gschneidner Jr, K.A. and V.K. Pecharsky, *Thirty years of near room temperature magnetic cooling: Where we are today and future prospects.* International Journal of Refrigeration, 2008. **31**(6): p. 945-961.

3. Blumenfeld, P.E., et al., *High temperature superconducting magnetic refrigeration.* AIP Conference Proceedings, 2002. **613**(1): p. 1019-1026.

4. Debye, P., *The fundamental laws of electric and magnetic excitation from standpoint of the quantum theory (Die Grundgesetze der elektrischen und magnetischen Erregung vom Standpunkte der Quantentherie).* Physikalische Zeitschrift, 1926. **27**(3): p. 67-74.

5. Giauque, W.F. and D.P. MacDougall, *Attainment of temperatures below 1^{o} absolute by demagnetization of $Gd_2(SO_4)_3 8H_2O$.* Phys. Rev., 1933. **43**: p. 768.

6. Dai, W., et al., *Application of high-energy Nd-Fe-B magnets in the magnetic refrigeration.* Journal of Magnetism and Magnetic Materials, 2000. **218**(1): p. 25-30.

7. Brown, G.V., *Magnetic heat pumping near room temperature.* Journal of Applied Physics, 1976. **47**(8): p. 3673-3680.

8. Zimm, C., et al., *Design and performance of a permanent-magnet rotary refrigerator.* International Journal of Refrigeration, 2006. **29**(8): p. 1302-6.

9. Yu, B., et al., *A review of magnetic refrigerator and heat pump prototypes built before the year 2010.* International Journal of Refrigeration, 2010. **33**(6): p. 1029-1060.

10. Bertotti, G., *Hysteresis in magnetism : for physicists, materials scientists, and engineers*. 1998, San Diego, CA: Academic Press. 558.

11. Jiles, D.C., J.B. Thoelke, and M.K. Devine, *Numerical determination of hysteresis parameters for the modeling of magnetic properties using the theory of ferromagnetic hysteresis.* IEEE Transactions on Magnetics, 1992. **28**(1): p. 27-35.

12. Jiles, D.C. and D.L. Atherton, *Theory of ferromagnetic hysteresis.* Journal of Magnetism and Magnetic Materials, 1986. **61**(1-2): p. 48-60.

13. LoBue, M., et al. *Entropy and entropy production in magnetic systems with hysteresis*. in *49th Annual Conference on Magnetism and Magnetic Materials*. 2005. Jacksonville, Florida (USA): AIP.

14. Gschneidner, K.A. and V.K. Pecharsky, *Magnetocaloric Materials.* Annual Review of Materials Science, 2000. **30**(1): p. 387-429.

15. Dan'kov, S.Y., et al., *Magnetic phase transitions and the magnetothermal properties of gadolinium.* Physical Review B, 1998. **57**(6): p. 3478.

16. Fujieda, S., et al., *Thermal transport properties of magnetic refrigerants $La(Fe_xSi_{1-x})_{13}$ and their hydrides, and $Gd_5Si_2Ge_2$ and MnAs.* Journal of Applied Physics, 2004. **95**(5): p. 2429-2431.

17. Pecharsky, V.K. and K.A. Gschneidner Jr, *Magnetocaloric effect and magnetic refrigeration.* Journal of Magnetism and Magnetic Materials, 1999. **200**(1-3): p. 44-56.

18. Nikitin, S.A., et al., *Magnetocaloric effect in rare-earth alloys Gd-Ho and Gd-Er.* Physics of Metals and Metallography, 1985. **59**(2): p. 104-108.

19. Fujita, A., et al., *Itinerant-electron metamagnetic transition and large magnetocaloric effects in $La(Fe_xSi_{1-x})_{13}$ compounds and their hydrides.* Physical Review B, 2003. **67**(10): p. 104416.

20. Fujieda, S., A. Fujita, and K. Fukamichi, *Large magnetocaloric effect in $La(Fe_xSi_{1-x})_{13}$ itinerant-electron metamagnetic compounds.* Applied Physics Letters, 2002. **81**(7): p. 1276-1278.

21. Jin-liang, Z., et al., *Reduction of magnetic hysteresis loss in $La_{0.5}Pr_{0.5}Fe_{11.4}Si_{1.6}H_x$ hydrides with large magnetocaloric effects.* Journal of Applied Physics. **107**(11): p. 113911 (5 pp.).

22. Pecharsky, V.K. and J.K.A. Gschneidner, *Giant Magnetocaloric Effect in $Gd_5(Si_2Ge_2)$.* Physical Review Letters, 1997. **78**(23): p. 4494.

23. Pecharsky, A.O., K.A. Gschneidner Jr, and V.K. Pecharsky, *The giant magnetocaloric effect of optimally prepared Gd5Si2Ge2.* Journal of Applied Physics, 2003. **93**(8): p. 4722-4728.

24. Pecharsky, V.K. and K.A. Gschneidner, Jr., *Tunable magnetic regenerator alloys with a giant magnetocaloric effect for magnetic refrigeration from approx.20 to approx.290 K.* Applied Physics Letters, 1997. **70**(24): p. 3299-3299.

25. Nielsen, K.K., et al., *Review on numerical modeling of active magnetic regenerators for room temperature applications.* International Journal of Refrigeration. **34**(3): p. 603-16.

26. Engelbrecht, K., *A Numerical Model of an Active Magnetic Regenerator Refrigerator with Experimental Validation* in *Mechanical Engineering*. 2008, The University of Wisconsin at Madison: Madison, WI. p. 267.

Chapter 2 HYSTERESIS MODELING

2.1 Entropy Generation due to Magnetic Hysteresis

This chapter presents a rigorous thermodynamic analysis of magnetic hysteresis in magnetocaloric materials. In this analysis, magnetic hysteresis is treated as a source of entropy generation in a system defined by a magnetocaloric material. The entropy generation associated with hysteresis is proportional to the area swept by the hysteresis curve on a applied field – magnetization (*H-M*) curve [1]. The *H-M* curve for a material is split into two components: anhysteretic or reversible magnetization and hysteretic or irreversible magnetization. This model of anhysteretic and hysteretic magnetization is based on the Jiles-Atherton model of magnetic hysteresis proposed in 1986 [2]. The irreversible magnetization (or hysteretic magnetization) is considered an applied field rate-independent property in this thesis, which may not be a valid treatment for systems with slow phase transitions relative to the time rate of change of the applied magnetic field [1]. Thermal hysteresis is also neglected in this analysis.

2.1.1 Entropy Balance without Magnetic Hysteresis

Consider an adiabatic process undergone by a magnetocaloric material without hysteresis. Such a process is assumed to be reversible and therefore an entropy balance on this system, carried out on a unit mass basis, requires that:

$$\frac{ds}{dt} = 0 \tag{2-1}$$

The time rate of change of the specific entropy in Eq. (2-1) is divided into its magnetic field ($\mu_o H$) and temperature (T) driven components:

$$\frac{ds}{dt} = \left(\frac{\partial s}{\partial T}\right)_{\mu_0 H}\left(\frac{dT}{dt}\right) + \left(\frac{\partial s}{\partial \mu_0 H}\right)_{T}\left(\frac{d\mu_0 H}{dt}\right) = 0 \tag{2-2}$$

where the temperature T and applied magnetic field $\mu_0 H$ are only functions of time. The partial derivative of specific entropy with respect to temperature at constant applied field can be written in terms of the constant field specific heat capacity, $c_{\mu_0 H}$:

$$\left(\frac{\partial s}{\partial T}\right)_{\mu_0 H} = \frac{c_{\mu_0 H}}{T} \tag{2-3}$$

A Maxwell relation is used to write the partial derivative of specific entropy with respect to applied field at constant temperature in terms of the mass specific anhysteretic magnetization ($v\,M_{an}$) [3]:

$$\left(\frac{\partial s}{\partial \mu_0 H}\right)_T = \left(\frac{\partial v M_{an}}{\partial T}\right)_{\mu_0 H} \tag{2-4}$$

Substituting Eqs. (2-3) and (2-4) into Eq. (2-2) leads to:

$$\frac{ds}{dt} = \frac{c_{\mu_0 H}}{T}\left(\frac{dT}{dt}\right) + \left(\frac{\partial v M_{an}}{\partial T}\right)_{\mu_0 H}\left(\frac{d\mu_0 H}{dt}\right) = 0 \tag{2-5}$$

For magnetic refrigeration systems, the term of interest in Eq. (2-5) is often the change in temperature with respect to time $\frac{dT}{dt}$ since we are typically interested in characterizing an adiabatic temperature rise for a given material. By inspection of this equation, it is evident that the temperature rise is a direct function of the change in the applied magnetic field, the magnitude of the constant field specific heat $c_{\mu_0 H}$ and the partial derivative of mass-specific anhysteretic magnetization vM_{an} with respect to temperature at constant field.

2.1.2 Entropy Balance with Magnetic Hysteresis

Since hysteresis is an irreversible process, it is necessary to model the phenomenon as an internal entropy generation. Consider an adiabatic process undergone by a magnetocaloric material with hysteresis. Such a process will be irreversible and therefore an entropy balance on this system, carried out on a unit mass basis, requires that:

$$\frac{ds}{dt} = \frac{\dot{S}_{gen}}{m} \tag{2-6}$$

where m is the mass of the material and $\dot{S}_{gen}$ is the rate of entropy generation, which must have a positive value. The rate of entropy generation per unit mass is defined using the irreversible magnetization (M_{irr}) and it is assumed to be related to the area within a hysteresis curve. The rate at which the hysteretic curve area is being swept out per time is given by:

$$T\frac{\dot{S}_{gen}}{m} = vM_{irr}\left|\frac{d\mu_0 H}{dt}\right| \tag{2-7}$$

or, solving for the entropy generation rate per unit mass:

$$\frac{\dot{S}_{gen}}{m} = \frac{vM_{irr}}{T}\left|\frac{d\mu_0 H}{dt}\right| \tag{2-8}$$

where v is the specific volume of the magnetic material, M_{irr} is the irreversible magnetization per unit volume, T is the temperature of the magnetic material, and $\frac{d\mu_0 H}{dt}$ is the rate of change of the applied magnetic field. The irreversible magnetization is a function that must be unambiguously positive and represents the deviation of the magnetization from its anhysteretic value. The irreversible magnetization must be a function of temperature and applied field as well as the minimum and maximum values of the applied field experienced by the material during each cycle. Assuming that the degree of hysteresis does not depend on the rate of the process, the total magnetization induced in the material (M) is the sum of the anhysteretic (M_{an}) and hysteretic (M_{irr}) terms:

$$\begin{aligned} M\left(T, \mu_0 H, \mu_0 H_{min}, \mu_0 H_{max}, \frac{d\mu_o H}{dt}\right) &= M_{an}\left(T, \mu_0 H\right) \\ &\quad - M_{irr}\left(T, \mu_0 H, \mu_0 H_{min}, \mu_0 H_{max}\right)\text{sign}\left(\frac{d\mu_o H}{dt}\right) \end{aligned} \tag{2-9}$$

Note that the sign function returns the sign of its argument and causes the irreversible magnetization to subtract from the anhysteretic magnetization during the time that the applied field is increasing and add to it when it is decreasing.

The value of M_{irr} must be equal to zero when the applied field reaches its minimum and maximum values:

$$\begin{aligned} M_{irr}\left(T,\mu_0 H=\mu_0 H_{min},\mu_0 H_{min},\mu_0 H_{max}\right)=0 \\ M_{irr}\left(T,\mu_0 H=\mu_0 H_{max},\mu_0 H_{min},\mu_0 H_{max}\right)=0 \end{aligned} \tag{2-10}$$

Note that the absolute value of the rate of change of the applied field is used in Eq. (2-8) in order to ensure that the entropy generation rate is unambiguously positive. Defining the entropy generation rate with an irreversible magnetization term permits the calculation of the entropy generation rate at any point along the *M-H* curve. Graphically, the irreversible magnetization can be thought of as a method of "fattening out" the *M-H* curve by adding or subtracting (depending on the direction of the rate of applied field change) it from the anhysteretic magnetization function. An example of a hysteresis curve that is defined using the irreversible magnetization function is shown in Figure 2-2.

The rate of change of specific entropy is again separated into its magnetic and temperature driven components, which yields:

$$\frac{ds}{dt}=\frac{c_{\mu_0 H}}{T}\left(\frac{dT}{dt}\right)+\left(\frac{\partial v M_{an}}{\partial T}\right)_{\mu_0 H}\left(\frac{d\mu_0 H}{dt}\right)=\frac{\dot{S}_{gen}}{m} \tag{2-11}$$

Note that the anhysteretic magnetization term, M_{an}, remains in Eq. (2-11) because the irreversibility associated with hysteresis is accounted for within the entropy generation term. By substituting Eq. (2-8) into Eq. (2-11):

$$\frac{c_{\mu_0 H}}{T}\left(\frac{dT}{dt}\right)+\left(\frac{\partial v M_{an}}{\partial T}\right)_{\mu_0 H}\left(\frac{d\mu_0 H}{dt}\right)=\frac{v M_{irr}}{T}\left|\frac{d\mu_0 H}{dt}\right| \tag{2-12}$$

which represents the final relation between temperature, applied field, irreversible magnetization, anhysteretic magnetization, and time for an adiabatic process.

2.2 Adiabatic Magnetization and Demagnetization with Hysteresis

The model of irreversible magnetization suggested in Section 1.1 is tested by using it to simulate a single piece of magnetic material that is exposed to an alternating magnetic field under adiabatic conditions. First the process is simulated with no hysteresis effects. Then the simulation is repeated with the addition of an irreversible magnetization term in order to simulate hysteresis.

In order to illustrate this approach, the simple Curie law equation of state for a paramagnetic material is used as the basis for the anhysteretic portion of the volume magnetization:

$$M_{an}\left(T,\mu_0 H\right)=\frac{C}{\mu_0}\frac{\mu_0 H}{T} \tag{2-13}$$

where C is the Curie constant. Substituting Eq. (2-13) into Eq. (2-9) leads to:

$$\begin{aligned} M\left(T,\mu_0 H,\mu_0 H_{min},\mu_0 H_{max},\frac{d\mu_0 H}{dt}\right)=&\frac{C}{\mu_0}\frac{\mu_0 H}{T}\\ &-M_{irr}\left(T,\mu_0 H,\mu_0 H_{min},\mu_0 H_{max}\right)\text{sign}\left(\frac{d\mu_0 H}{dt}\right)\end{aligned} \tag{2-14}$$

One requirement for the irreversible magnetization function is that it must be equal to zero at the minimum and maximum applied fields experienced by the material, as shown in Eq. (2-10). One possibility for M_{irr} is therefore:

$$M_{irr}\left(T,\mu_0 H,\mu_0 H_{min},\mu_0 H_{max}\right)=\Delta M\sin\left(\frac{\pi\left(\mu_0 H-\mu_0 H_{\min}\right)}{\mu_0 H_{\max}-\mu_0 H_{\min}}\right) \tag{2-15}$$

where ΔM is a constant that represents the maximum irreversible magnetization. Substituting Eq. (2-15) into Eq. (2-14) provides:

$$M\left(T,\mu_0 H,\mu_0 H_{min},\mu_0 H_{max},\frac{d\mu_0 H}{dt}\right)=\frac{C}{\mu_0}\frac{\mu_0 H}{T} -\Delta M\sin\left(\frac{\pi\left(\mu_0 H-\mu_0 H_{\min}\right)}{\mu_0 H_{\max}-\mu_0 H_{\min}}\right)\operatorname{sign}\left(\frac{d\mu_0 H}{dt}\right) \tag{2-16}$$

For the cases considered in this report, $\mu_o H_{\min} = 0$ and therefore the magnetization is described by:

$$M\left(T,\mu_0 H,\mu_0 H_{min},\mu_0 H_{max},\frac{d\mu_0 H}{dt}\right)=\frac{C}{\mu_0}\frac{\mu_0 H}{T}-\Delta M\sin\left(\frac{\pi\mu_0 H}{\mu_0 H_{\max}}\right)\operatorname{sign}\left(\frac{d\mu_0 H}{dt}\right) \tag{2-17}$$

Figure 2-1 shows the irreversible magnetization function given by Eq. (2-15) as a function of the applied magnetic field for various values of $v\Delta M$ with $\mu_0 H_{\max} = 2$ T. Note that it satisfies the constraints of Eq. (2-10) as it is zero at the minimum and maximum applied field.

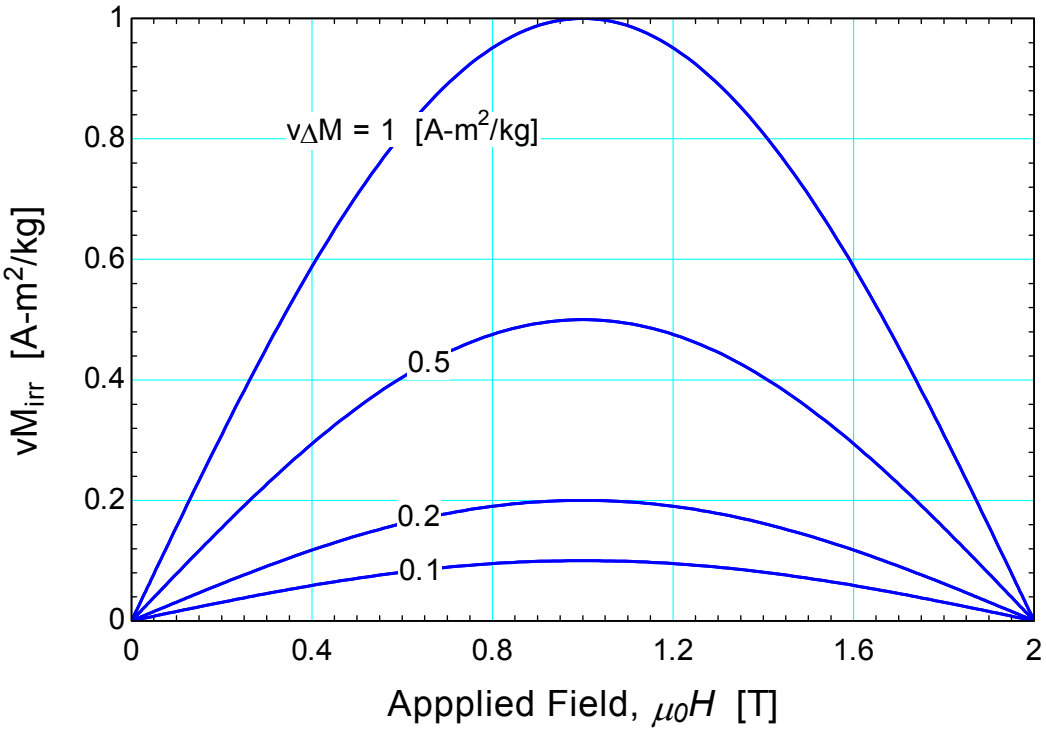

Figure 2-1. Irreversible magnetization function as a function of applied magnetic field for various values of $v\Delta M$ for the model considered.

For the magnetization-demagnetization adiabatic process, the material is exposed to an oscillating magnetic field that varies between zero and a maximum applied field, $\mu_0 H_{\max}$, in an assumed sinusoidal manner:

$$\mu_0 H(t) = \frac{\mu_0 H_{\max}}{2}\left(1 - \cos\left(\frac{2\pi t}{\tau}\right)\right) \tag{2-18}$$

where τ is the period of each cycle. The derivative of the applied field with respect to time is:

$$\frac{d\mu_0 H}{dt} = \frac{\mu_0 H_{\max}\pi}{\tau}\sin\left(\frac{2\pi t}{\tau}\right) \tag{2-19}$$

Equation (2-12) is solved for the temperature rate of change:

$$\frac{dT}{dt} = \frac{\left[\frac{vM_{irr}}{T}\left|\frac{d\mu_0 H}{dt}\right| - \left(\frac{\partial vM_{an}}{\partial T}\right)_{\mu_0 H}\left(\frac{d\mu_0 H}{dt}\right)\right]}{\frac{c_{\mu_0 H}}{T}} \tag{2-20}$$

Equation (2-15) is used to evaluate the first term in Eq. (2-20) and the Curie law, Eq. (2-13), is used to evaluate the second term:

$$\frac{dT}{dt} = \frac{\left[\frac{v\Delta M}{T}\sin\left(\frac{\pi\mu_0 H}{\mu_0 H_{\max}}\right)\operatorname{sign}\left(\frac{d\mu_0 H}{dt}\right)\left|\frac{d\mu_0 H}{dt}\right| + \frac{C}{\mu_0}\frac{v\mu_0 H}{T^2}\left(\frac{d\mu_0 H}{dt}\right)\right]}{\frac{c_{\mu_0 H}(\mu_0 H, T)}{T}} \tag{2-21}$$

or

$$\frac{dT}{dt} = \frac{v\Delta M}{c_{\mu_0 H}}\sin\left(\frac{\pi\mu_0 H}{\mu_0 H_{\max}}\right)\operatorname{sign}\left(\frac{d\mu_0 H}{dt}\right)\left|\frac{d\mu_0 H}{dt}\right| + \frac{C}{\mu_0}\frac{v\mu_0 H}{T c_{\mu_0 H}}\left(\frac{d\mu_0 H}{dt}\right) \tag{2-22}$$

Note that the ordinary differential equation has no simple closed form solution that would allow the temperature to be expressed explicitly in terms of time; therefore, numerical methods must be employed

to solve Eq. (2-22). The first-order Euler method can be employed, which approximates the temperature at the end of each time step according to:

$$T_{i+1} \approx T_i + \left(\frac{dT}{dt}\right)_i \Delta t \qquad i = 1 \ldots N \tag{2-23}$$

where N is the total number of time steps and Δt is a finite valued time step. This is an approximation using the first two terms of the Taylor expansion for T. For this approximation, the initial temperature must be known as an initial condition used to approximate the temperature at the first step forward in time. The single shot model was evaluated using the inputs listed in Table 2-1.

Table 2-1. Properties specified for magnetization-demagnetization model simulation

Variable	**Value**	**Variable**	**Value**
$\mu_0 H_{\max}$	2 *Tesla*	C/μ_0	273 $A-K/T-m$
$\mu_0 H_{\min}$	0 *Tesla*	τ	4 *s*
$c_{\mu_0 H=0}$	0.5 $J/kg-K$	ΔM	0.1 A/m
ρ	1 kg/m^3	$T(t=0)$	293 *K*

The values of the parameters used in Table 1 are arbitrary and were chosen in order to illustrate the impact of hysteresis in the model. The purpose of the simulation is to verify that the method described to add an irreversible magnetization term to the entropy balance equation is valid. Figure 2-2 illustrates the magnetization of the material as a function of applied field with the anhysteretic and hysteretic lines predicted by Eqs. (2-13) and (2-15), respectively, indicated. Note that the M_{irr} term essentially widens the curve by reducing the magnetization from the anhysteretic value as the field increases and increasing the magnetization from its anhysteretic value as the field is removed.

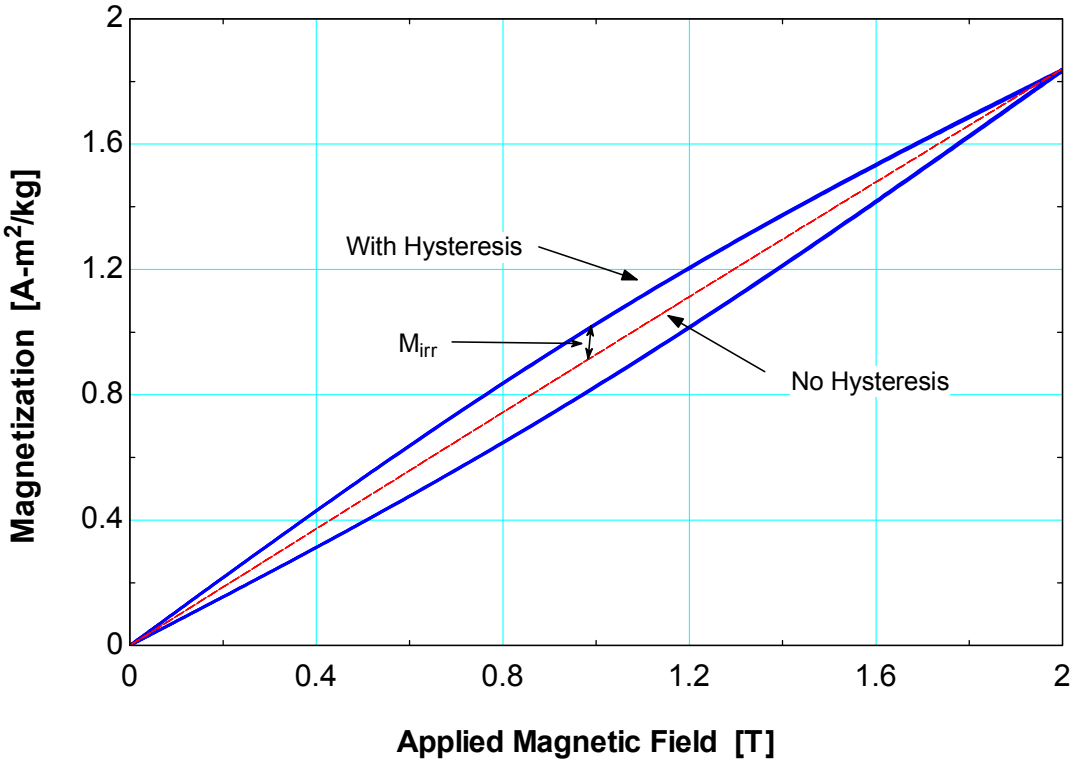

Figure 2-2. Magnetization as a function of applied magnetic field for a magnetic material predicted using Eqs. (2-13) and (2-15).

Figure 2-3 shows the temperature of the magnetic material as a function of time as it is exposed to the alternating applied magnetic field. For the case where it is modeled with no hysteresis ($\Delta M = 0$), the material experiences an isentropic temperature rise and then returns to its initial temperature as the field is removed. When hysteretic effects are included, the material experiences an adiabatic temperature change that is accompanied by an entropy increase due to the entropy generation. Therefore, when the field is removed the material does not return to its initial temperature because its entropy increases. Instead the temperature gradually rises as entropy increases during each successive cycle.

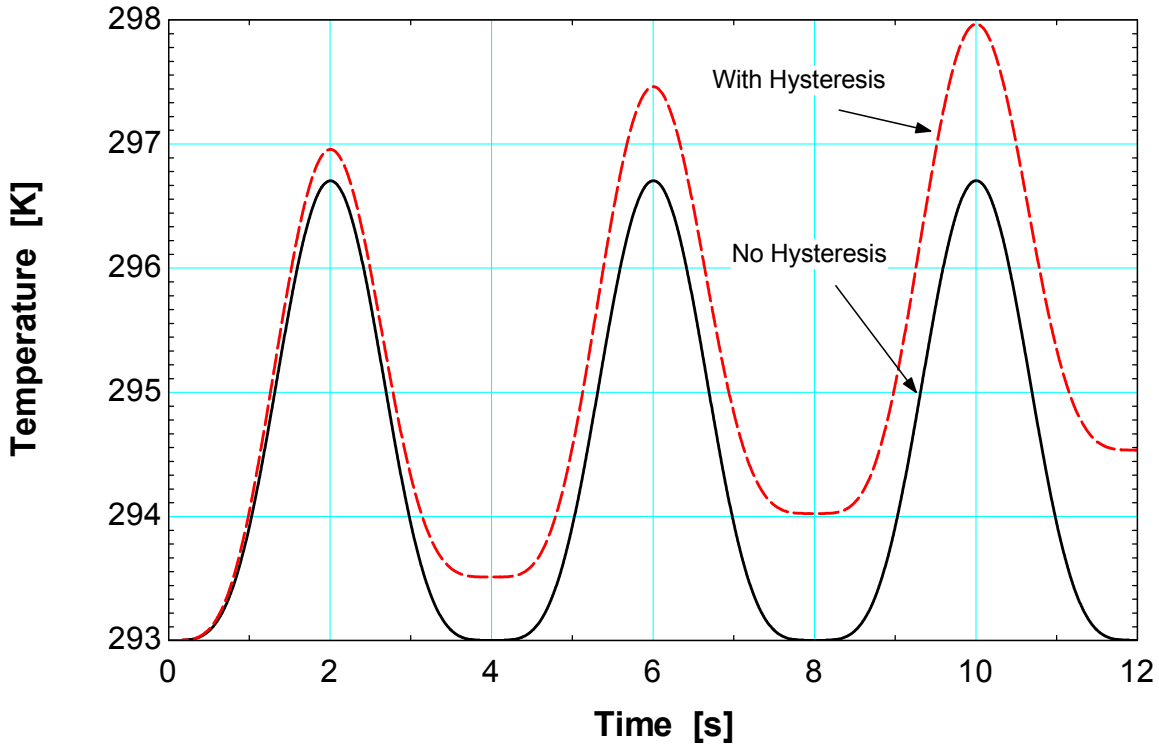

Figure 2-3. Temperature as a function of time for an adiabatic material exposed a sinusoidal applied field with and without hysteresis.

A temperature-specific entropy diagram for the adiabatic magnetization-demagnetization model is shown in Figure 2-4, with the isofield entropy lines shown. The results of the simulation with and without hysteresis are indicated.

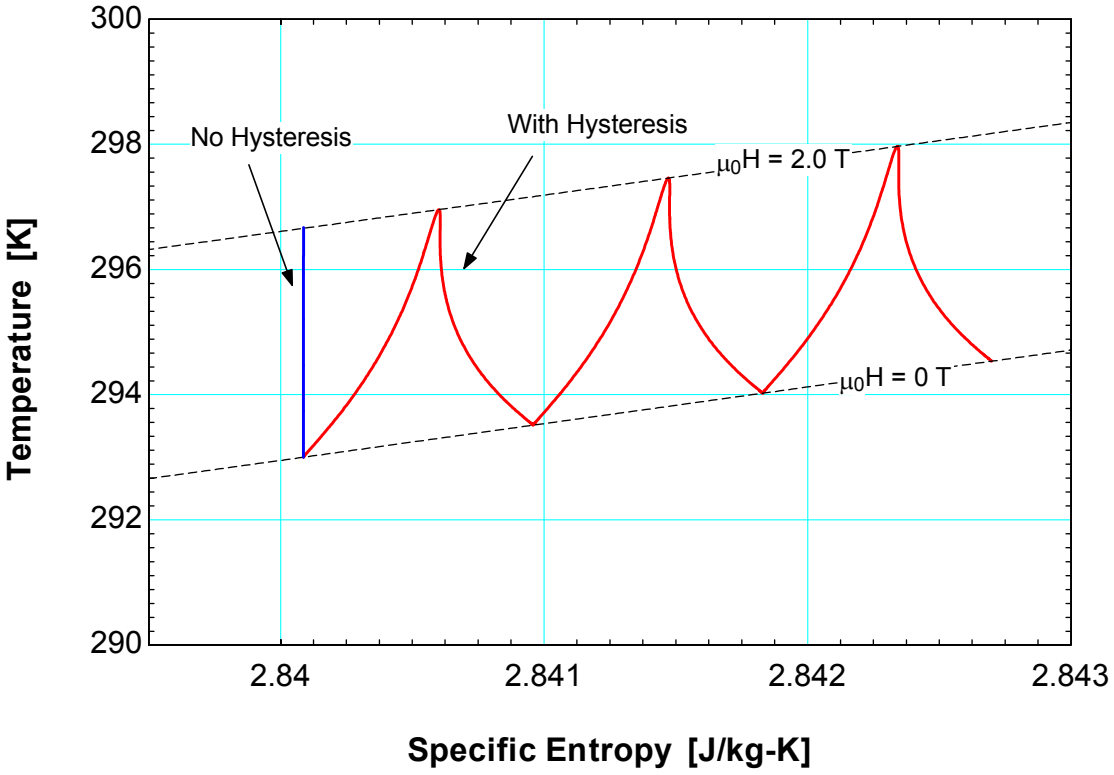

Figure 2-4. T-s diagram for single-shot model with and without hysteresis showing isofield entropy lines

The specific entropy values used to generate Figure 2-4 are calculated by eliminating the time derivatives and integrating Eq. (2-5) from a reference entropy (s_{ref}) at a reference applied field and temperature ($\mu_o H_{ref}$ and T_{ref}) to a final entropy (s) at an arbitrary applied field and temperature ($\mu_o H_f$ and T_f). The integration path proceeds first along a line of constant applied field ($\mu_o H_{ref}$) from T_{ref} to T_f:

$$s\left(T=T_f,\mu_0 H=\mu_0 H_{ref}\right)-s_{ref}=\int_{T_{ref}}^{T_f}\frac{c_{\mu_0 H=\mu_0 H_{ref}}}{T}dT=c_{\mu_0 H=\mu_0 H_{ref}}\ln\left(\frac{T_f}{T_{ref}}\right) \tag{2-24}$$

and then along a line of constant temperature (T_f) from the reference field $\mu_0 H_{ref}$ to $\mu_0 H_f$:

$$s\left(T=T_f,\mu_0 H_f\right)-s\left(T=T_f,\mu_0 H=\mu_0 H_{ref}\right)=\int_{\mu_0 H_{ref}}^{\mu_0 H_f}\left(\frac{\partial v M_{an}}{\partial T}\right)_{\mu_0 H,T=T_f}d\mu_0 H \tag{2-25}$$

where $c_{\mu_0 H=\mu_0 H_{ref}}$ is the constant field specific heat at $\mu_o H_{ref}$. Substituting Eq. (2-13) into Eq. (2-25) provides:

$$s\left(T=T_f,\mu_0 H_f\right)-s\left(T=T_f,\mu_0 H=\mu_0 H_{ref}\right)=-\int_{\mu_0 H_{ref}}^{\mu_0 H_f}\frac{C}{\mu_0}\frac{v\,\mu_o H}{T_f^2}\,d\,\mu_0 H=\frac{C}{\mu_0}\frac{v}{2T_f^2}\left(\mu_o H_{ref}^2-\mu_o H_f^2\right) \quad (2\text{-}26)$$

Adding Eqs. (2-25) and (2-26) together and defining $s_{ref} = 0$ at $T_{ref} = 1$ K and $\mu_o H_{ref} = 0$ provides:

$$s\left(T,\mu_0 H\right)=c_{\mu_0 H=0}\ln\left(T\right)-\frac{C}{\mu_0}\frac{v\left(\mu_o H\right)^2}{2T^2} \quad (2\text{-}27)$$

From Eq. (2-27), the constant field derivative of entropy with respect to temperature is:

$$\left(\frac{\partial s}{\partial T}\right)_{\mu_0 H}=\frac{c_{\mu_0 H}}{T}=\frac{c_{\mu_0 H=0}}{T}+\frac{C}{\mu_0}\frac{v\left(\mu_o H\right)^2}{T^3} \quad (2\text{-}28)$$

which shows that the constant field specific heat must be a function of temperature in order to agree with the Curie law equation of state:

$$c_{\mu_0 H}=c_{\mu_0 H=0}+\frac{C}{\mu_0}\frac{v\left(\mu_o H\right)^2}{T^2} \quad (2\text{-}29)$$

As the plot in Figure 2-4 indicates, the specific entropy remains constant for the case where there is no hysteresis. In the case where hysteresis is modeled, the entropy increases gradually as more cycles are completed, due to the entropy generation related to the irreversible magnetization term. The discontinuous slope in the entropy for the model with hysteresis is a consequence of the absolute value of the $\frac{d\,\mu_0 H}{dt}$ term in Eq. (2-8).

The entropy generation rate is plotted as a function of time in Figure 2-5 according to the relation given in Eq. (2-8). It reaches a minimum where the field is at either the maximum or minimum value, and it reaches a maximum where the irreversible magnetization is maximum (halfway between the minimum and maximum fields). This behavior is consistent with the idea that entropy generation is

related to the area of the hysteresis curve; Figure 2-2 shows that the differential area of the hysteresis curve approaches zero at $\mu_o H_{min}$ and $\mu_o H_{max}$. Figure 2-6 shows the entropy generation rate as a function of time over a larger range of times and with a larger maximum irreversible magnetization of $v\Delta M = 0.5\ \frac{A-m^2}{kg}$. The plot demonstrates that the entropy generation rate decreases steadily over time as the temperature of the material increases, which is a consequence of the entropy generation rate being inversely proportional to the material temperature per Eq. (2-8). The larger value of the maximum irreversible magnetization was chosen so that the behavior of the entropy generation rate as a function of time is obvious.

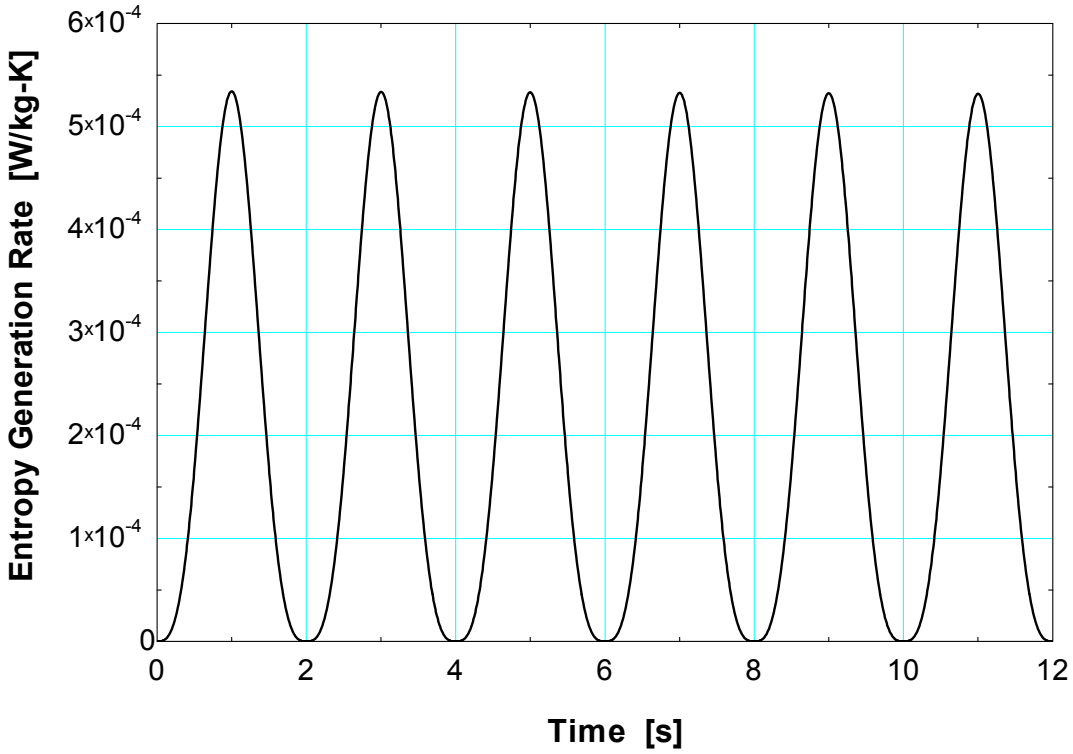

Figure 2-5. Entropy generation as a function of time as a result of hysteresis in the single-shot model. Note that the time scale is not large enough to show decrease in entropy generation rate with time.

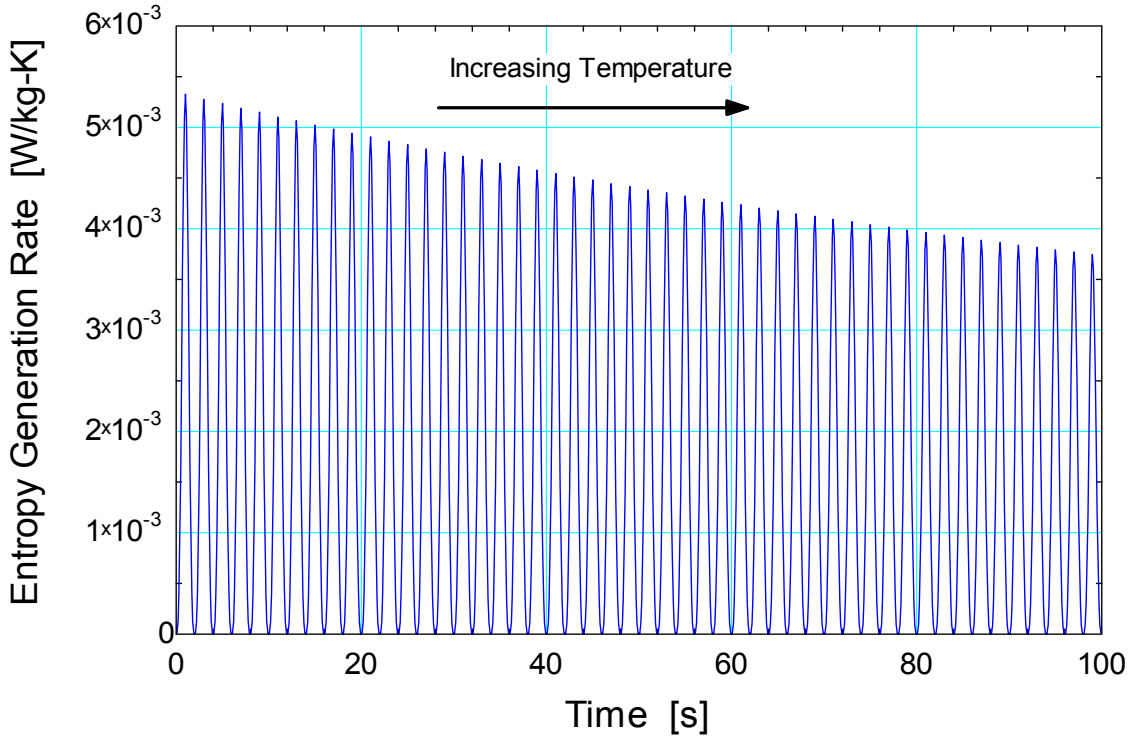

Figure 2-6. Entropy generation rate as a function of time with $v\Delta M$ = 0.5 [A-m^2/kg] to show steady decline in rate over time.

The total entropy generated should be equal to the difference in entropy between the initial and final states of the process since this is an adiabatic, closed process. In other words the area underneath the curve in Figure 2-5 should be equal to the difference between final entropy and initial entropy for the process with hysteresis shown in Figure 2-4. Mathematically, this can be stated in an integral:

$$s_f - s_i = \int_0^{t_f} \frac{\dot{S}_{gen}}{m} dt \tag{2-30}$$

where $t_f = 12$ sec in this case. By utilizing the trapezoidal method for integration, the integral in (2-30) yields a value of 0.0026 $^{J}/_{\text{kg-K}}$, which is exactly the same value of $s_f - s_i$. The MATLAB code used to generate these plots and data is included in Appendix A.

Also, the area of the hysteresis loop should be equivalent to the area swept by the irreversible magnetization function. Since the irreversible magnetization function is always positive and symmetrical, the total area swept by the irreversible magnetization function is equal to:

$$Area = T\frac{S_{gen}}{m} = \oint_{cycle} vM_{irr}\left|d\mu_0 H\right| = 2\int_0^{\mu_0 H_{\max}} vM_{irr}\, d\mu_0 H \tag{2-31}$$

This area is also equal to the area of the hysteresis loop for one complete cycle:

$$Area = T\frac{S_{gen}}{m} = \oint_{cycle} vM\, d\mu_0 H \tag{2-32}$$

By numerical integration of Eq. (2-31) using the trapezoidal rule function in MATLAB, the area is found to be $0.2546\ {}^{J}/_{kg}$ and by numerically integrating Eq. (2-32) in the same fashion, the area is found to be $0.2535\ {}^{J}/_{kg}$. This is a 0.43% difference, which is attributable to numerical estimation error. Figure 2-7 is a plot of the exergy loss per cycle as a function of the maximum irreversible magnetization constant ΔM. The solid line shows the energy loss calculated via Eq. (2-32) and the data points show the calculation via Eq. (2-31). There is very little difference in the values, and therefore the entropy generation is directly related to the area under the *M-H* curve for this model.

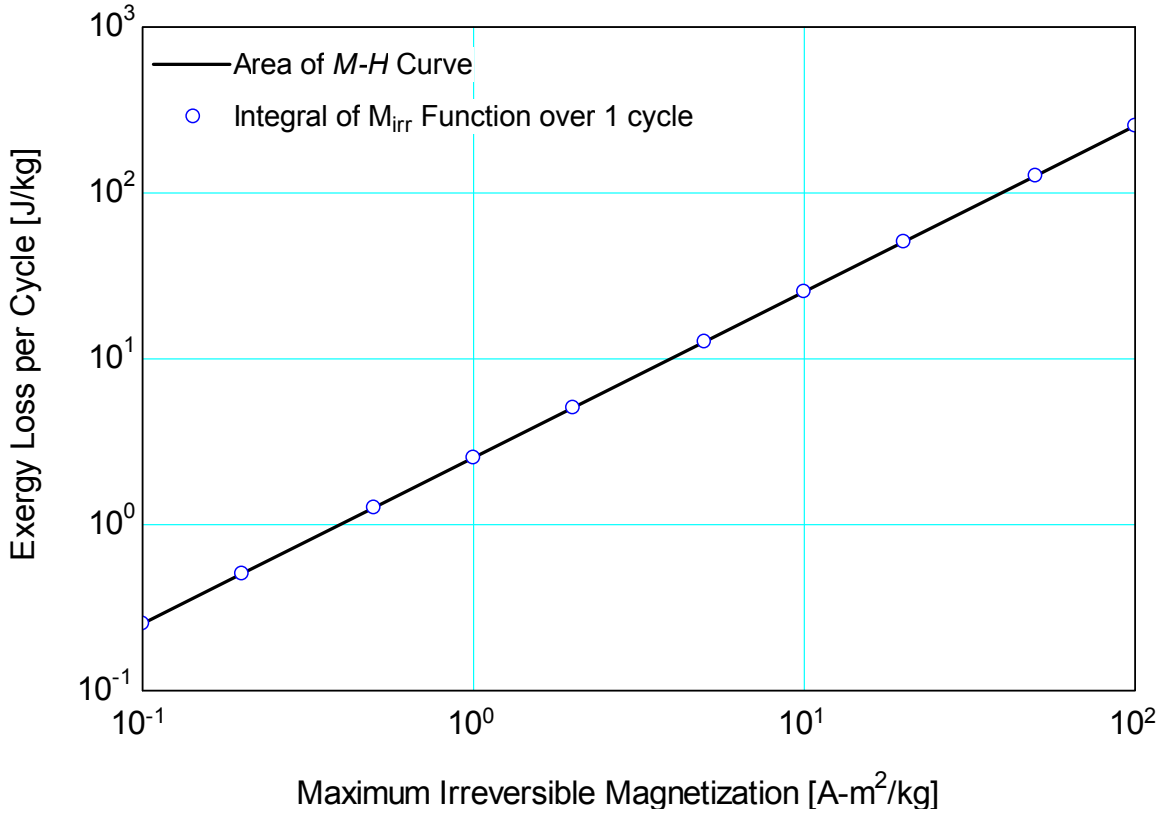

Figure 2-7. Comparison of calculation of exergy loss for various values of ΔM

2.3 Carnot Cycle Analysis

As an extension to the investigation of hysteretic effects on a single shot adiabatic magnetization/demagnetization model, a magnetic Carnot refrigeration cycle (or ADR cycle) is modeled to investigate the deterioration in its performance that occurs due to the entropy generation that arises from hysteresis. The magnetic Carnot cycle consists of four distinct processes listed as follows:

1. Adiabatic magnetization
2. Isothermal heat rejection
3. Adiabatic demagnetization
4. Isothermal heat addition

The same entropy generation term introduced in Eq. (2-8) is added to the entropy balance for the magnetization and demagnetization processes in order to simulate the irreversibility associated with magnetic hysteresis.

2.3.1 Governing Equations

Adiabatic magnetization and demagnetization

By performing an entropy balance on the magnetic material of interest, the following equation is obtained in the same manner as the single-shot model:

$$\frac{dS}{dt} = \dot{S}_{gen} \tag{2-33}$$

which can be rewritten on a mass specific basis in terms of the mass of the magnetic material *m*:

$$\frac{ds}{dt} = \frac{\dot{S}_{gen}}{m} \tag{2-34}$$

The derivative in Equation 34 can be expressed in terms of its magnetic and thermal contributions to entropy:

$$\frac{ds}{dt} = \frac{c_{\mu_0 H}}{T}\left(\frac{dT}{dt}\right) + \left(\frac{\partial v M_{an}}{\partial T}\right)_{\mu_0 H}\left(\frac{d\mu_0 H}{dt}\right) = \frac{\dot{S}_{gen}}{m} \tag{2-35}$$

which is identical to Eq. (2-11) in Section 2.1.2 . Similarly, the entropy generation can be expressed according to Eq. (2-8):

$$\frac{c_{\mu_0 H}}{T}\left(\frac{dT}{dt}\right) + \left(\frac{\partial v M_{an}}{\partial T}\right)_{\mu_0 H}\left(\frac{d\mu_0 H}{dt}\right) = \frac{v M_{irr}}{T}\left|\frac{d\mu_0 H}{dt}\right| \tag{2-36}$$

which is identical to Eq. (2-12). These equations are valid for both adiabatic magnetization and demagnetization because the processes are thermodynamically equivalent.

Isothermal heat rejection and addition

By performing an entropy balance on the magnetic material of interest:

$$\frac{dS}{dt} = \dot{S}_{gen} + \frac{\dot{Q}}{T} \tag{2-37}$$

and by dividing by the mass of the magnetic material *m*:

$$\frac{ds}{dt} = \frac{\dot{S}_{gen}}{m} + \frac{\dot{q}}{T} \tag{2-38}$$

where $\dot{q}$ is the rate of heat transfer per unit mass of magnetic material and *T* is the temperature of the material. Again by expanding the rate of change in entropy into its magnetic and thermal terms provides:

$$\frac{c_{\mu_0 H}}{T}\left(\frac{dT}{dt}\right) + \left(\frac{\partial v M_{an}}{\partial T}\right)_{\mu_0 H}\left(\frac{d\mu_0 H}{dt}\right) = \frac{\dot{S}_{gen}}{m} + \frac{\dot{q}}{T} \tag{2-39}$$

Since processes 2 and 4 are isothermal, the change in temperature with respect to time $\frac{dT}{dt}$ is equal to zero. Applying this relation and substituting the expression for the entropy generation from Eq. (2-8) leads to:

$$\left(\frac{\partial v M_{an}}{\partial T}\right)_{\mu_0 H}\left(\frac{d\mu_0 H}{dt}\right) = \frac{v M_{irr}}{T}\left|\frac{d\mu_0 H}{dt}\right| + \frac{\dot{q}}{T} \tag{2-40}$$

By rearranging this equation, the rate of heat transfer per unit mass of magnetic material can be recovered for both the heat rejection process ($\dot{q}_H$) and heat absorption process ($\dot{q}_C$). For the heat rejection to the hot thermal reservoir:

$$\dot{q}_H = T_H\left[\left(\frac{\partial v M_{an}}{\partial T}\right)_{\mu_0 H}\left(\frac{d\mu_0 H}{dt}\right) - \frac{v M_{irr}}{T_H}\left|\frac{d\mu_0 H}{dt}\right|\right] \tag{2-41}$$

and for the heat absorption from the cold thermal reservoir:

$$\dot{q}_C = T_C \left[\left(\frac{\partial v M_{an}}{\partial T} \right)_{\mu_0 H} \left(\frac{d\mu_0 H}{dt} \right) - \frac{v M_{irr}}{T_C} \left| \frac{d\mu_0 H}{dt} \right| \right] \tag{2-42}$$

It is important to note that the positive direction for heat flow is defined to be *into* the material, and thus $\dot{q}_H$ is a negative quantity and $\dot{q}_C$ is a positive quantity for this model.

2.3.2 Model Parameters

For this model, the equation of state relating the magnetization and applied magnetic field that is used is the Curie law (the same equation of state that was used previously in the single-shot model):

$$M_{an} = \frac{C}{\mu_0} \frac{\mu_0 H}{T} \tag{2-43}$$

The irreversible magnetization will again be applied to describe the effects of hysteresis on the magnetization of the material:

$$M = M_{an} - M_{irr} \operatorname{sign}\left(\frac{d\mu_0 H}{dt} \right) \tag{2-44}$$

For simplicity, M_{irr} can be described by a sinusoidal relationship described in Eq. (2-15) which is positive for all values of applied field except at the minimum and maximum applied fields, where it is equal to zero. In this simple model the minimum applied field will be equal to zero, $\mu_0 H_{\min} = 0$, which yields and equation for the magnetization *M* of the form:

$$M = \frac{C}{\mu_0} \frac{\mu_0 H}{T} - \Delta M \sin\left(\pi \frac{\mu_0 H}{\mu_0 H_{\max}} \right) \operatorname{sign}\left(\frac{d\mu_0 H}{dt} \right) \tag{2-45}$$

Substituting the equation of state in (2-43) into Eq. (2-36) and eliminating the time derivatives provides:

$$\frac{c_{\mu_0 H}}{T} dT - \frac{C}{\mu_0} \frac{v \mu_0 H}{T^2} d\mu_0 H = \frac{v M_{irr}}{T} \left| d\mu_0 H \right| \tag{2-46}$$

Doing the same for equations (2-41) and (2-42) respectively:

$$\delta q_H = T_H \left[\frac{C}{\mu_0} \frac{v \mu_0 H}{T_H^{\,2}} d\mu_0 H - \frac{v M_{irr}}{T_H} \left| d\mu_0 H \right| \right] \tag{2-47}$$

$$\delta q_C = T_C \left[\frac{C}{\mu_0} \frac{v \mu_0 H}{T_C^{\,2}} d\mu_0 H - \frac{v M_{irr}}{T_C} \left| d\mu_0 H \right| \right] \tag{2-48}$$

where δq_H and δq_C are the differential heat transfers per unit mass of magnetic material to the hot and cold reservoirs, respectively.

2.3.3 Model Results

Table 2-2 is a summary of the input parameters used in this model. These inputs are arbitrary and are chosen to be realistic; however, they are not specific to any magnetic refrigerant material.

Table 2-2. Properties specified for Carnot cycle model simulation

Variable	Value	Variable	Value
$\mu_0 H_{\max}$	2 *Tesla*	C	20 K
$\mu_0 H_{\min}$	0 *Tesla*	τ	4 s
$c_{\mu_0 H=0}$	0.5 $^{J}/_{kg-K}$	T_H	280 K
ρ	7900 $^{kg}/_{m^3}$	T_C	273 K

In this model, each of the equations were evaluated numerically using a second order Runge-Kutta method. This method solves for a point one step forward in magnetic field by using the slope of the function evaluated halfway between the current point and the point 1 step forward, multiplying that slope by the step size, and adding it to the value of the current point. Mathematically, this process appears as:

$$\left[f(\mu_0 H) \right]_{i+1} = \left[f(\mu_0 H) \right]_i + \Delta\mu_0 H \frac{df}{d\mu_0 H} \left(\mu_0 H_i + \tfrac{\Delta\mu_0 H}{2}, f_i + \tfrac{\Delta\mu_0 H}{2} \tfrac{df}{d\mu_0 H} (\mu_0 H_i, f_i) \right) \quad i = 1..N \tag{2-49}$$

where $\Delta\mu_0 H$ is a finite step size for the magnetic field and *i* is the current step. The function $f(\mu_0 H)$ can be any function that has a known derivative with respect to magnetic field and a known initial condition. For this problem, *f* can be the temperature *T*, specific entropy *s*, or heat transfer q for the isothermal heat addition/rejection processes. The entropy is defined using the same method described in Eqs. (2-24)-(2-27), where a reference field is set at 0 Tesla and a reference temperature is 1 K.

By applying the equations for adiabatic magnetization or demagnetization outlined in Section 2.3.1 the state of the system can be described. Writing numerical estimates explicitly based on Eq. (2-49), the temperature during the adiabatic magnetization or demagnetization at any node step in magnetic field *i* can be expressed as:

$$T_{i+1} \cong T_i + \frac{v M_{irr,mid,i}}{\left(c_{\mu_0 H}\right)_{mid,i}} \left|\Delta\mu_0 H\right| + \frac{C}{\mu_0} \frac{v\left(\mu_0 H\right)_{mid,i}}{\left(c_{\mu_0 H}\right)_{mid,i} T_{mid,i}} \Delta\mu_0 H \quad i = 1..N \tag{2-50}$$

where $\left(\mu_0 H\right)_{mid}$ and T_{mid} are evaluated at the midpoint between the steps *i* and $i+1$. Note that the irreversible magnetization function is also evaluated at $\left(\mu_0 H\right)_{mid}$. The midpoint applied magnetic field is:

$$\left(\mu_0 H\right)_{mid,i} = \mu_0 H_i + \tfrac{\Delta\mu_0 H}{2} \tag{2-51}$$

and midpoint temperature:

$$T_{mid,i} \cong T_i + \frac{v M_{irr,i}}{\left(c_{\mu_0 H}\right)_i} \left|\tfrac{\Delta\mu_0 H}{2}\right| + \frac{C}{\mu_0} \frac{v\left(\mu_0 H\right)_i}{\left(c_{\mu_0 H}\right)_i T_i} \tfrac{\Delta\mu_0 H}{2} \tag{2-52}$$

The constant field specific heat is a function of the temperature and applied magnetic field as well:

$$\left(c_{\mu_0 H}\right)_{mid,i} = c_{\mu_0 H=0} + \frac{C}{\mu_0} \frac{v\left(\mu_o H\right)^2_{mid,i}}{T^2_{mid,i}} \tag{2-53}$$

The irreversible magnetization is described in terms of the applied magnetic field for this problem by:

$$M_{irr,i} = \Delta M \sin\left(\pi \frac{\mu_0 H_i}{\mu_0 H_{\max}}\right)$$
$$M_{irr,mid,i} = \Delta M \sin\left(\pi \frac{\mu_0 H_i + \frac{\Delta\mu_0 H}{2}}{\mu_0 H_{\max}}\right) \tag{2-54}$$

For the entropy calculation, the midpoint temperature is also used:

$$s_{i+1} = s_i + \frac{v M_{irr,mid,i}}{T_{mid,i}} \left|\Delta\mu_0 H\right| \quad i = 1..N \tag{2-55}$$

Note that in these equations, $\Delta\mu_0 H$ is positive for magnetization and negative for demagnetization.

The isothermal heat addition/rejection processes are treated with a different set of equations (described in Section 2.3.1) and therefore must be solved separately. Since the temperature at any time is known, it does not have to be determined numerically: it is T_H for the heat rejection process and T_C for the heat addition process. However, since the magnetic field is not constant during these processes, the entropy changes according to:

$$s_{i+1} = s_i - \frac{C}{\mu_0} \frac{v \mu_0 H_{mid,i}}{T_H^{\,2}} \Delta\mu_0 H \tag{2-56}$$

$$s_{i+1} = s_i - \frac{C}{\mu_0} \frac{v \mu_0 H_{mid,i}}{T_C^{\,2}} \Delta\mu_0 H \tag{2-57}$$

and the total amount of heat transferred up to node *i* is expressed as follows:

$$q_{i+1} = q_i - \frac{C}{\mu_0} \frac{v \mu_0 H_{mid,i}}{T_H} \Delta\mu_0 H - v M_{irr,mid,i} \left|\Delta\mu_0 H\right| \tag{2-58}$$

$$q_{i+1} = q_i - \frac{C}{\mu_0} \frac{v \mu_0 H_{mid,i}}{T_C} \Delta\mu_0 H - v M_{irr,mid,i} \left|\Delta\mu_0 H\right| \tag{2-59}$$

In the previous equations (2-56)-(2-59), the temperature is the temperature of the thermal sink (T_H for heat rejection and T_C for heat addition). Again it should be noted that the magnetic field step $\Delta\mu_0 H$ is positive for isothermal heat rejection and negative for heat addition..

These equations are evaluated numerically (using the MATLAB code included in Appendix A) and the resulting Carnot cycles are plotted on a *T*-*s* diagram. Figures 2-8, 2-9 and 2-10 show the cycle plotted on a *T*-*s* diagram for $v\Delta M$ = 0, 0.5, and 5 $\frac{A-m^2}{kg}$, respectively, with pertinent isofield entropy lines drawn. The hot and cold reservoirs are 280 K and 273 K respectively for each plot. These diagrams also show the numerical result for entropy as a function of temperature obtained from Eqs. (2-55) and (2-56) or (2-57) as compared to the analytical result obtained from evaluating Eq. (2-27). As these plots illustrate, there is nearly perfect agreement between the numerical results to the analytical results, which verifies the numerical calculations. Also, by examining the plots, it is evident that as the irreversible magnetization is increased, the adiabatic magnetization and demagnetization processes have a characteristic curvature (seen in Figure 2-10) in the direction of increasing entropy. This behavior is a direct result of entropy generation and has a significant effect on the performance of the refrigeration cycle.

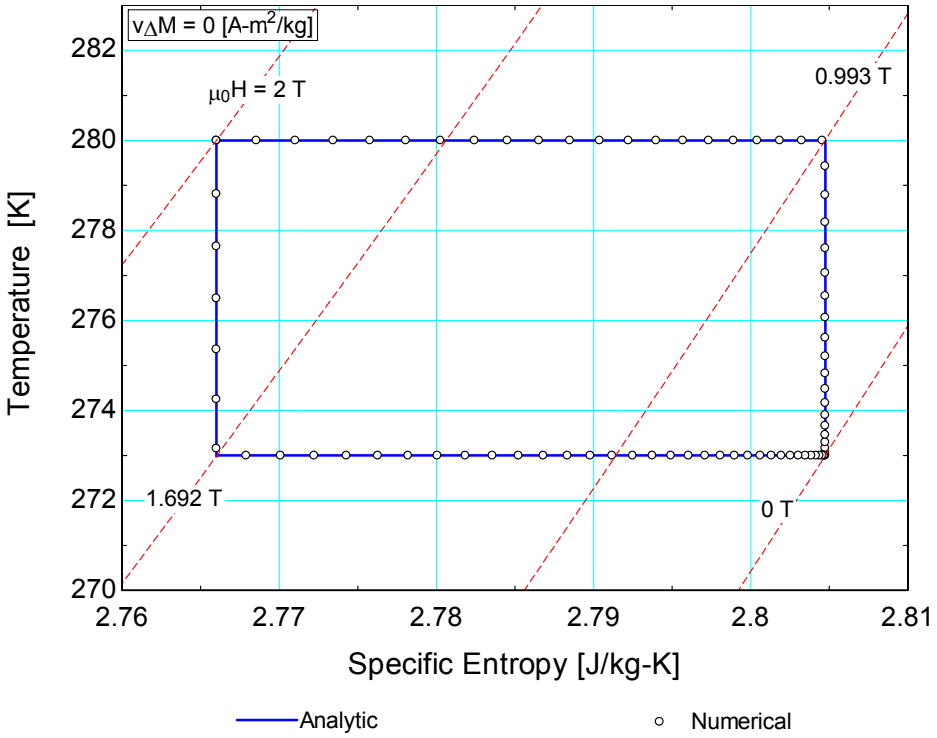

Figure 2-8. *T-s* diagram for Carnot cycle operating between T_H = 280 K and T_C = 273 K with ΔM = 0 A-m^2/kg and isofield entropy lines shown

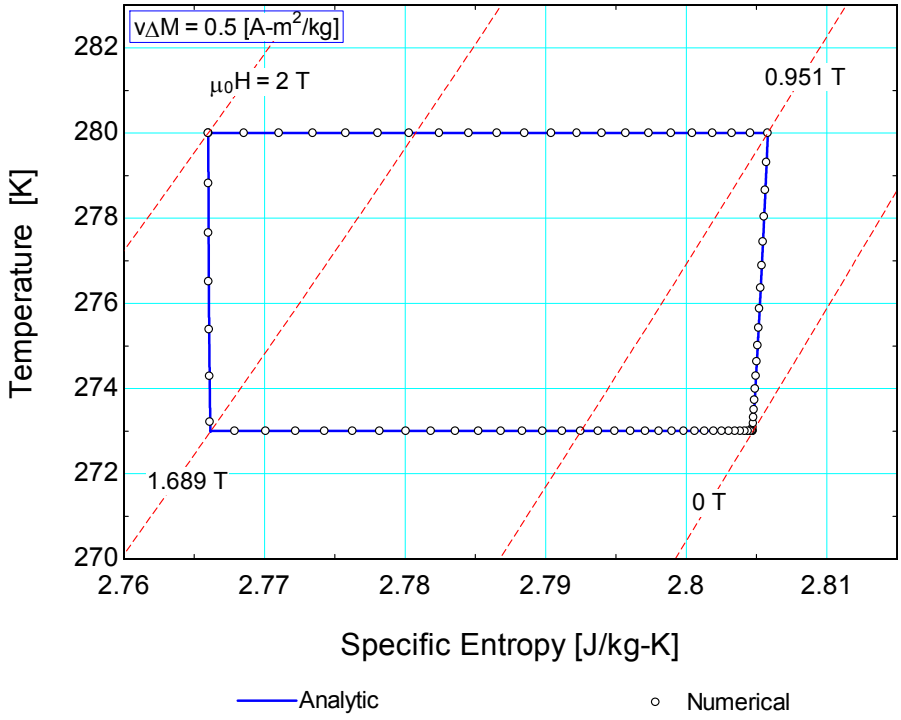

Figure 2-9. *T-s* diagram for Carnot cycle operating between T_H = 280 K and T_C = 273 K with ΔM = 0.5 A-m^2/kg and isofield entropy lines shown

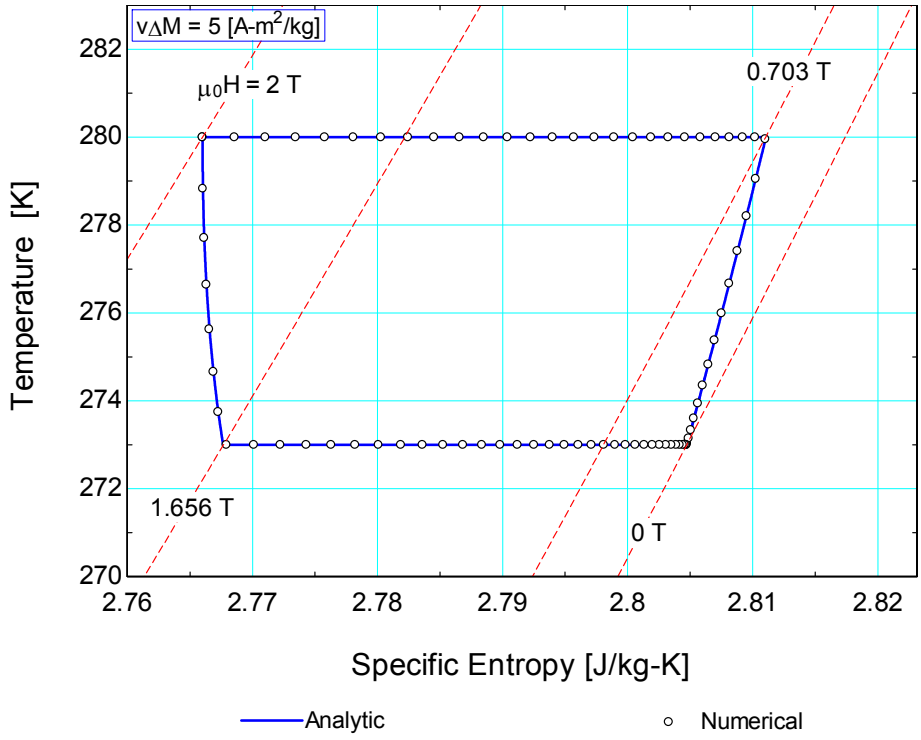

Figure 2-10. *T-s* diagram for Carnot cycle operating between T_H = 280 K and T_C = 273 K with vΔM = 5 A-m²/kg

Figure 2-11 shows the coefficient of performance as a function of the maximum irreversible magnetization $v\Delta M$ for the magnetic Carnot cycle presented in Figure 2-8, Figure 2-9, and Figure 2-10. The *COP* decreases sharply with increasing maximum irreversible magnetization, with the Carnot *COP* occurring where $v\Delta M = 0$. Such a sharp decline in *COP* relative to a small increase in $v\Delta M$ suggests that the performance of a magnetic refrigerator is adversely affected by even a small amount of hysteresis that occurs in the material. However, magnetic materials that exhibit hysteresis also exhibit larger adiabatic temperature changes of magnetization, which may offset the negative effect of hysteresis and the characteristics of an AMRR cycle may be substantially different than this Carnot cycle.

Figure 2-12 shows the coefficient of performance of a Carnot refrigerator with hysteresis as a function of the refrigeration temperature (T_C) for various values of $v\Delta M$ with the hot reservoir held fixed at $T_H = 293$ K. Like Figure 2-11, it shows that the *COP* decreases as $v\Delta M$ increases for all refrigeration temperatures. Also, it indicates that as the temperature difference between the hot and cold

thermal reservoirs increases, the relative impact of increasing $v\Delta M$ on the *COP* remains approximately the same. For example, the *COP* with $v\Delta M = 0.2\ \frac{A-m^2}{kg}$ is approximately $\frac{1}{3}$ the value of the *COP* with $v\Delta M = 0\ \frac{A-m^2}{kg}$ for all values of T_C.

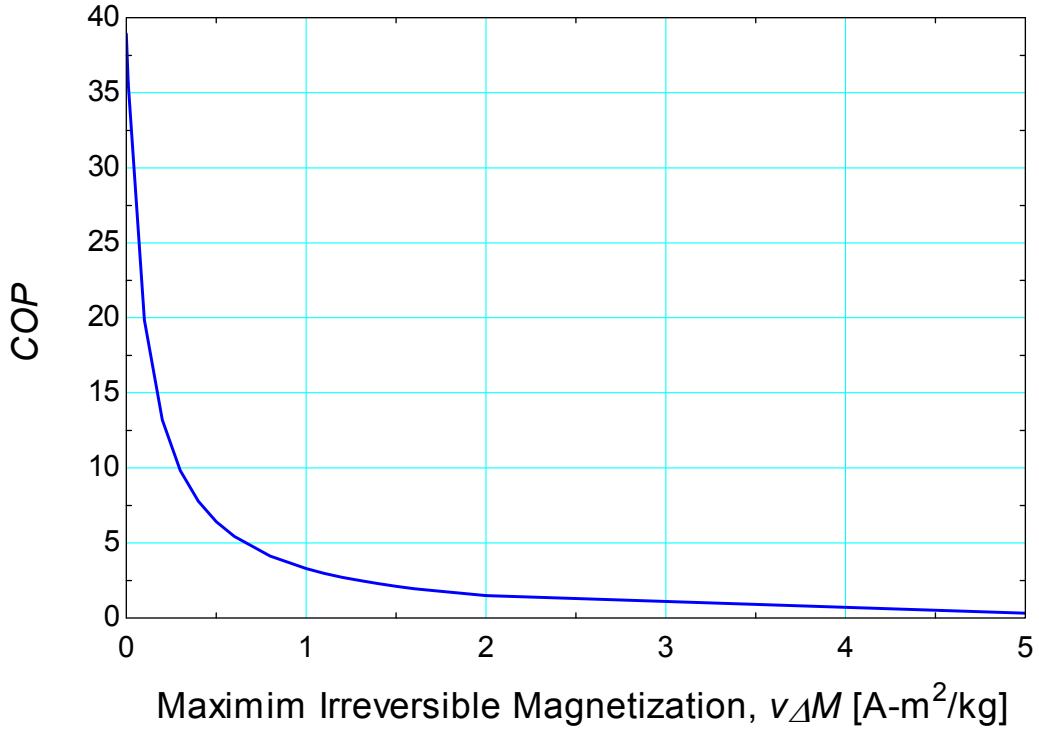

Figure 2-11. COP as a function of the maximum irreversible magnetization for magnetic Carnot cycle with T_H = 280 K and T_C = 273 K

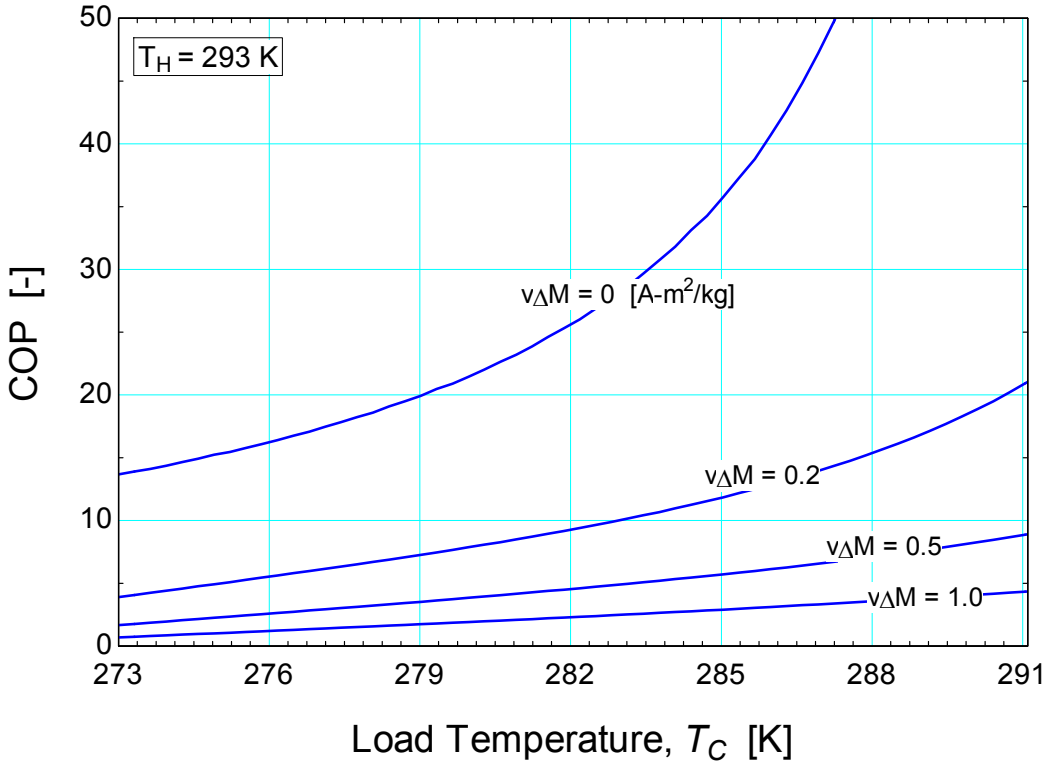

Figure 2-12. COP as a function of the load temperature (T_C) for various values of the maximum irreversible magnetization and T_H = 293 K

Figure 2-13 illustrates the refrigeration capacity per mass of a Carnot refrigerator with hysteresis as a function of the refrigerator temperature (T_C) for various values of ΔM with the hot reservoir held fixed at $T_H = 293$ K. Like the *COP*, the refrigeration capacity decreases with increasing ΔM for all T_C.

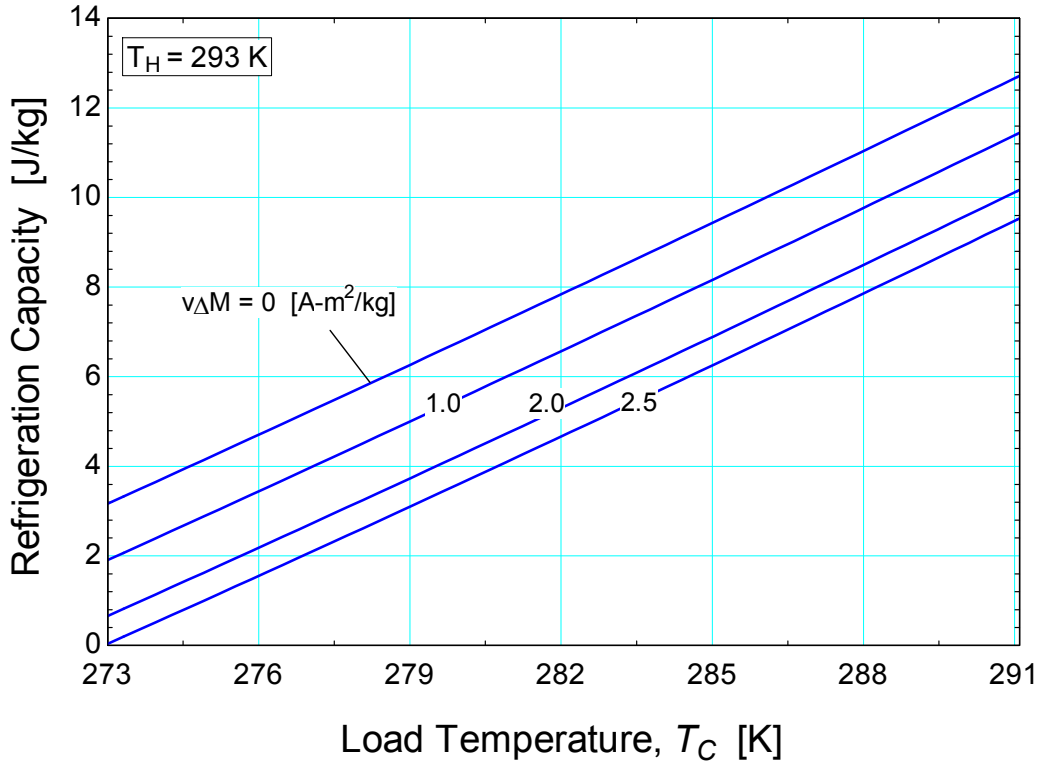

Figure 2-13. Refrigeration capacity per mass as a function of the load temperature (T_C) for various values of the maximum irreversible magnetization and T_H = 293 K

REFERENCES

1. Bertotti, G., *Hysteresis in magnetism : for physicists, materials scientists, and engineers*. 1998, San Diego, CA: Academic Press. 558.

2. Jiles, D.C. and D.L. Atherton, *Theory of ferromagnetic hysteresis.* Journal of Magnetism and Magnetic Materials, 1986. **61**(1-2): p. 48-60.

3. Nellis, G., *Stirling/Magnetic Cryocooler*, in *Department of Mechanical Engineering*. 1997, Massachusettes Institute of Technology: Cambridge, MA. p. 198.

Chapter 3 NUMERICAL MODEL DESCRIPTION

The numerical model used in this this thesis is described by Engelbrecht (2004, 2008) with modifications to account for magnetic hysteresis in the regenerator energy balance equations [1, 2]. The modified MATLAB code for the model is included in Appendix C. Engelbrecht (2008) provides a detailed description of the AMR model used in this thesis, and outlines the governing heat transfer fluid energy equations as well as Nusselt number, pressure drop, and heat transfer fluid property correlations used in the model. Corrections for internal temperature gradients that exist in a packed sphere regenerator are also discussed in depth. This chapter focuses on the modification of the regenerator magnetocaloric material governing energy equations presented by Engelbrecht (2008) to account for magnetic hysteresis.

3.1 Model Input Parameters

Figure 3-1 is a conceptual schematic of the one-dimensional AMRR regenerator bed model with important model input parameters shown. The model requires input parameters that define the heat transfer fluid, the magnetic regenerator material, the regenerator geometry, and the applied magnetic field.

The heat transfer fluid properties required by the model are the fluid specific heat capacity (c_f), density (ρ_f), thermal conductivity (k_f), and viscosity (μ_f). The temperatures of the fluid hot (T_H) and cold (T_C) reservoirs must also be specified, and are assumed to be constant. The time-dependent mass flow ($\dot{m}$) profile of the heat transfer fluid must also be defined, and should be based on the profile of the applied magnetic field ($\mu_o H$), which also must be specified in space (x) and time (t). A positive mass flow rate indicates flow from the hot to cold reservoir and a negative mass flow rate flows from the cold to hot reservoir. The heat transfer fluid is assumed to be incompressible and the flow is assumed to be perfectly distributed, meaning there is no spatial variation in the flow.

The magnetocaloric material properties required by the model are the regenerator material thermal conductivity (k_r), partial derivative of entropy with applied field at constant temperature $\left(\frac{\partial s_r}{\partial \mu_o H}\right)_T$, constant

field specific heat capacity ($c_{\mu_o H}$), and density (ρ_f). Also, if the bed is layered, the model requires a spatially-dependent Curie temperature (T_{Curie}) input. The regenerator geometry is specified by the cross-sectional area (A_c), bed length (L), volume specific particle surface area (a_s), particle hydraulic diameter (d_h), and bed porosity (ε). A Nusselt number dependent on the regenerator geometry, Reynolds number of the flow (Re_f), and Prandtl number of the fluid (Pr_f) is required. Likewise, a friction factor (f_f) that is dependent on the regenerator geometry and the Reynolds number of the fluid flow is required. Finally, an effective thermal conductivity of the regenerator matrix is specified (k_{eff}) that depends on the thermal conductivity of the fluid, the thermal conductivity of the magnetocaloric material, the regenerator geometry, the Reynolds number of the fluid flow, and the Prandtl number of the fluid.

The outputs of the model are the regenerator material (T_r) and heat transfer fluid (T_f) temperature distributions as a function of regenerator position (x) and cycle time (t). These temperature distributions are used along with the material property data to calculate performance parameters that characterize the system, such as refrigeration capacity ($\dot{Q}_{ref}$) and the system coefficient of performance (COP).

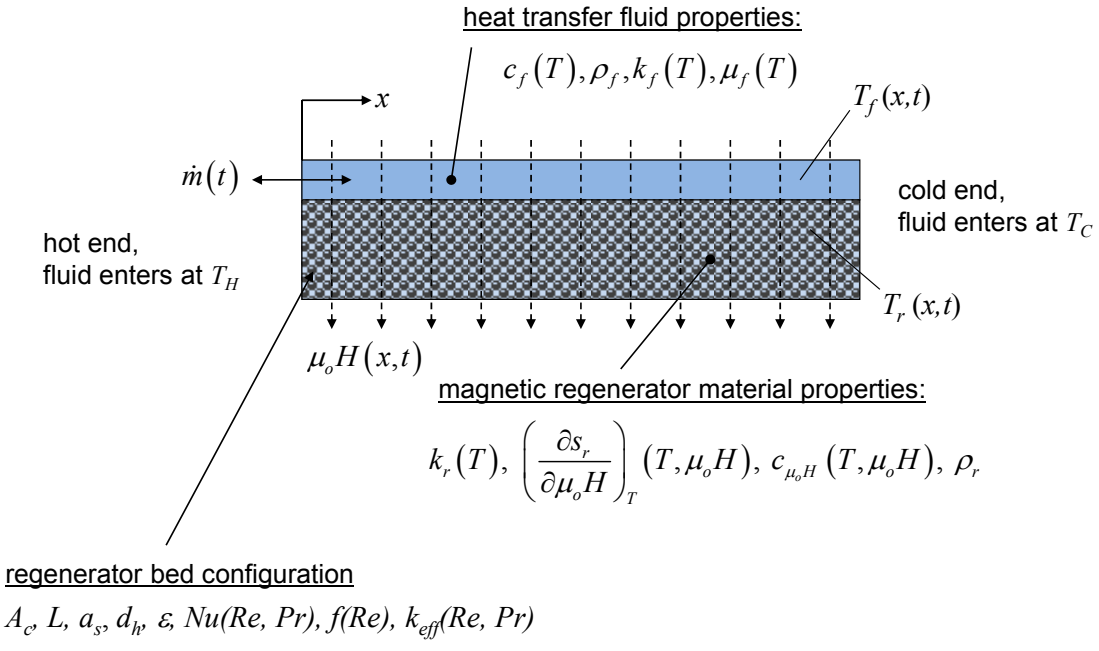

Figure 3-1. Conceptual schematic of the one-dimensional regenerator bed showing heat transfer fluid, magnetocaloric regenerator material, and bed geometry input parameters.

The coefficient of performance (*COP*) used in this thesis is defined as:

$$COP = \frac{\left|Q_{ref}\right|}{\left|W_{pump}\right| + \left|W_{motor}\right|} \tag{3-1}$$

where Q_{ref} is the refrigeration load, W_{pump} is the pump work, and W_{motor} is the motor work per cycle. The motor work per cycle is defined as:

$$W_{motor} = \frac{W_{mag}}{\eta_{motor}} \tag{3-2}$$

where W_{mag} is the magnetic work per cycle and η_{motor} is the motor efficiency. The pump work per cycle is defined in terms of the pressure gradient ($\frac{dP}{dx}$) across the regenerator bed:

$$W_{pump} = \frac{1}{\eta_{pump}} \int_0^L \int_0^\tau \left(\left| \frac{\dot{m}(t)}{\rho_f} \frac{dP}{dx} \right| \right) dt\, dx \tag{3-3}$$

where η_{pump} is the pump efficiency, L is the length of the regenerator bed, and τ is the cycle time.

Engelbrecht (2008) presents correlations for the pressure gradient in packed sphere and parallel plate regenerator geometries. A typographical error exists in this reference in the presentation of the Ergun (1952) equation to model the pressure drop in a packed sphere regenerator (Eqs. (2.57) and (2.58) in reference [2]). The Ergun equation for the pressure gradient in a packed sphere regenerator is [3]:

$$\frac{dP}{dx} = \left(\frac{A \alpha \mu_f}{d_p^2} \right) v + \left(\frac{B \beta \mu_f}{d_p} \right) v^2 \tag{3-4}$$

where the parameters *A* and *B* are based on the surface roughness of the particles and d_p is the particle diameter. Kaviany suggests values of $A = 180$ and $B = 1.8$ for smooth particles [4]. The particle diameter is expressed in terms of the hydraulic diameter (d_h) according to:

$$d_p = \frac{3}{2} \frac{1-\varepsilon}{\varepsilon} d_h \tag{3-5}$$

where ε is the porosity of the packed sphere bed. Eq. (3-4) can be rearranged and the spatial pressure gradient can be converted into a friction factor according to:

$$\frac{dP}{dx} = \frac{f_f \dot{m}^2}{2 \rho_f A_c^2 d_h} \tag{3-6}$$

Combining Eqs. (3-4) and (3-6) yields an equation for the friction factor based on the particle hydraulic diameter:

$$f_f = \frac{8}{9} \frac{A}{Re_f \varepsilon} + \frac{4}{3} \frac{B}{\varepsilon} \tag{3-7}$$

where Re_f is the Reynolds number of the fluid based on the hydraulic diameter of the packed particles.

The refrigeration load per cycle (Q_{ref}) is defined as:

$$Q_{ref} = \int_0^{\tau} \left[h_f\left(T_C\right) - h_f\left(T_{f,x=L}\right) \right] \dot{m}(t)\, dt \qquad \text{for } \dot{m}(t) > 0 \tag{3-8}$$

where $h_f\left(T_C\right)$ is the enthalpy of the fluid evaluated at the cold reservoir temperature and $h_f\left(T_{f,x=L}\right)$ is the enthalpy of the fluid evaluated at the temperature of the fluid at the cold end of the bed ($x = L$) at cycle time t. Note that a positive mass flow rate indicates a hot-to-cold blow providing refrigeration and the integral in Eq. (3-8) is only evaluated during cycle times where the mass flow rate is positive.

3.2 Regenerator Governing Equations

For the spatially one-dimensional active magnetic refrigerator model developed at the UW, the regenerator energy balance equation is modified to include an irreversible entropy generation source that can be used to represent the effect of hysteresis on the thermodynamic cycle. The model solves a pair of coupled partial differential equations in time and space for a cycle steady state condition. One equation describes the energy balance for the fluid flow through the matrix, and the other describes the energy

balance for magnetocaloric material and entrained fluid in the matrix. A schematic of the energy balance for a differential segment of the regenerator is shown in Figure 3-2:

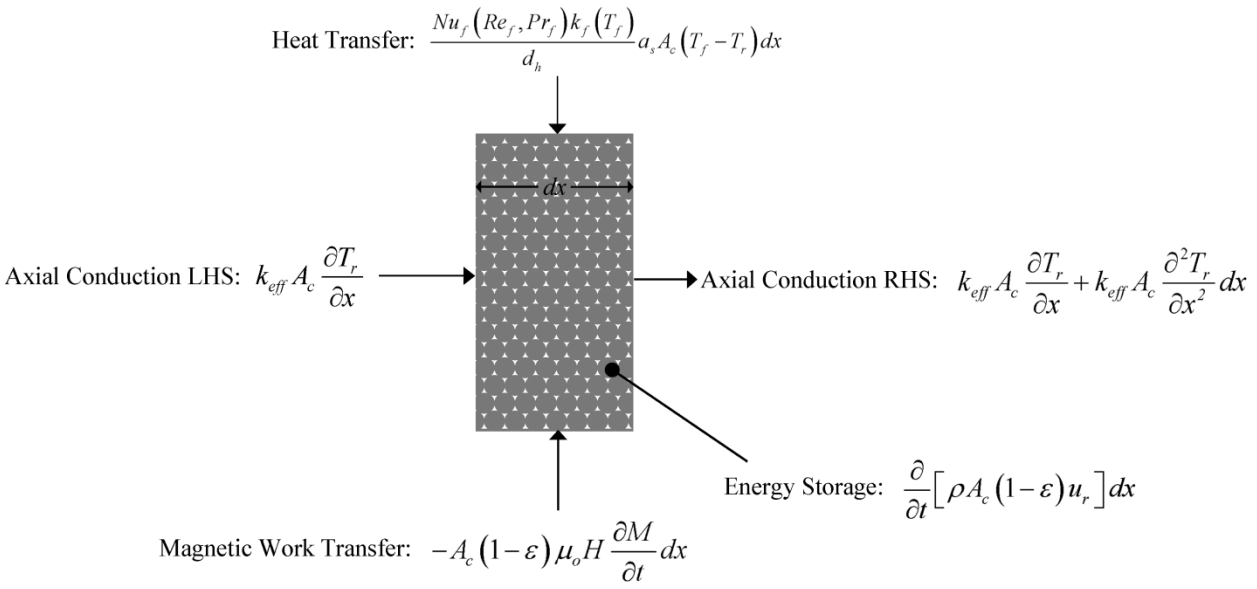

Figure 3-2. Differential segment of the regenerator with energy balance terms included

where the differential control volume has differential length *dx* and cross-sectional area A_c.

The energy balance in Figure 3-2 is written as:

$$\frac{Nu\cdot k_f}{d_h}a_sA_s\left(T_f-T_r\right)+A_c\left(1-\varepsilon\right)\mu_0 H\frac{\partial M}{\partial t}+k_{eff}A_c\frac{\partial^2 T_r}{\partial x^2}=\rho_r A_c(1-\varepsilon)\frac{\partial u_r}{\partial t} \tag{3-9}$$

An entropy balance on a differential piece of magnetocaloric material is given by:

$$dS=\frac{\delta Q}{T_r}+S_{gen} \tag{3-10}$$

where S_{gen} is the internal entropy generation related to hysteresis. By combining the energy balance for a magnetocaloric material represented by Eq. (1-4) and the entropy balance for the same magnetocaloric material represented by Eq. (3-10) we obtain:

$$dU=T_r\,dS-T_r\,S_{gen}+\mu_0 H\cdot d\left(V\cdot M\right) \tag{3-11}$$

Dividing through by the mass of the material leads to:

$$du = T_r\, ds - T_r\left(\frac{S_{gen}}{m}\right) + \mu_0 H \cdot d\left(v \cdot M\right) \tag{3-12}$$

where (S_{gen}/m) is the mass specific entropy generation. Equation (3-12) can be rearranged:

$$\frac{\partial u}{\partial t} - \frac{\mu_0 H}{\rho_r}\frac{\partial M}{\partial t} = T_r\frac{\partial s}{\partial t} - T_r\left(\frac{\dot{S}_{gen}}{m}\right) \tag{3-13}$$

Substituting Eq. (3-13) into Eq. (3-9) provides the overall energy balance equation for the regenerator:

$$\frac{Nu \cdot k_f}{d_h} a_s A_s \left(T_f - T_r\right) + k_{eff} A_c \frac{\partial^2 T_r}{\partial x^2} = \rho_r A_c (1-\varepsilon) \cdot T_r\left(\frac{\partial s_r}{\partial t} - \frac{\dot{S}_{gen}}{m}\right) \tag{3-14}$$

which can be further simplified by expressing the change in the regenerator specific entropy in terms of the its magnetic field and temperature driven components:

$$\frac{Nu \cdot k_f}{d_h} a_s A_s \left(T_f - T_r\right) + k_{eff} A_c \frac{\partial^2 T_r}{\partial x^2} = \rho_r A_c (1-\varepsilon) \cdot \left[c_{\mu_0 H}\frac{\partial T_r}{\partial t} + T_r\left(\left.\frac{\partial s_r}{\partial \mu_0 H}\right|_T \cdot \frac{\partial \mu_0 H}{\partial t} - \frac{\dot{S}_{gen}}{m}\right)\right] \tag{3-15}$$

The last term in Eq. (3-15) is related to internal entropy generation due to hysteresis. From Chapter 2, the specific entropy generation rate is resolved in terms of an irreversible magnetization according to Eq. (2-8). Substituting Eq. (2-8) into Eq. (3-15) yields:

$$\frac{Nu \cdot k_f}{d_h} a_s A_s \left(T_f - T_r\right) + k_{eff} A_c \frac{\partial^2 T_r}{\partial x^2} = \rho_r A_c (1-\varepsilon) \cdot \left[c_{\mu_0 H}\frac{\partial T_r}{\partial t} + T_r \left.\frac{\partial s_r}{\partial \mu_0 H}\right|_T \cdot \frac{\partial \mu_0 H}{\partial t} - v_r M_{irr}\left|\frac{\partial \mu_0 H}{\partial t}\right|\right] \tag{3-16}$$

as the final regenerator energy balance equation including hysteresis effects, which are expressed in terms of the irreversible mass specific magnetization (vM_{irr}).

3.3 Discretization of Governing Regenerator Equations

The regenerator is discretized into Nx spatial nodes where the axial location of each node is given by:

$$x_i = \left(i - \frac{1}{2} \right) \frac{L}{Nx} \quad i = 1..Nx \tag{3-17}$$

where i is the axial subscript and L is the length of the regenerator bed. The temporal grid is similarly separated into Nt nodes where the cycle time is given by:

$$t_j = j \frac{\tau}{Nt} \quad j = 0..Nt \tag{3-18}$$

where j is the temporal subscript.

Following Eq. (3-16), the regenerator energy balance equation for each control volume can be discretized as follows:

$$\begin{aligned} &\frac{Nu_{f\,i,j}\, k_{f\,i,j}}{d_h} a_s A_s \frac{L}{Nx} \left(T_{r\,i,j+1} - T_{f\,i,j+1} \right) + A_c \frac{L}{Nx} (1-\varepsilon) \rho_r c_{\mu_0 H\,i,j} \frac{\left(T_{r\,i,j+1} - T_{r\,i,j} \right) Nt}{\tau} \\ &+ \frac{Nx\, k_{eff\,i,j} A_c}{L} \left[T_{r\,i,j+1} - T_{r\,i-1,j+1} \right] + \frac{Nx\, k_{eff\,i,j} A_c}{L} \left[T_{r\,i,j+1} - T_{r\,i+1,j+1} \right] = \\ &- A_c (1-\varepsilon) \rho_r T_{r\,i,j} \left(\frac{\partial s_r}{\partial \mu_0 H} \right)_{i,j} \frac{\partial \mu_0 H}{\partial t} \left(x_i, \frac{t_{j+1} + t_j}{2} \right) + \\ &A_c (1-\varepsilon) \rho_r \left(v_r M_{irr} \right)_{i,j} \left| \frac{\partial \mu_0 H}{\partial t} \left(x_{Nx}, \frac{t_{j+1} + t_j}{2} \right) \right| \qquad i = 2..Nx-1 \end{aligned} \tag{3-19}$$

Since the ends of the bed are assumed to be insulated, the conduction terms vanish at the hot end ($i = 1$) and the cold end ($i = Nx$). The regenerator energy balance at the hot end is:

$$\frac{Nu_{f\ 1,j}\,k_{f\ 1,j}}{d_h}a_s A_s\frac{L}{Nx}\left(T_{r\ 1,j+1}-T_{f\ 1,j+1}\right)+A_c\frac{L}{Nx}\left(1-\varepsilon\right)\rho_r c_{\mu_0 H\ 1,j}\frac{\left(T_{r\ 1,j+1}-T_{r\ 1,j}\right)Nt}{\tau}$$
$$+\frac{Nx\,k_{eff\ 1,j}A_c}{L}\left[T_{r\ 1,j+1}-T_{r\ 2,j+1}\right]=-A_c\left(1-\varepsilon\right)\rho_r T_{r\ 1,j}\left(\frac{\partial s_r}{\partial\mu_0 H}\right)_{1,j}\frac{\partial\mu_0 H}{\partial t}\left(x_1,\frac{t_{j+1}+t_j}{2}\right) \qquad (3\text{-}20)$$
$$+A_c\left(1-\varepsilon\right)\rho_r\left(v_r M_{irr}\right)_{i,j}\left|\frac{\partial\mu_0 H}{\partial t}\left(x_{Nx},\frac{t_{j+1}+t_j}{2}\right)\right|$$

Similarly, by neglecting conduction at the cold end of the bed, the regenerator energy balance at the cold end is:

$$\frac{Nu_{f\ Nx,j}\,k_{f\ Nx,j}}{d_h}a_s A_s\frac{L}{Nx}\left(T_{r\ Nx,j+1}-T_{f\ Nx,j+1}\right)+A_c\frac{L}{Nx}\left(1-\varepsilon\right)\rho_r c_{\mu_0 H\ 1,j}\frac{\left(T_{r\ Nx,j+1}-T_{r\ Nx,j}\right)Nt}{\tau}$$
$$+\frac{Nx\,k_{eff\ Nx,j}A_c}{L}\left[T_{r\ Nx,j+1}-T_{r\ Nx\text{-}1,j+1}\right]=-A_c\left(1-\varepsilon\right)\rho_r T_{r\ Nx,j}\left(\frac{\partial s_r}{\partial\mu_0 H}\right)_{Nx,j}\frac{\partial\mu_0 H}{\partial t}\left(x_{Nx},\frac{t_{j+1}+t_j}{2}\right) \qquad (3\text{-}21)$$
$$+A_c\left(1-\varepsilon\right)\rho_r\left(v_r M_{irr}\right)_{i,j}\left|\frac{\partial\mu_0 H}{\partial t}\left(x_{Nx},\frac{t_{j+1}+t_j}{2}\right)\right|$$

where $\left(v_r M_{irr}\right)$ is the mass specific irreversible magnetization due to magnetic hysteresis. The final term in Eqs. (3-19) - (3-21) represents the energy lost due to the hysteresis entropy generation rate.

REFERENCES

1. Engelbrecht, K., *A Numerical Model of an Active Magnetic Regenerator Refrigeration System*, in *Mechanical Engineering*. 2004, The University of Wisconsin at Madison: Madison, WI. p. 157.

2. Engelbrecht, K., *A Numerical Model of an Active Magnetic Regenerator Refrigerator with Experimental Validation* in *Mechanical Engineering*. 2008, The University of Wisconsin at Madison: Madison, WI. p. 267.

3. Ergun, S., *Fluid flow through packed columns.* Chemical Engineering Progress, 1952. **48**(2): p. 89-94.

4. Kaviany, M., *Principles of Heat Transfer in Porous Media*. 1995, New York, NY: Springer.

Chapter 4 MAGNETIC EQUATIONS OF STATE

The thermodynamics of the magnetic phase change has become a growing field of interest since the discovery of the near room temperature giant magnetocaloric effect (GMCE) in $Gd_5(Si_xGe_{1-x})_4$ type compounds by Pecharsky and Gschneider in 1997 [1].

Despite the magnetocaloric effect being well-documented, it is difficult to model accurately for most materials since a general magnetic equation of state (akin to the Redlich-Kwong-Soave or Peng-Robinson equations of state for compressible substances) does not exist. The Brillouin function is widely used as the general equation of state for magnetic materials, and works well for second-order magnetic transition (SOMT) materials such as pure gadolinium [2, 3]. The second-order magnetic transition is a continuous phase transition, meaning that the partial derivative of the free energy with respect to any intensive state variable is continuous [4]. Jiles (1998) presents equations of state for paramagnetic and ferromagnetic materials based on the Brillouin function.

For first-order magnetic transition (FOMT) materials, where the magnetic phase change is discontinuous, the quantum Brillouin model presented by Jiles is not accurate. Von Ranke, Oliveira, and Gama (2004) propose a model for the first-order magnetic phase change through modifications to the Brillouin equation of state [5]. Their model is a two-parameter equation of state that also accounts for pressure effects.

4.1 Paramagnetic Equation of State

At temperatures above the Curie temperature (T_{Curie}), a ferromagnetic material becomes completely paramagnetic. A fundamental equation of state for paramagnetism allows the thermodynamic properties of a magnetic material to be evaluated above these temperatures. The quantum mean-field theory of paramagnetism states that the volumetric magnetization for a multi-electron magnetic material can be expressed as a function of applied field ($\mu_0 H$) and temperature (T) [3]:

$$M\left(\mu_0 H,T\right)=M_s\,B_J\left(z\right)=N\,g_L\,J\,\mu_B\,B_J\left(\frac{g_L J\mu_B\mu_o H}{k_B T}\right) \tag{4-1}$$

where M_s is the saturation magnetization, N is the number of atoms per unit volume, g_L is the material-dependent Lande factor, J is the total molecular angular momentum number, μ_B is the Bohr magneton, and k_B is the Boltzmann constant. The Brillouin function ($B_J\left(z\right)$) is defined as [3]:

$$B_J\left(z\right)=\left(\frac{2J+1}{2J}\right)\coth\left(\frac{2J+1}{2J}z\right)-\left(\frac{1}{2J}\right)\coth\left(\frac{z}{2J}\right) \tag{4-2}$$

where the argument $z=g_L J\mu_B\mu_o H/(k_B T)$ is the ratio of the energy due to the applied magnetic field to the thermal energy. In the limit of an ideal paramagnet (in small fields or high temperatures), the Brillouin function can be estimated by a first order series expansion:

$$N\,g_L\,J\,\mu_B B_J\left(z\right)\approx\frac{N\,g_L^2\,\mu_B^2\,J\left(J+1\right)\mu_o H}{3k_B T} \tag{4-3}$$

Eq. (4-3) is simply the Curie law:

$$M=\frac{N\,g_L^2\,\mu_B^2\,J\left(J+1\right)\mu_o}{3k_B}\frac{H}{T}=C\frac{H}{T} \tag{4-4}$$

which implies that:

$$C=\frac{N\,\mu_o g_L^2\,\mu_B^2\,J\left(J+1\right)}{3k_B} \tag{4-5}$$

where C is the Curie constant.

Eq. (4-1) is effectively a two-parameter magnetic equation of state, where the Lande factor (g_L) and the total angular momentum (J) can be adjusted to fit the characteristics of a certain material.

4.2 Ferromagnetic Equation of State

For temperatures below the Curie temperature, a magnetic material exists in the ferromagnetic phase. The quantum mean-field equation of state for a ferromagnetic material is related to the quantum mean-field equation of state for a paramagnetic material, the difference is that ferromagnetic materials have magnetic domains that interact with one another. The interaction leads to an effective internal field (H_{eff}) that is dependent on both the applied field and magnetization. Thus the equation of state for a ferromagnetic material can be written as:

$$M\left(\mu_0 H, T\right) = N\, g_L\, J\, \mu_B\, B_J\left(\frac{g_L J \mu_B \mu_o \left(H + \alpha M\right)}{k_B T}\right) \tag{4-6}$$

where α is the domain coupling constant that is representative of the strength of interactions between neighboring domains. The magnetization of a ferromagnetic material is thus implicitly defined by itself. Eq. (4-6) has three free parameters: α , *J*, and g_L . In a high temperature limit, a ferromagnetic system becomes paramagnetic, and the Brillouin function can be estimated by a first order series expansion:

$$N\, g_L\, J\, \mu_B B_J\left(z\right) \approx \frac{N\, g_L^2\, \mu_B^2\, J\left(J+1\right) \mu_o \left(H + \alpha M\right)}{3 k_B T} \tag{4-7}$$

where the argument $z = g_L J \mu_B \mu_o \left(H + \alpha M\right) \big/ \left(k_B T\right)$. The volumetric magnetization is thus:

$$M = \frac{N\, g_L^2\, \mu_B^2\, J\left(J+1\right) \mu_o \left(H + \alpha M\right)}{3 k_B T} \tag{4-8}$$

which can be rearranged to solve explicitly for *M*:

$$M = \frac{N\, g_L^2\, \mu_B^2\, J\left(J+1\right) \mu_o H \big/ \left(3 k_B T\right)}{1 - \alpha N\, g_L^2\, \mu_B^2\, J\left(J+1\right) \mu_o H \big/ \left(3 k_B T\right)} = \frac{N\, g_L^2\, \mu_B^2\, J\left(J+1\right) \mu_o H \big/ \left(3 k_B\right)}{T - \alpha N\, g_L^2\, \mu_B^2\, J\left(J+1\right) \mu_o H \big/ \left(3 k_B\right)} \tag{4-9}$$

Under close inspection, Eq. (4-9) is the Curie-Weiss law:

$$M = \frac{C_W}{T - T_{Curie}} H \tag{4-10}$$

where the Curie-Weiss constant is $C_W = N\mu_o g_L^2 \mu_B^2 J(J+1)/(3k_B)$ and the Curie temperature is $T_{Curie} = \alpha N \mu_o g_L^2 \mu_B^2 J(J+1)/(3k_B)$. Since the Curie temperature is a measurable quantity, it is useful to express the domain coupling constant (α) as a function of T_{Curie}:

$$\alpha = \frac{3k_B T_{Curie}}{N\mu_o g_L^2 \mu_B^2 J(J+1)} \tag{4-11}$$

The expression for the domain coupling constant can be substituted into the argument of the Brillouin function in Eq. (4-6) to yield:

$$M(\mu_0 H, T) = N g_L J \mu_B B_J\left(\frac{g_L J \mu_B \mu_o H}{k_B T} + \frac{3T_{Curie} M}{N g_L \mu_B (J+1) T}\right) \tag{4-12}$$

which is dependent on the Curie temperature rather than the domain coupling constant.

Figure 4-1 shows the isothermal magnetic entropy change for pure gadolinium predicted by Eq. (4-12) compared to experimental data for an applied field change from 0 to 1.5 Tesla. For gadolinium, the Landé g-factor has a value of g_L = 2 and the total angular momentum has a value of J = 3.5; these values were used to generate the curve in Figure 4-1 [3]. The ferromagnetic equation of state generally over-predicts the magnitude of the magnetic entropy change for temperatures below the Curie temperature (293 K) and under-predicts it for temperatures above the Curie temperature.

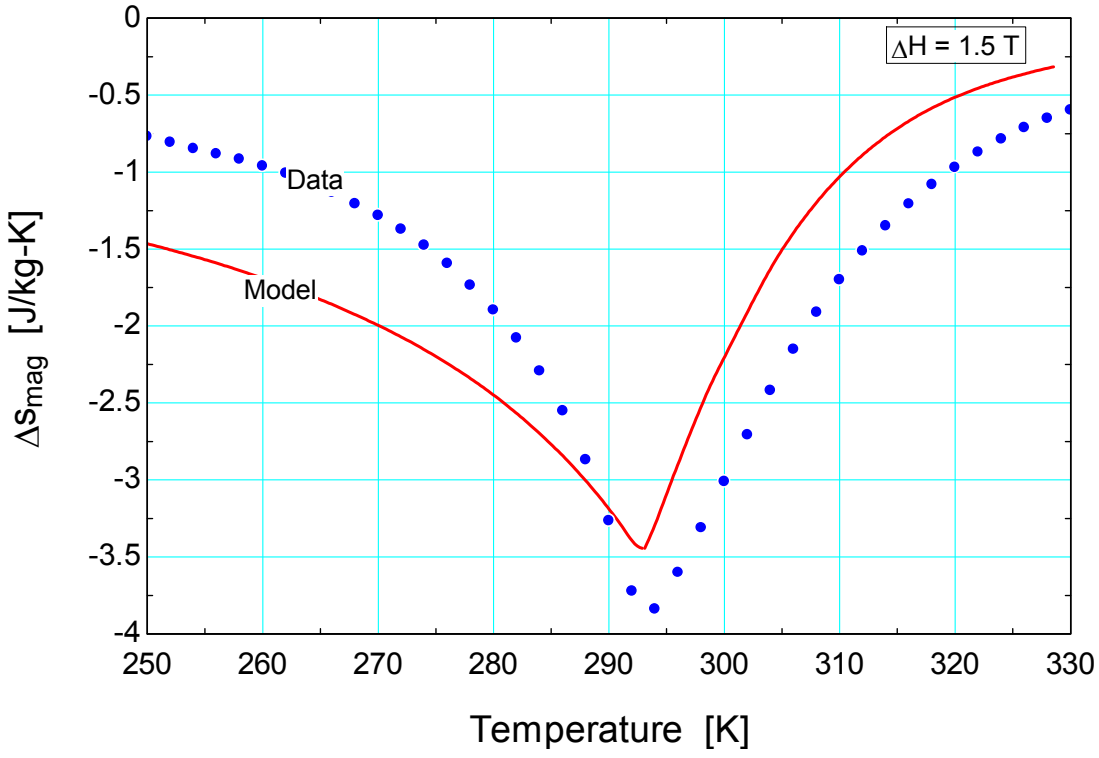

Figure 4-1. Isothermal magnetic entropy change for gadolinium for a magnetic field change of 0 to 1.5 Tesla computed using the mean field model and from experimental specific heat data. Data provided by Astronautics Corporation of America.

4.3 Metamagnetic Phase Transitions

4.3.1 Equation of State Model

Von Ranke et al. (2004) propose an equation of state model for the metamagnetic phase transition of first-order magnetic transition materials. The underlying assumption of the model is that the Curie temperature (T_{Curie}) is linearly dependent on the change in volume due to magnetostriction that occurs during the phase change:

$$T_{Curie} = T_0\left(1+\beta\omega\right) \tag{4-13}$$

where T_0 is the Curie temperature in the absence of an external magnetic field at atmospheric pressure, ω is the dimensionless change in volume, and β is a material-dependent, dimensionless parameter that

is proportional to the derivative of Curie temperature with respect to volume (dT_{Curie}/dV). The dimensionless change in volume ω is defined as:

$$\omega = \frac{V - V_0}{V_0} \tag{4-14}$$

where V_0 is the material volume in the absence of an external magnetic field at the reference pressure. In general, the Gibbs free energy for a magnetic, compressible material is defined as:

$$G \equiv U + PV - H M - T S \tag{4-15}$$

where U is the internal energy, P is pressure, V is volume, H is the external magnetic field, M is the total magnetic moment, T is the temperature, and S is the entropy. Using a molecular field approximation for a ferromagnetic lattice that includes exchange, Zeeman, distortion, and pressure effects, the Gibbs free energy is:

$$G = -\frac{3}{2}\left(\frac{J}{J+1}\right)\frac{N}{V_0}k_B T_C \sigma^2 - H g_L \mu_B J N \sigma + \frac{1}{2K}\omega^2 + P\omega - T S \tag{4-16}$$

where J is the total angular momentum, N is the number of magnetic spins, k_B is the Boltzmann constant, T_C is the Curie temperature, σ is the dimensionless magnetization, H is the external magnetic field, g_L is the Landé g-factor, K is the compressibility, P is the externally applied pressure, and S is the magnetic entropy. The dimensionless magnetization (σ) is defined as:

$$\sigma = \frac{M}{g_L \mu_B J N} \tag{4-17}$$

The minimum of the Gibbs free energy defined in Eq. (4-16) determines the equilibrium condition. To determine the equilibrium condition, the partial derivative of the Gibbs free energy with respect to the dimensionless change in volume at constant temperature, pressure, applied magnetic field, and number of magnetic spins is set to zero:

$$\left(\frac{\partial G}{\partial \omega}\right)_{T,P,H,N} = -\frac{3}{2}\left(\frac{J}{J+1}\right)\frac{N}{V_0}k_B T_0 \beta\sigma^2 + \frac{\omega}{K} + P = 0 \tag{4-18}$$

Rearranging Eq (4-18), the dimensionless volume change that minimizes the Gibbs free energy is:

$$\omega = \frac{3}{2}\frac{J^2}{J(J+1)}\frac{N}{V_0}k_B K T_0 \beta\sigma^2 - PK \tag{4-19}$$

By substituting Eq. (4-19) into Eq. (4-16) and taking the derivative of the Gibbs free energy with respect to the dimensionless magnetization (σ), the magnetic equation of state is obtained:

$$\sigma = B_J\left[3\frac{T_0}{T}\left(\frac{J}{J+1}\right)\sigma + \frac{g_L \mu_B J}{k_B T}H + \frac{9}{5}\left(\frac{(2J+1)^4 - 1}{[2(J+1)]^4}\right)\frac{T_0 \eta \sigma^3}{T} - 3\frac{J\beta PK}{(J+1)}\frac{T_0}{T}\sigma\right] \tag{4-20}$$

where B_J indicates the Brillouin function, which is defined as:

$$B_J(x) = \left(\frac{2J+1}{2J}\right)\coth\left(\frac{2J+1}{2J}x\right) - \left(\frac{1}{2J}\right)\coth\left(\frac{1}{2J}x\right) \tag{4-21}$$

The parameter η indicates the order of the magnetic phase transition and is directly related to the parameter β by:

$$\eta = \frac{5}{2}\frac{[4J(J+1)]^2}{[(2J+1)^4 - 1]}\frac{N}{V_0}k_B K T_0 \beta^2 \tag{4-22}$$

Thus, η is proportional to the square of the derivative of the Curie temperature with respect to volume. In other words, it is indicative of the magnitude of the magneto-structural volume change.

4.3.2 Application to $La(Fe_{1-x}Si_x)_{13}H_y$

A promising material for use in magnetic coolers is the $La(Fe_{1-x}Si_x)_{13}H_y$ family of compounds. These materials exhibit a large magnetocaloric effect resulting from a first order magnetic phase change. For compositions with $0.87 \leq x \leq 0.90$, the Curie temperature ranges from approximately 180 K to 330 K, depending on the concentration of hydrogen (y).

The only element to exhibit ferromagnetism in $La(Fe_{1-x}Si_x)_{13}H_y$ near its transition temperature is iron (Fe). Hence, the total angular momentum of isolated elemental iron is used to approximate that of $La(Fe_{1-x}Si_x)_{13}H_y$. The Landé g-factor for isolated iron is approximately equal to its value for gadolinium and is $g_L = 2$ and the total angular momentum has a value of $J = 1.5$ [3].

Entropy data for the specific composition of $La(Fe_{1-x}Si_x)_{13}H_y$ with $x \approx 0.115$ and $y \approx 1.21$ is available for comparison. For this specific composition, the number of magnetic spins per mole is $N = 11.5 N_A$, where the coefficient of N_A represents the number of iron atoms per mole. Figure 4-2 shows the isothermal entropy change predicted by the mean field model and experimental magnetization data for a applied magnetic field change from 0 to 1.5 Tesla for $La(Fe_{0.885}Si_{0.115})_{13}H_{1.21}$. The parameters chosen for the mean field model are η =1.39 and T_0 = 283.5 K. These parameters most closely match the data and were chosen based on trial-and-error. The model is fairly accurate in predicting the isothermal entropy change for this material, but tends to over-predict the effect below 290 K, and under-predict for temperatures above 290 K.

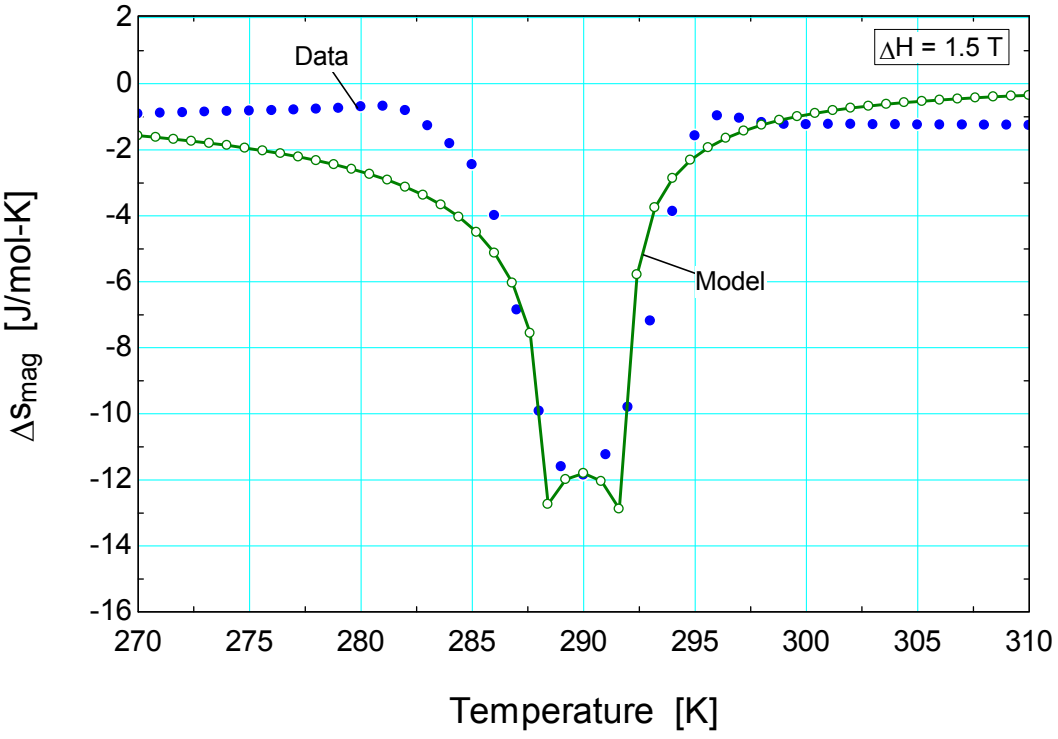

Figure 4-2. Isothermal entropy change for $La(Fe_{0.885}Si_{0.115})_{13}H_{1.21}$ predicted by mean field model and from experimental magnetization data. Data provided by Astronautics Corporation of America.

4.4 Raw Data

Another method for characterizing magnetic material properties is through interpolation of raw data for that material. The purpose of this section is to demonstrate how raw magnetization and specific heat data can be used in lieu of an equation of state.

The raw data used in this demonstration were provided from Astronautics Corporation of America and include four sets of magnetization measurements as a function of applied field taken along 12 isotherms for the FOMT material $La(Fe_{0.885}Si_{0.115})_{13}H_{1.21}$. A set of data was taken for increasing applied field and temperature, another for decreasing applied field and increasing temperature, a third for increasing applied field and decreasing temperature, and a final set for decreasing applied field and temperature. Table 4-1 lists the physical properties of the sample tested. Figure 4-3 is a photo of the mounting apparatus used for a magnetization sample.

Table 4-1. Test specimen details

Density	7170 $^{kg}/_{m^3}$
Sample Mass	0.0163 g
Geometry	Packed spheres w/~0.37 porosity inside cylindrical housing with 0.10 *in* diameter.
Applied Field Direction	Parallel to the axis of cylindrical sample holder.
Chemical Formula	$La(Fe_{1-x}Si_x)_{13}H_y$ where $x \approx 0.115$ and $y \approx 1.21$

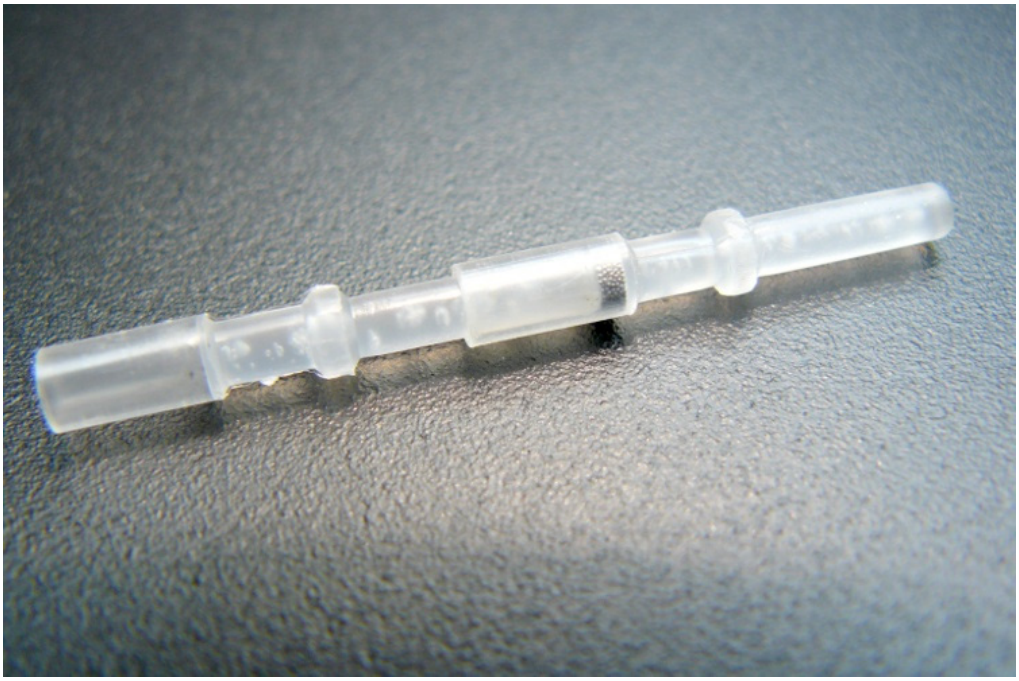

Figure 4-3. Typical mounting apparatus for a magnetization sample. Photo courtesy of Astronautics Corporation of America.

Figure 4-4 shows the mass-specific magnetization as a function of applied field for various temperatures when the temperature is increasing. The solid lines are representative of the magnetization while the field is increasing with time, and the dotted lines represent the magnetization in a decreasing field. Figure 4-5 is the mass-specific magnetization as a function of applied field for various temperatures when the temperature is decreasing. Comparison of these two plots indicate that $La(Fe_{0.885}Si_{0.115})_{13}H_{1.21}$ exhibits large magnetic hysteresis but little thermal hysteresis near the Curie temperature.

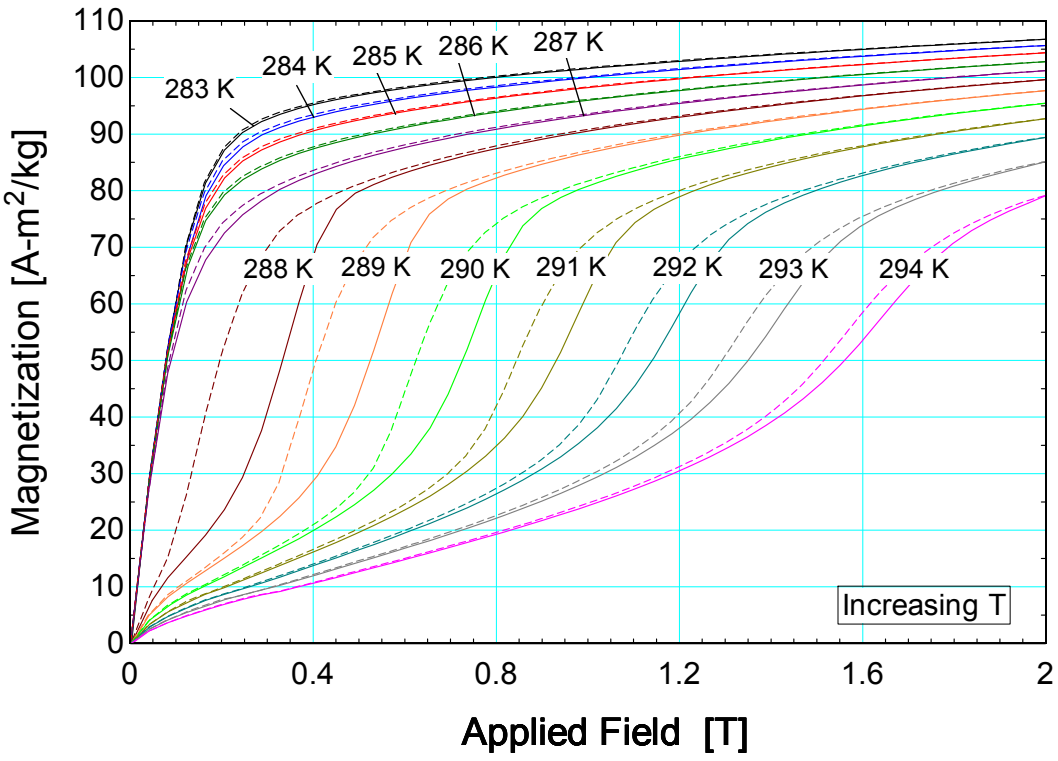

Figure 4-4. Magnetization as a function of applied field for increasing temperatures in JF1-142A. Solid lines indicate increasing field and dotted lines indicate decreasing field.

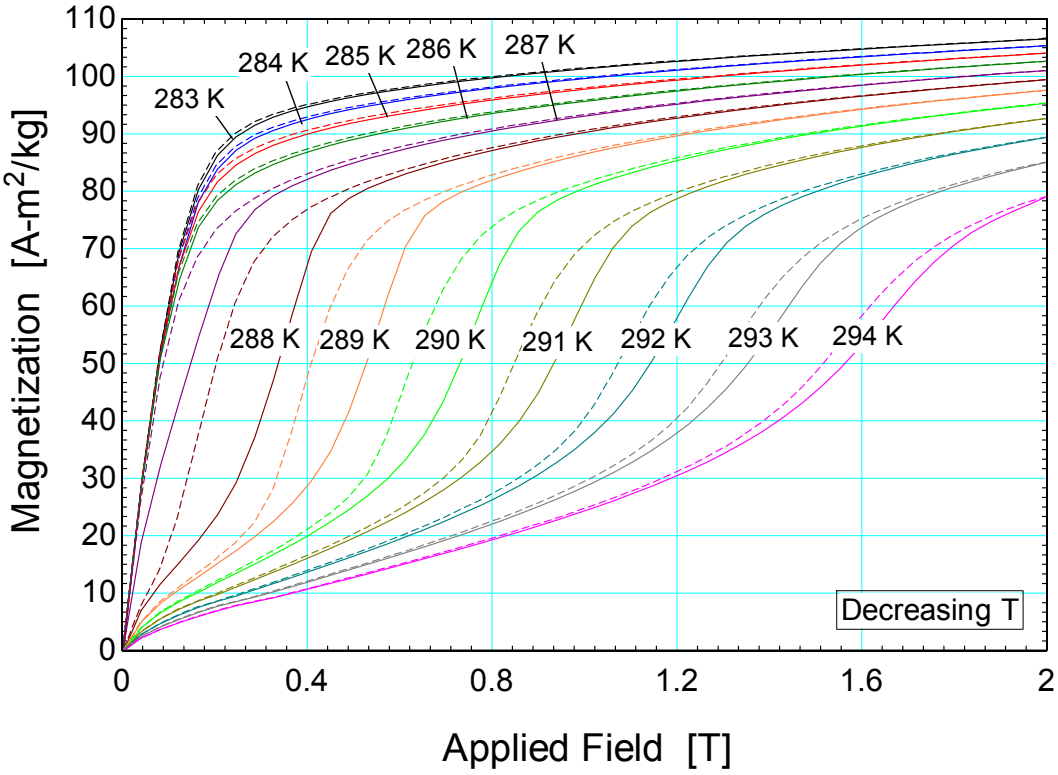

Figure 4-5. Magnetization as a function of applied field for decreasing temperatures in JF1-142A. Solid lines indicate increasing field and dotted lines indicate decreasing field.

4.4.1 Demagnetization Effects

A magnetization (M) is induced within the material when it is subjected to an applied magnetic field (H_a). Inside a material of finite geometry, these fields are oriented in opposite directions and result in an internal magnetic field (H_{int}) that is smaller in magnitude than the applied magnetic field [3]. To calculate the internal field, first the demagnetizing field (H_d) is defined as:

$$H_d = N_d M \tag{4-23}$$

where M is the volume magnetization of the material and N_d is the material demagnetization factor. The demagnetization factor is a function of material geometry, applied field, and temperature. The demagnetization factor must be determined experimentally for complex geometries, but it can be found analytically for simple geometries such as cylinders and spheres. Suggested values for the demagnetization factor for many simple geometries have been published in the literature [3, 6]. Since the

demagnetizing field vector is opposite the applied field vector, the magnitude of internal field vector is simply expressed as:

$$H_{\text{int}} = H_a - H_d = H_a - N_d M \tag{4-24}$$

Expressing the magnetization as a function of the calculated internal field and temperature yields the corrected magnetization function. Demagnetizing effects should be accounted for in an efficient AMRR design and can be detrimental to the performance for cycles using low applied field (< 2 Tesla) permanent magnets [7].

4.4.2 Anhysteretic and Irreversible Magnetization

The anhysteretic magnetization function (M_{an}) is the hypothetical magnetization curve of a material in the absence of magnetic hysteresis. The anhysteretic magnetization is calculated by taking the average of the positive (M_{pos}) and negative (M_{neg}) magnetization curves for a given applied field and temperature:

$$M_{an}\left(\mu_0 H, T\right) = \frac{M_{pos}\left(\mu_0 H, T\right) + M_{neg}\left(\mu_0 H, T\right)}{2} \tag{4-25}$$

where M_{pos} is the magnetization when the change in field with time is positive and M_{neg} is the magnetization when the change in field with time is negative. Bozorth (1951) states that the average of the positive (M_{pos}) and negative (M_{neg}) magnetization branches of the hysteresis curve at a given applied field is an accurate estimate of the anhysteretic magnetization [8]. Figure 4-6 is the anhysteretic magnetization taken from the decreasing temperature magnetization data depicted in Figure 4-5 (not corrected for demagnetization effects).

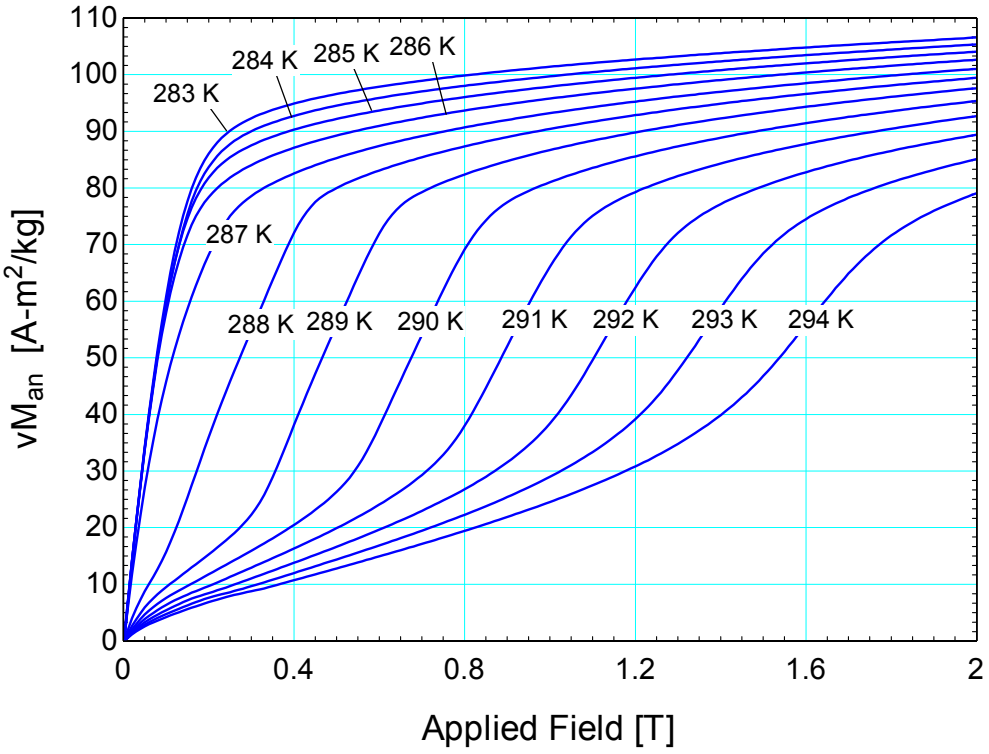

Figure 4-6. Anhysteretic magnetization for $La(Fe_{0.885}Si_{0.115})_{13}H_{1.21}$ for the decreasing temperature measurement. Not corrected for demagnetization.

Figure 4-7 shows the anhysteretic magnetization for $La(Fe_{0.885}Si_{0.115})_{13}H_{1.21}$ after correcting for demagnetization effects. The raw data were first corrected using Eq. (4-24), and the anhysteretic magnetization was subsequently calculated with Eq. (4-25). The magnetization curves below the Curie point (approximately 288 K for $La(Fe_{0.885}Si_{0.115})_{13}H_{1.21}$) should be tangent to the vertical axis at zero applied field. The demagnetization factor was therefore empirically determined in order to satisfy this requirement. The resulting demagnetization factor is approximately 0.15 for these data. For a perfect sphere, the demagnetization factor is 0.33 [3]. Since the total geometry consists of many closely packed spheres, the demagnetizing field will differ from that of a perfect sphere. There is no explicit recommendation in the literature for packed spheres, but air gaps in samples are known to reduce the effective demagnetizing field [9]. Thus, a value of 0.15 for the demagnetization factor is reasonable in this case. Note that the graphical effect of the demagnetization factor is counterclockwise rotation of each magnetization curve about the origin for the anhysteretic magnetization function.

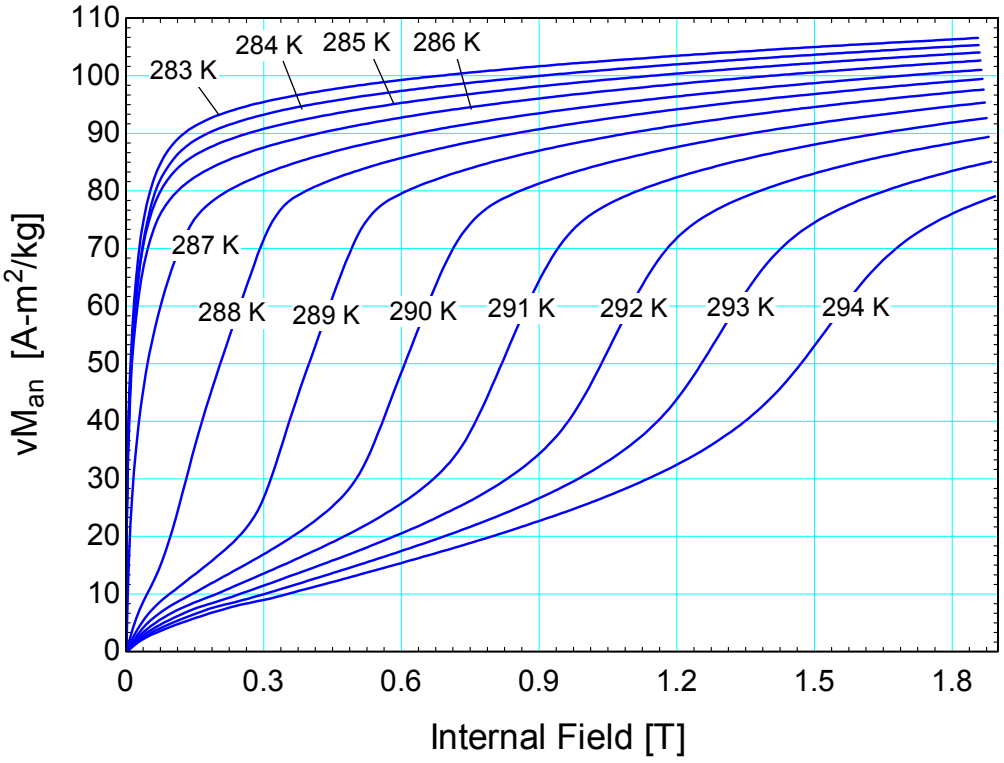

Figure 4-7. Anhysteretic magnetization for $La(Fe_{0.885}Si_{0.115})_{13}H_{1.21}$ for the decreasing temperature measurement. Corrected for demagnetization with $N_d = 0.15$.

The irreversible magnetization (M_{irr}) is defined in order to recover the area swept by a given hysteresis curve. The irreversible magnetization can be calculated according to:

$$M_{irr}\left(\mu_0 H,T\right)=\frac{\left|M_{neg}\left(\mu_0 H,T\right)-M_{pos}\left(\mu_0 H,T\right)\right|}{2} \tag{4-26}$$

The absolute value in Eq. (4-26) ensures a positive value for the irreversible magnetization which is necessary since it is directly related to the entropy generation. The positive and negative magnetization curves can be expressed in terms of the anhysteretic and irreversible magnetization:

$$M_{pos}\left(\mu_0 H,T\right)=M_{an}\left(\mu_0 H,T\right)-M_{irr}\left(\mu_0 H,T\right) \tag{4-27}$$

$$M_{neg}\left(\mu_0 H,T\right)=M_{an}\left(\mu_0 H,T\right)+M_{irr}\left(\mu_0 H,T\right) \tag{4-28}$$

Figure 4-8 shows the irreversible magnetization for $La(Fe_{0.885}Si_{0.115})_{13}H_{1.21}$ calculated using the data associated with temperatures between 287 and 294 K. At temperatures below the Curie point (~288 K), the irreversible magnetization becomes small. These data were extracted from the data shown in Figure 4-5 without the correction for demagnetization.

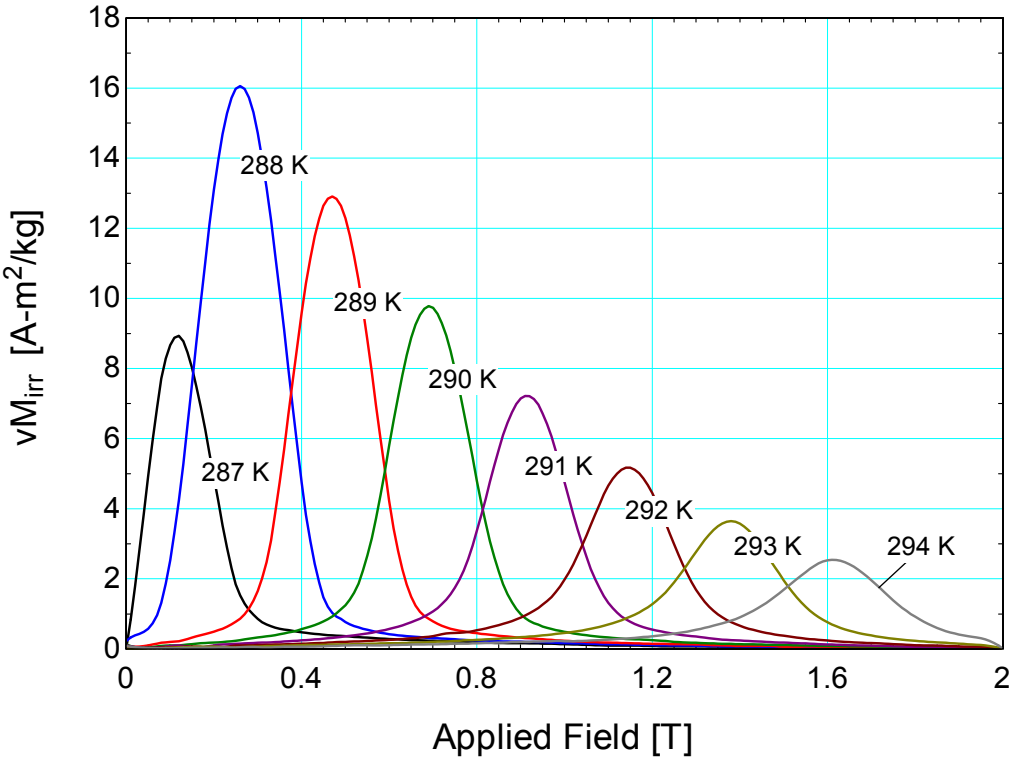

Figure 4-8. Irreversible magnetization for $La(Fe_{0.885}Si_{0.115})_{13}H_{1.21}$ for the decreasing temperature measurement. Not corrected for demagnetization effects.

Figure 4-9 is the irreversible magnetization for the decreasing temperature measurement after it has been corrected for demagnetization. Like the anhysteretic magnetization, the raw data were first corrected, and then the anhysteretic magnetization was derived from the corrected data. By comparing Figure 4-8 and Figure 4-9, the effect of applying the demagnetization factor becomes apparent. Graphically, it reduces the width of the peaks but also causes their peaks to become higher. Since the area underneath the curve is proportional the entropy generation and the entropy generation is constant

whether or not demagnetization effects occur, the area underneath each curve should remain constant before and after the application Eq. (4-24).

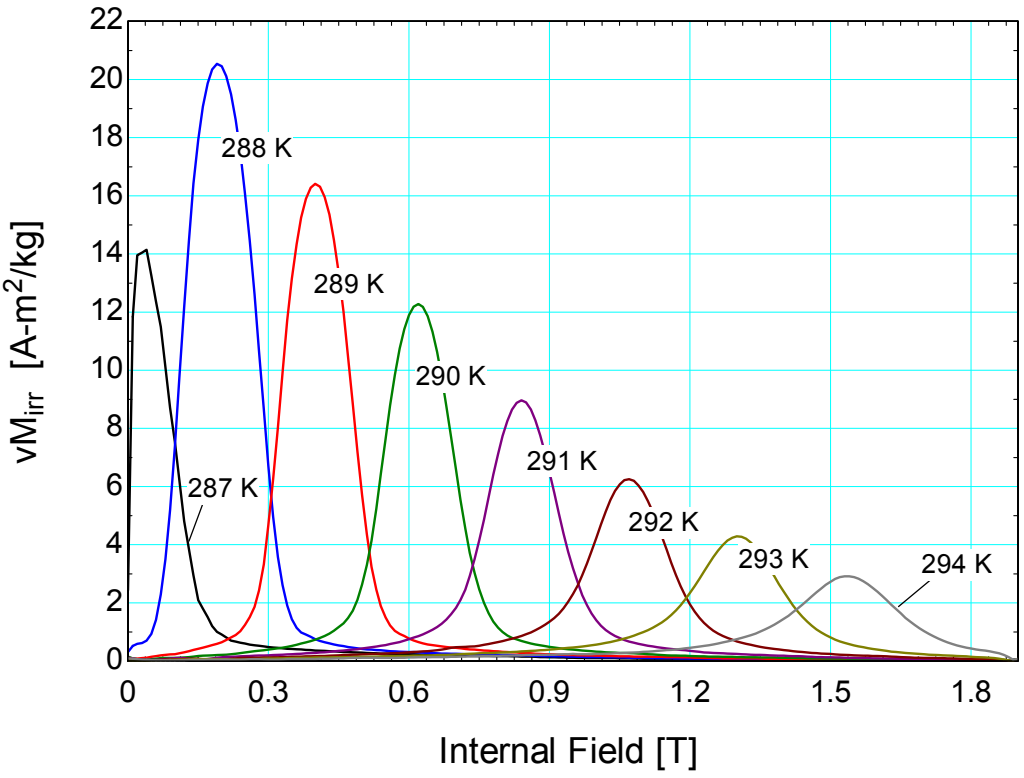

Figure 4-9. Irreversible magnetization for $La(Fe_{0.885}Si_{0.115})_{13}H_{1.21}$ for the decreasing temperature measurement. Corrected for demagnetization effects with $N_d = 0.15$.

4.4.3 Specific Entropy Calculation

With the anhysteretic and irreversible magnetization calculated, the specific entropy of $La(Fe_{0.885}Si_{0.115})_{13}H_{1.21}$ can be mapped as a function of both applied field and temperature. The total differential of the specific entropy (ds) of the material can be divided into its temperature-driven and applied magnetic field-driven components:

$$ds = \left(\frac{\partial s}{\partial T}\right)_{\mu_0 H} dT + \left(\frac{\partial s}{\partial \mu_0 H_{int}}\right)_T d\mu_0 H_{\text{int}} \tag{4-29}$$

where $\mu_0 H_{int}$ is the internal field. The Maxwell relation that relates the entropy to the anhysteretic magnetization can be utilized:

$$\left(\frac{\partial s}{\partial \mu_0 H}\right)_T = \left(\frac{\partial v M_{an}}{\partial T}\right)_{\mu_0 H} \tag{4-30}$$

as well as the definition of specific heat:

$$\left(\frac{\partial s}{\partial T}\right)_{\mu_0 H} = \frac{c_{\mu_0 H}}{T} \tag{4-31}$$

where $c_{\mu_0 H}$ is the constant field specific heat. Substituting Eqs. (4-30) and (4-31) into Eq. (4-29) yields:

$$ds = \frac{c_{\mu_0 H}}{T} dT + \left(\frac{\partial v M_{an}}{\partial T}\right)_{\mu_0 H} d\mu_0 H_{int} \tag{4-32}$$

Since only the zero-field specific heat is known for this material (this information was also obtained from Astronautics), Eq. (4-32) must be integrated first along a line of constant reference applied field ($\mu_0 H_{ref}$ = 0 Tesla) from a reference temperature (T_{ref}) to the temperature of interest (T) :

$$s\left(T = T, \mu_0 H = \mu_0 H_{ref}\right) - s\left(T = T_{ref}, \mu_0 H = \mu_0 H_{ref}\right) = \int_{T_{ref}}^{T} \frac{c_{\mu_0 H = \mu_0 H_{ref}}}{T} dT \tag{4-33}$$

where $c_{\mu_0 H = \mu_0 H_{ref}}$ is the constant field specific heat at the reference field. Note that the second term on the right hand side of Eq. (4-32) vanishes for this integration since the field is not changing ($d\mu_0 H = 0$). Equation (4-32) can subsequently be integrated from the reference field and the temperature of interest to the field of interest ($\mu_0 H$):

$$s\left(T = T, \mu_0 H = \mu_0 H\right) - s\left(T = T, \mu_0 H = \mu_0 H_{ref}\right) = \int_{\mu_0 H_{ref}}^{\mu_0 H} \left(\frac{\partial v M_{an}}{\partial T}\right)_{\mu_0 H, T} d\mu_0 H_{int} \tag{4-34}$$

Now note that, in this case, the first term on the right side of Eq. (4-32) vanishes since the temperature is not changing. Also, the derivative of the anhysteretic magnetization with respect to temperature at constant field must be evaluated at the temperature of interest (T). Adding Eqs. (4-33) and (4-34) allows for a full mapping of the entropy function:

$$s\left(T,\mu_0 H\right)-s\left(T=T_{ref},\mu_0 H=\mu_0 H_{ref}\right)=\int_{T_{ref}}^{T}\frac{c_{\mu_0 H=\mu_0 H_{ref}}}{T}dT+\int_{\mu_0 H_{ref}}^{\mu_0 H}\left(\frac{\partial v M_{an}}{\partial T}\right)_{\mu_0 H,T}d\mu_0 H_{int} \qquad (4\text{-}35)$$

For this data set, a reference entropy of 0 was set at a reference temperature of 283 K and a reference field of 0 Tesla:

$$s\left(T=283\text{ K},\mu_0 H=0\text{ T}\right)=0 \qquad (4\text{-}36)$$

Substituting these reference states into (4-35) provides:

$$s\left(T,\mu_0 H\right)=\int_{283\text{ K}}^{T}\frac{c_{\mu_0 H=0}}{T}dT+\int_{0}^{\mu_0 H}\left(\frac{\partial v M_{an}}{\partial T}\right)_{\mu_0 H,T}d\mu_0 H_{\text{int}} \qquad (4\text{-}37)$$

The zero field specific heat capacity ($c_{\mu_0 H=0}$) is known as a function of temperature for $La(Fe_{0.885}Si_{0.115})_{13}H_{1.21}$ and is presented in Figure 4-10 below. Note that the zero field specific heat becomes very large at the Curie temperature due to the ferromagnetic to paramagnetic phase transition.

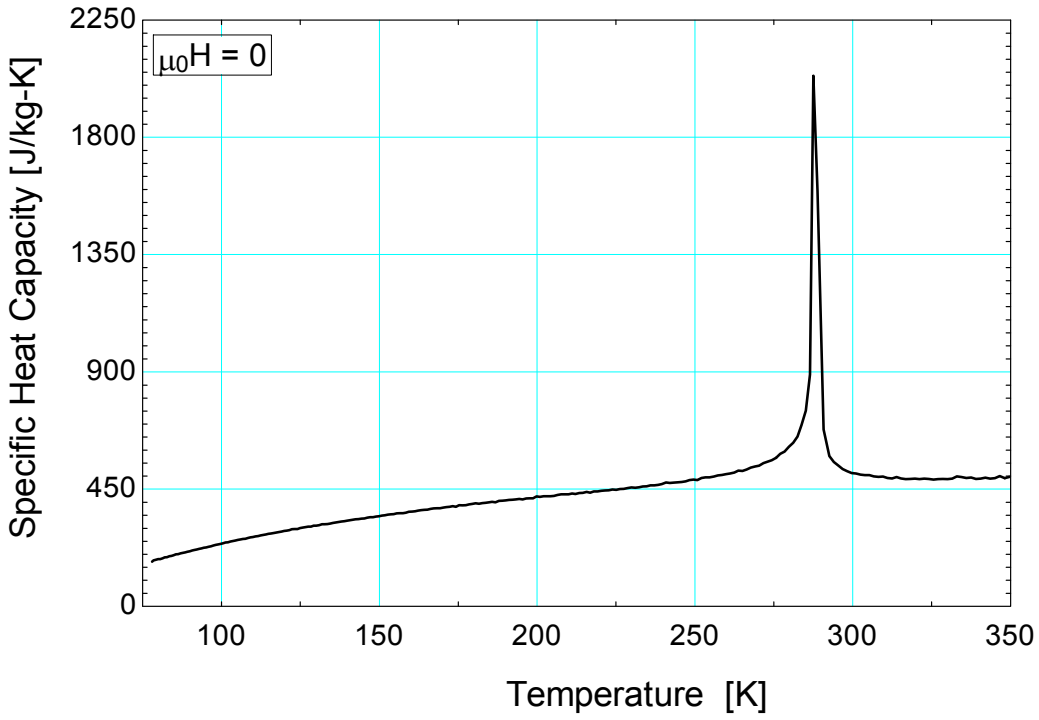

Figure 4-10. Zero field specific heat for $La(Fe_{0.885}Si_{0.115})_{13}H_{1.21}$ as a function of temperature.

Utilizing the specific heat capacity data presented in Figure 4-10 and the adjusted anhysteretic magnetization data provided in Figure 4-7, the specific entropy can be calculated with Eq. (4-37). The specific entropy as a function of temperature and applied field near the Curie temperature for $La(Fe_{0.885}Si_{0.115})_{13}H_{1.21}$ is shown in Figure 4-11. The large dip in the specific entropy surface along the Curie temperature isotherm illustrates the magnetocaloric effect. For this material, the maximum isothermal specific entropy decrease is approximately 15.7 $\frac{J}{kg\text{-}K}$ for a field change from 0 to 2 Tesla.

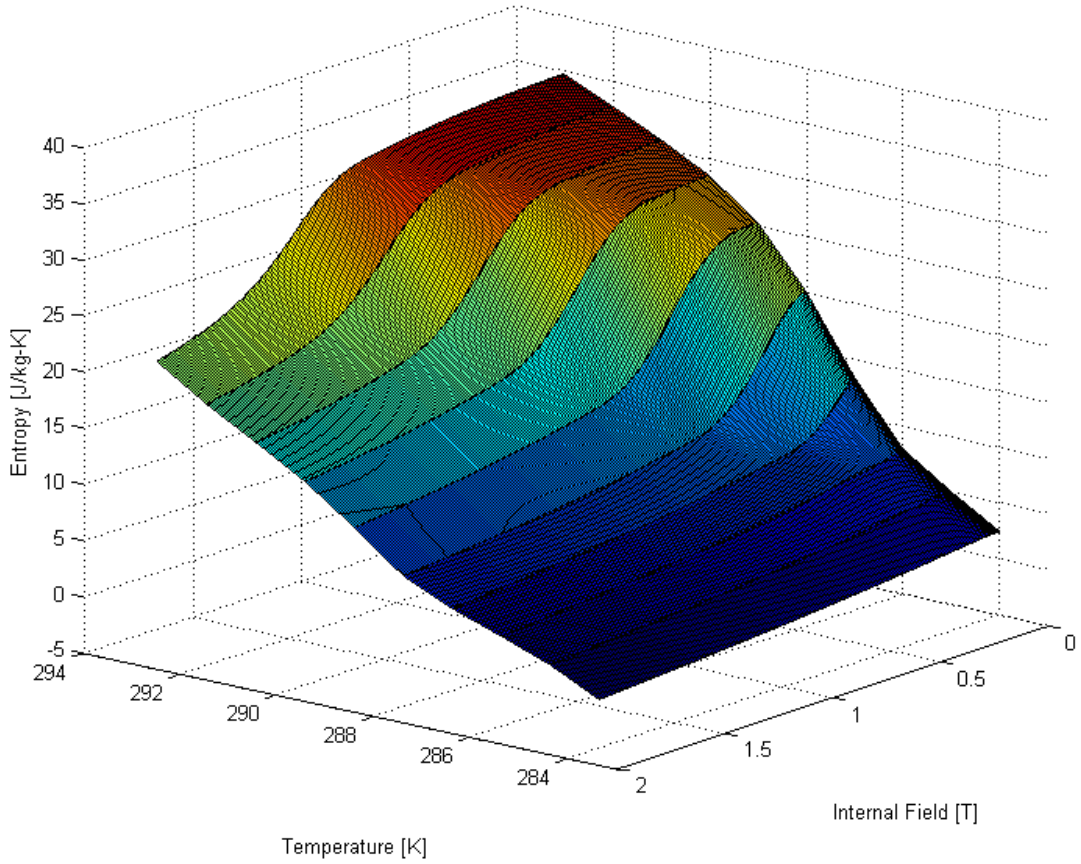

Figure 4-11. Specific entropy of $La(Fe_{0.885}Si_{0.115})_{13}H_{1.21}$ as a function of temperature and internal field with. Reference entropy of 0 is set at 283 K and 0 applied field.

REFERENCES

1. Pecharsky, V.K. and J.K.A. Gschneidner, *Giant Magnetocaloric Effect in $Gd_5(Si_2Ge_2)$.* Physical Review Letters, 1997. **78**(23): p. 4494.

2. Brillouin, L., *Les moments de rotation et le magnétisme dans la mécanique ondulatoire.* J. Phys. Radium, 1927. **8**(2): p. 74-84.

3. Jiles, D., *Introduction to Magnetism and Magnetic Materials*. 2nd Edition ed. 1998: CRC Press. 568.

4. Gschneidner, K.A., V.K. Pecharsky, and A.O. Tsokol, *Recent developments in magnetocaloric materials.* Reports on Progress in Physics, 2005. **68**(6): p. 1479.

5. Von Ranke, P.J., N.A. de Oliveira, and S. Gama, *Understanding the influence of the first-order magnetic phase transition on the magnetocaloric effect: application to Gd5(SixGe1-x)4.* Journal of Magnetism and Magnetic Materials, 2004. **277**(1-2): p. 78-83.

6. Goldfarb, R.B., *Demagnetization Factors*, in *Concise Encyclopedia of Magnetic & Superconducting Materials*, J. Evetts, Editor. 1992: Oxford.

7. Peksoy, O. and A. Rowe, *Demagnetizing effects in active magnetic regenerators.* Journal of Magnetism and Magnetic Materials, 2005. **288**: p. 424-432.

8. Bozorth, R.M., *Ferromagnetism*. Bell Telephone Laboratories series. 1951: Van Nostrand. xvii, 968 p.

9. Dai, W., et al., *Application of high-energy Nd-Fe-B magnets in the magnetic refrigeration.* Journal of Magnetism and Magnetic Materials, 2000. **218**(1): p. 25-30.

Chapter 5 PARAMETRIC STUDIES

5.1 Refrigeration Capacity Curves

Magnetic coolers, like vapor compression refrigeration systems, have characteristic refrigeration capacity curves that show the refrigeration capacity and coefficient of performance (*COP*) as a function of the heat transfer fluid mass flow rate. In the case of vapor compression systems, the working fluid is both the refrigerant and the heat transfer fluid. For an AMRR system, the thermodynamic working substance is the solid magnetocaloric material and the mass flow rate refers to the heat transfer fluid. Figure 5-1 shows the *COP* and refrigeration capacity ($\dot{Q}_{ref}$) as a function of the heat transfer fluid mass flow rate amplitude for a properly configured AMRR system with SOMT material Gd-Er as the magnetic refrigerant. Shown are curves depicting beds that are consist of a single material and infinitely layered. Table 5-1 presents the inputs to the AMRR model used to generate Figure 5-1 and Figure 5-2. The mass flow and magnetic field profiles used for this study are shown in Figure 5-3 and Figure 5-4, respectively.

Table 5-1. Inputs to AMRR model for refrigeration curves

Parameter	Value	Parameter	Value
cycle time	0.2 s	dwell ratio	1/2
max magnetic field	1.5 T	regenerator type	packed sphere
heat transfer fluid	water	particle diameter	0.0002 m
porosity	0.36	motor efficiency	0.9
heat rejection temperature	310 K	pump efficiency	0.7
load temperature	299 K	number of beds	6
aspect ratio	0.2	regenerator volume	6 L

In the case of an infinitely layered bed, the Curie temperature (T_{Curie}) is assumed to vary linearly between the hot and cold reservoirs according to:

$$T_{Curie}(x) = T_H - (T_H - T_C)\frac{x}{L} \tag{5-1}$$

where x/L is the dimensionless regenerator position, and T_H and T_C are the hot and cold reservoir temperatures, respectively. In the case of a bed composed of a single material (i.e., a single layer bed), the Curie temperature is assumed to be a constant and is evaluated as the arithmetic mean of the hot and cold reservoir temperatures:

$$T_{Curie} = \frac{(T_H + T_C)}{2} \tag{5-2}$$

Note the Curie temperature is not a function of regenerator position in this case.

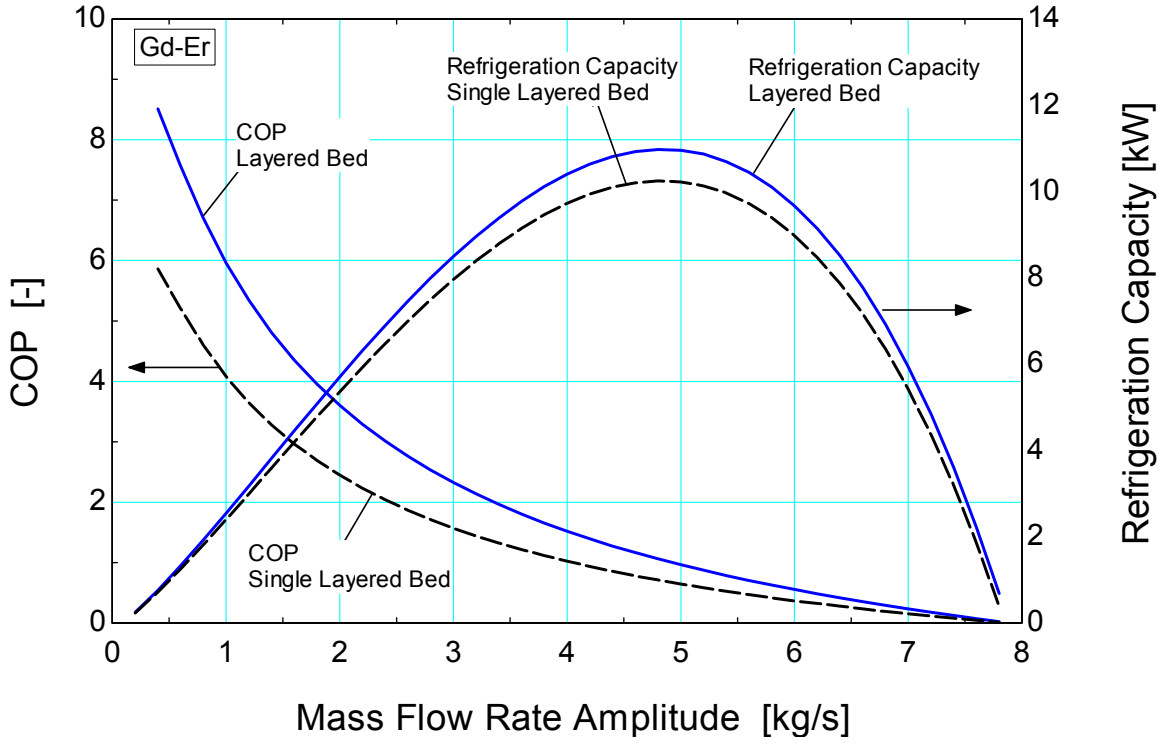

Figure 5-1. *COP* and refrigeration capacity as a function of heat transfer fluid mass flow rate amplitude for Gd-Er. Curves for single layered and infinitely layered beds are shown.

As Figure 5-1 illustrates, there exist two mass flow rate amplitudes that can achieve a given refrigeration capacity, up to some maximum possible refrigeration capacity for the bed. The larger mass flow rate amplitude value corresponds to a condition where the regenerator matrix is flooded with heat transfer fluid. This condition is undesirable since the value of the *COP* is reduced dramatically by an increased pump work requirement. For a given refrigeration capacity, the operating condition that

corresponds to the smaller value of mass flow rate should be chosen, since this condition yields a higher *COP*. Also, shown in Figure 5-1 is the effect of layering the regenerator bed. For a given refrigeration capacity, the *COP* at the optimal operating condition is increased by layering.

Figure 5-2 is the refrigeration capacity curve for the FOMT hysteretic material $La(Fe_{1-x}Si_x)_{13}H_y$ showing the curves for cases with and without magnetic hysteresis modeled. The bed is infinitely layered and operates under the condition listed in Table 5-1. The effect of hysteresis on cycle performance becomes less significant at large mass flow rate amplitudes, since hysteretic losses are becoming small relative to the pump work. Additionally, by comparison of Figure 5-2 and Figure 5-1, the potential advantage of FOMT materials over SOMT materials is an increased refrigeration capacity for a given operating condition. For example, the refrigeration capacity for a layered bed with hysteretic $La(Fe_{1-x}Si_x)_{13}H_y$ is approximately five greater than that of the same system operating with a layered bed of Gd-Er for an operating point where the *COP* = 4. Also, Figure 5-2 shows that FOMT type materials may be particularly advantageous for applications requiring large refrigeration capacities.

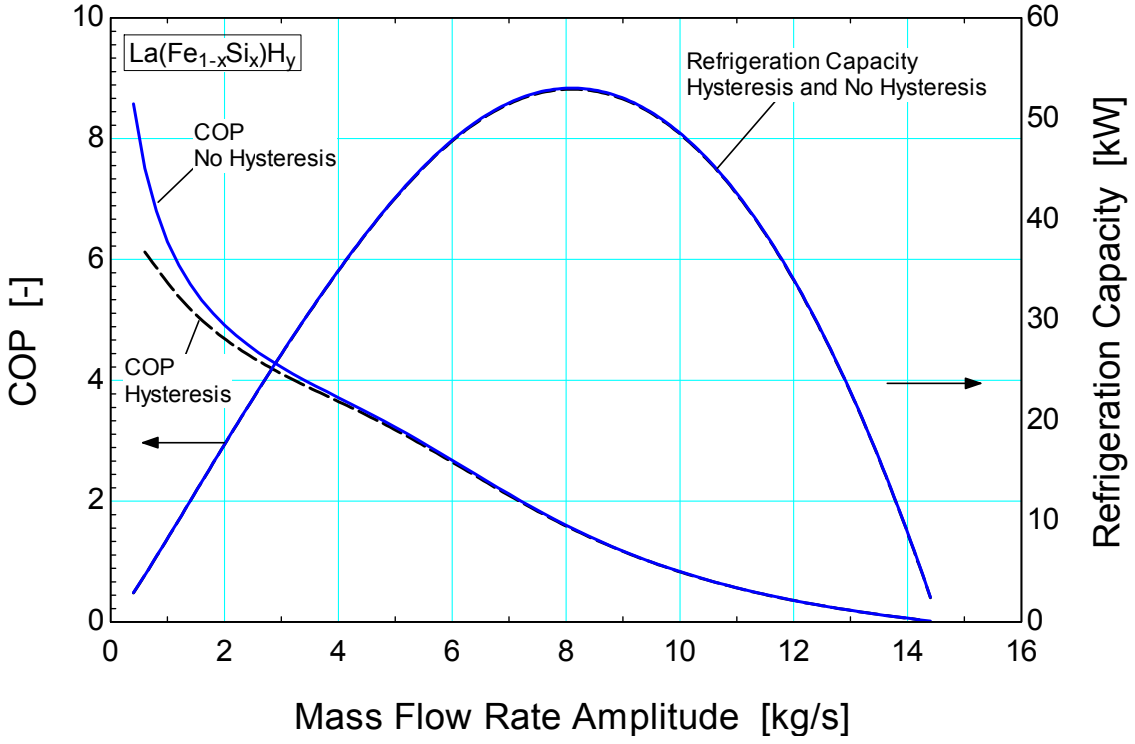

Figure 5-2. *COP* and refrigeration capacity as a function of heat transfer fluid mass flow rate amplitude for $La(Fe_{1-x}Si_x)_{13}H_y$. Curves for infinitely layered beds with and without hysteresis are shown.

5.2 Space Conditioning Study

One potential use for magnetic coolers is space conditioning. A refrigeration capacity of $\dot{Q}_{ref,d} = 5.00$ kW is chosen as a design criteria for a typical space cooling application in this study. A gadolinium-erbium compound ($Gd_{1-x}Er_x$) with a tunable Curie temperature is used to model a second-order magnetic transition (SOMT) material and a lanthanum-iron-silicon hydride compound ($La(Fe_{1-x}Si_x)_{13}H_y$) with a tunable Curie temperature is used to model a first-order magnetic transition (FOMT) material. The beds are layered such that the Curie temperature of each layer varies linearly between load and heat rejection temperatures. Heat exchangers are not explicitly modeled in this study.

5.2.1 Model Inputs

Table 5-2 lists the inputs for the AMRR model for the space conditioning parametric study. These parameters are held constant, while the total regenerator volume (V), aspect ratio (AR), mass flow rate

amplitude ($\dot{m}_{amp}$) are varied. The dwell ratio is defined as the ratio of the time in which the mass flow rate is zero to the total cycle time. The aspect ratio is defined as the length of a single regenerator bed to its diameter.

Table 5-2. Inputs to AMRR model for space conditioning study

Parameter	Value	Parameter	Value
cycle time	0.2 s	dwell ratio	1/2
max magnetic field	1.5 T	regenerator type	packed sphere
heat transfer fluid	water	particle diameter	0.0002 m
porosity	0.36	motor efficiency	0.9
heat rejection temperature	310 K	pump efficiency	0.7
load temperature	299 K	number of beds	6

Figure 5-3 illustrates the mass flow rate as a function of cycle time, where the peak and trough represent the positive and negative of the specified mass flow rate amplitude, respectively. Note that the mass flow rate is zero for half of the cycle time, as specified by the dwell ratio listed in Table 5-2.

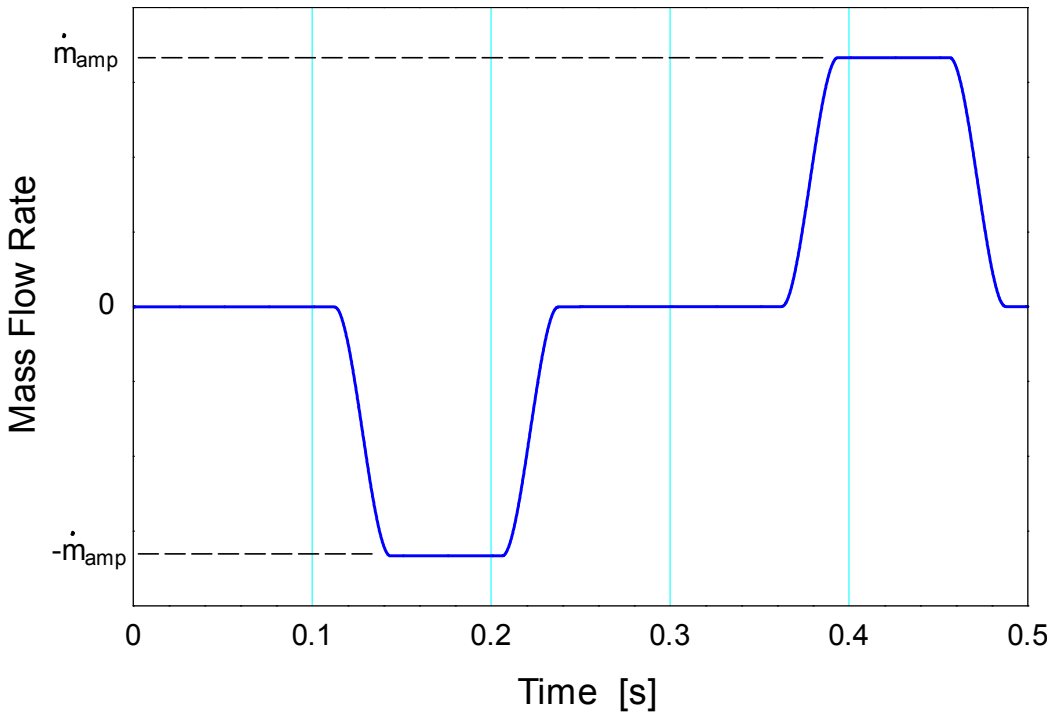

Figure 5-3. Mass flow rate as a function of cycle time.

Figure 5-4 shows the applied magnetic field as a function of time. During the first quarter of the cycle, the magnetic field is linearly ramped from zero to its maximum value; it then remains at its maximum value for the next quarter, decreases linearly from its maximum value to zero during the third quarter, and finally is zero for the final quarter of cycle time. The mass flow rate and magnetic field profiles are only functions of time, and do not vary spatially across the regenerator bed.

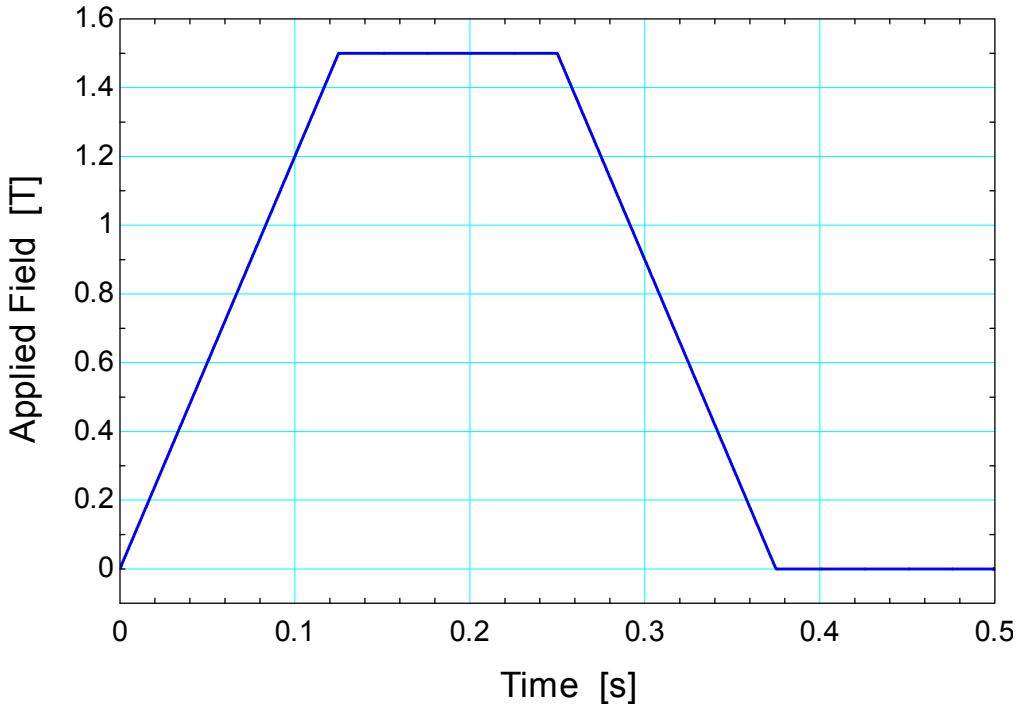

Figure 5-4. Applied magnetic field as a function of cycle time.

5.2.2 Design Strategy

The UW AMRR model requires inputs such as an initial temperature distribution, magnetocaloric refrigerant material, working fluid, regenerator geometry, magnetic field profile, and mass flow profile. The model begins with an initial temperature distribution and numerically iterates the partial differential equations forward through time until it reaches a temperature distribution that satisfies the convergence criteria for steady state regenerator operation. The main outputs of the model include the regenerator and fluid temperature distributions, from which important performance metrics such as the coefficient of

performance (*COP*) and refrigeration capacity ($\dot{Q}_{ref}$) can be calculated for a given magnetocaloric refrigerant. The list of required inputs is outlined in detail in Chapter 3.

In order to specify a refrigeration capacity for a given regenerator volume and aspect ratio and determine the corresponding mass flow rate amplitude, it is necessary to provide a guess value for the fluid flow rate amplitude and check the refrigeration capacity that is output against the desired capacity. It is best to provide a small mass flow rate as a guess value. A "small" mass flow rate in this sense is taken relative to the size of the regenerator and desired cooling capacity. A small mass flow rate initial guess ensures that the bed is not in the overloaded region of the refrigeration curve (as explained in Section 5.1), which ensures that the operating condition that is ultimately identified will correspond to the optimal *COP*. If the refrigeration capacity is above the design refrigeration capacity, then a smaller mass flow rate amplitude than the initial guess is required to achieve the desired cooling capacity at the optimal *COP*. If it is less than the design refrigeration capacity, then the mass flow rate amplitude must be incrementally increased until the design refrigeration capacity is reached. The iterative process is outlined in the flow diagram presented as Figure 5-5. This process is repeated for various combinations of volume and aspect ratio.

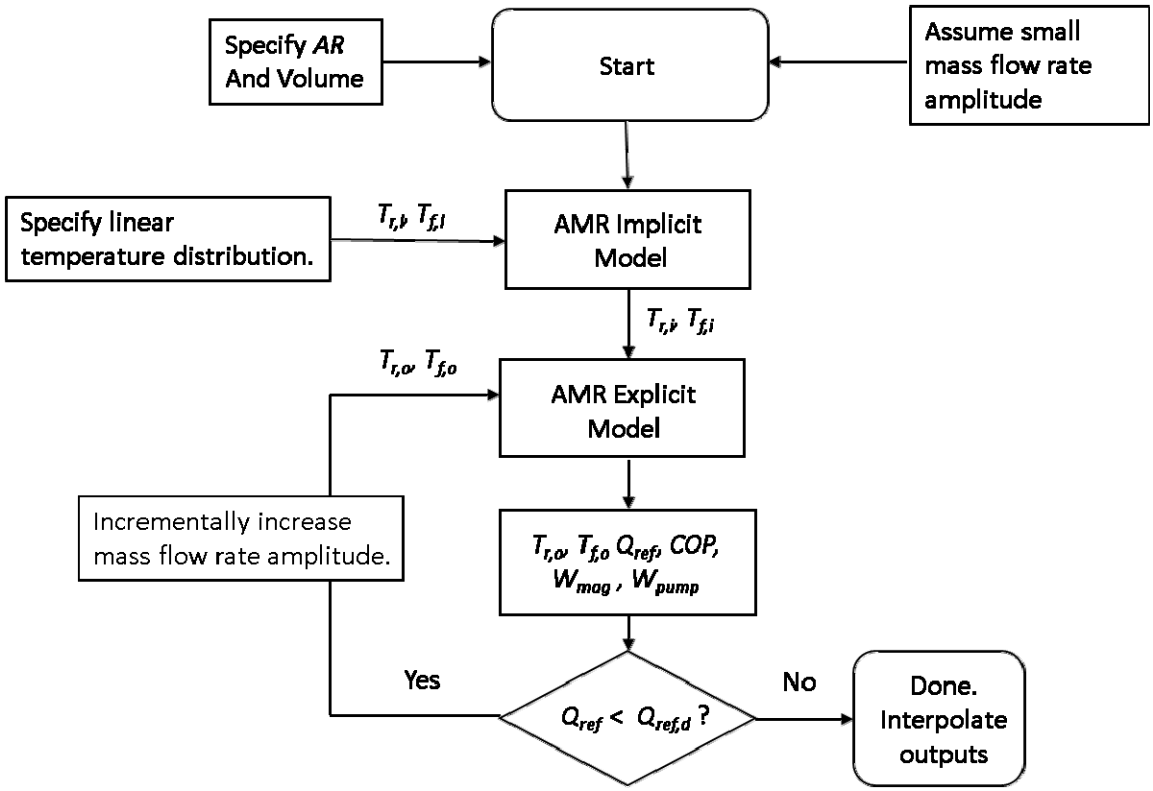

Figure 5-5. Model flow chart to find specified refrigeration capacity.

5.2.3 Modeling Results

For a given regenerator volume and refrigeration capacity, there exists an optimal aspect ratio that balances axial conduction and pressure drop losses and therefore yields a maximum coefficient of performance. Thus, for each volume, the aspect ratio is varied until an optimal value of the *COP* is found using the golden section search optimization technique.

Regenerator Volume

For a fixed load temperature of T_C = 299 K, the regenerator volume is varied to examine its effect on *COP* at the optimal aspect ratio for each volume. All other model parameters are held constant at the values listed in Table 5-2. Figure 5-6 shows the coefficient of performance (*COP*) as a function of regenerator volume; each point on the curve is associated with a unique, optimal aspect ratio and assumes

a layered bed with 60 layers for each material. Figure 5-7 shows the corresponding optimal aspect ratio as a function of volume for each material. The three materials simulated are the SOMT material $Gd_{1-x}Er_x$, and the FOMT material $La(Fe_{1-x}Si_x)_{13}H_y$; the FOMT material is modeled with and without hysteresis effects.

By inspection of Figure 5-6, it is clear that the hysteresis losses become greater with an increasing volume. Consequently, for a given refrigeration capacity and temperature span, there exists an optimal regenerator volume where the *COP* is maximized. For a 5 kW application with T_C = 299 K and T_H = 310 K, Figure 5-6 demonstrates that a magnetic cooler with layered $La(Fe_{1-x}Si_x)_{13}H_y$ as the active refrigerant performs better at this optimal volume (~ 4.3 L) than it would with layered $Gd_{1-x}Er_x$. At larger regenerator volumes, above approximately 7 liters, the layered gadolinium-erbium refrigerant outperforms the FOMT $La(Fe_{1-x}Si_x)_{13}H_y$ refrigerant.

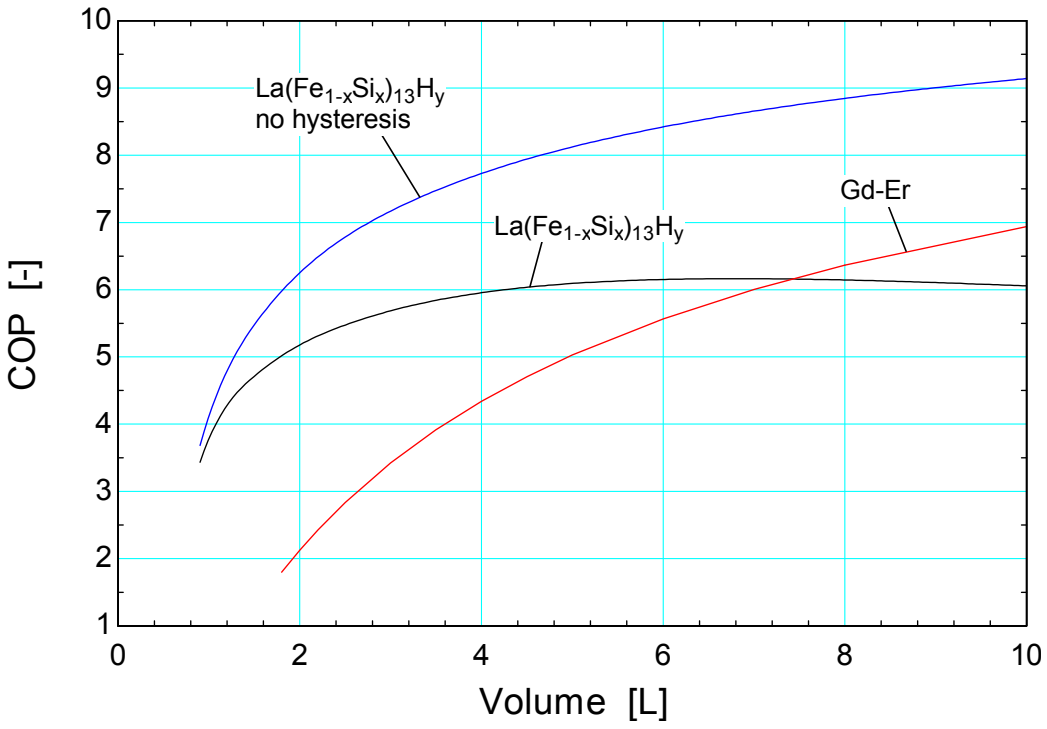

Figure 5-6. *COP* as a function of regenerator volume at its optimal aspect ratio and a load temperature of T_C = 299 K for a layered bed with each material indicated.

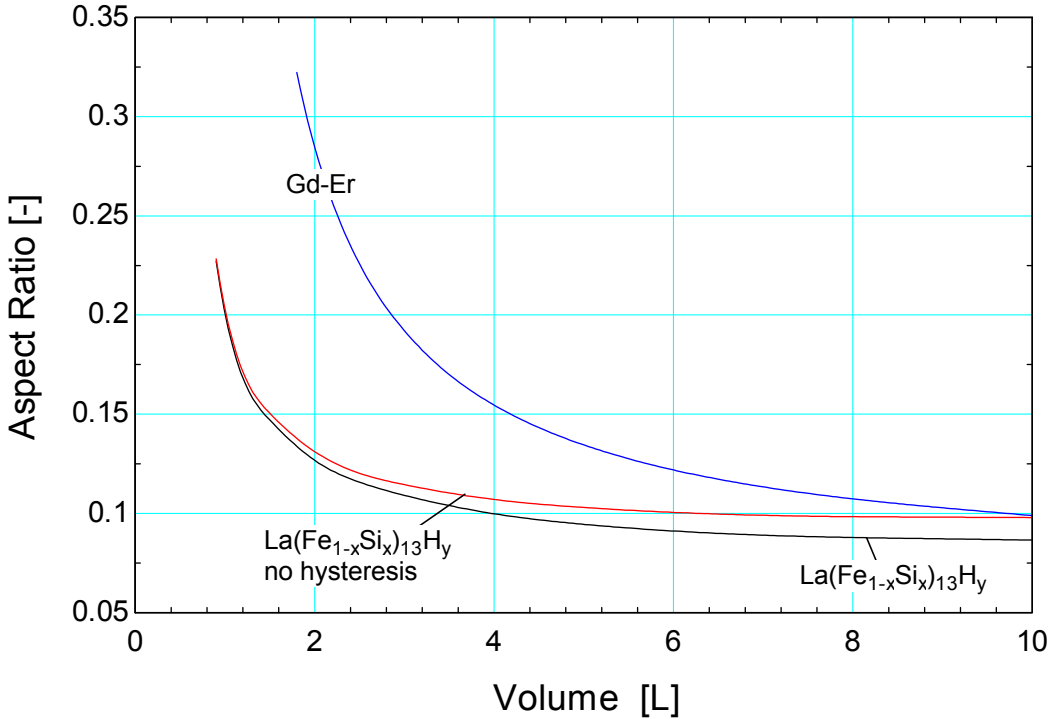

Figure 5-7. Optimal *AR* as a function of regenerator volume at a load temperature of T_C = 299 K for each material.

Load Temperature

In this study, the load temperature (T_C) is varied while the volume is held constant at 8 liters in order to examine the effect of load temperature on the cycle *COP*. The aspect ratio is optimized at each value of load temperature in order to yield the highest *COP*. The number of bed layers for each material is fixed at N_L = 60. Other pertinent model inputs are listed in Table 5-2. Figure 5-8 illustrates the *COP* as a function of the load temperature with the bed set to its optimal aspect ratio for each material. Figure 5-9 shows the aspect ratio that yields the optimal *COP* as a function of the load temperature.

If hysteresis is neglected for $La(Fe_{1-x}Si_x)_{13}H_y$ then it is more efficient than the gadolinium-erbium compound for all load temperatures. However, when hysteresis is accounted for, $La(Fe_{1-x}Si_x)_{13}H_y$ is only more efficient than $Gd_{1-x}Er_x$ at load temperatures that are below approximately 297.5 K, for this particular application and bed volume. For a load temperature of 294 K, the *COP* resulting from $La(Fe_{1-x}Si_x)_{13}H_y$ is approximately 25% greater than that of $Gd_{1-x}Er_x$.

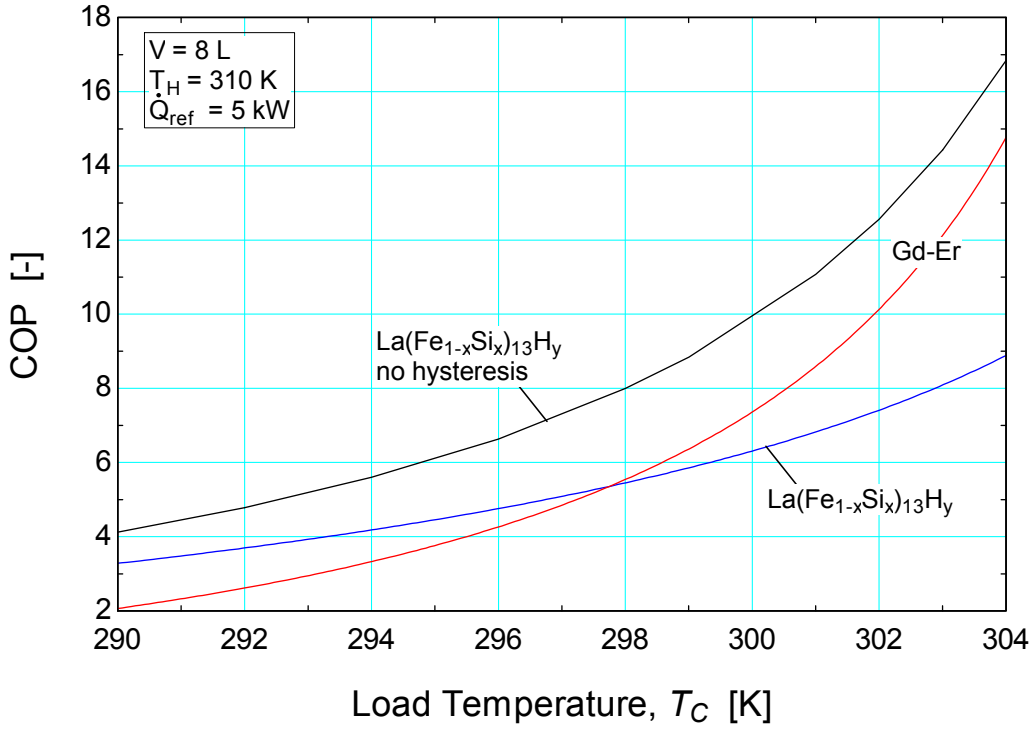

Figure 5-8. *COP* as a function of load temperature (T_C) at the optimal aspect ratio for an infinitely layered regenerator bed with volume of 8 liters.

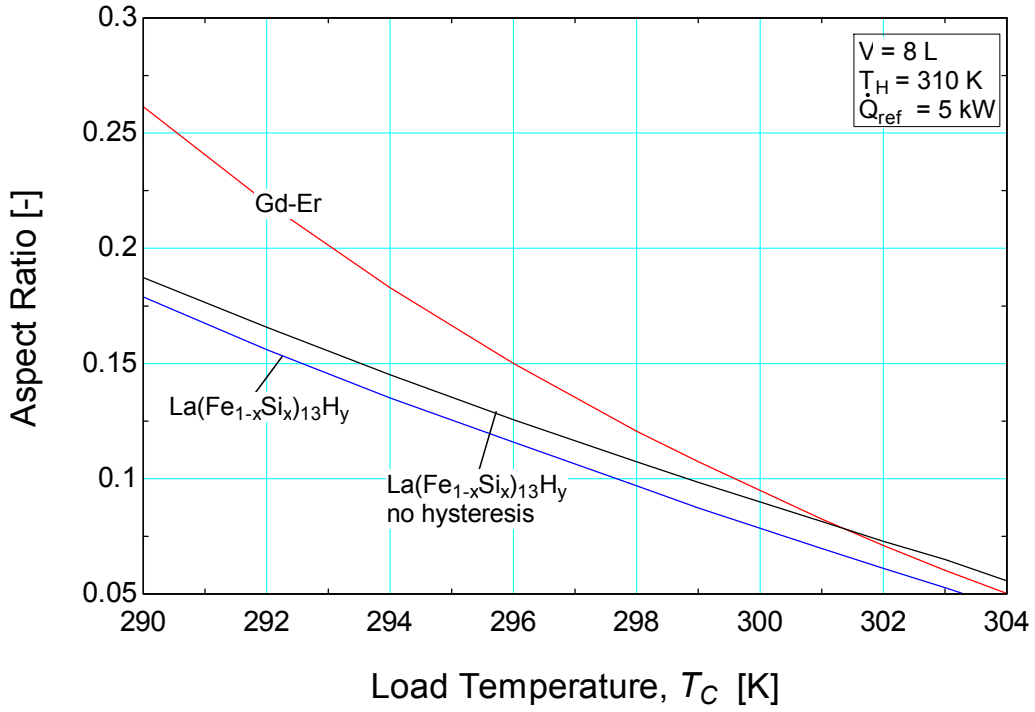

Figure 5-9. Optimal aspect ratio as a function of load temperature (T_C) for a, an infinitely layered regenerator with volume of 8 L.

Figure 5-10 shows the *COP* as a function of load temperature (T_C) at the optimal aspect ratio for a regenerator bed volume of 2 liters. Figure 5-11 and Figure 5-12 show the *COP* as a function of load temperature (T_C) at the optimal aspect ratio for a regenerator bed volume of 4 and 6 liters, respectively. Comparing the figures for regenerator volumes between 2 and 8 liters, the performance of a layered bed with lanthanum-iron-silicon hydride is less sensitive to changes in regenerator volumes than the performance of a bed layered with gadolinium-erbium. As the volume is increased, the load temperature at which the *COP* of an AMR cycle with layered $La(Fe_{1-x}Si_x)_{13}H_y$ and layered Gd-Er is identical decreases. Hence for smaller volumes (2 L), $La(Fe_{1-x}Si_x)_{13}H_y$ will outperform Gd-Er for load temperatures below at least 304 K with a heat rejection temperature (T_H) of 310 K for a 5 kW cooling application.

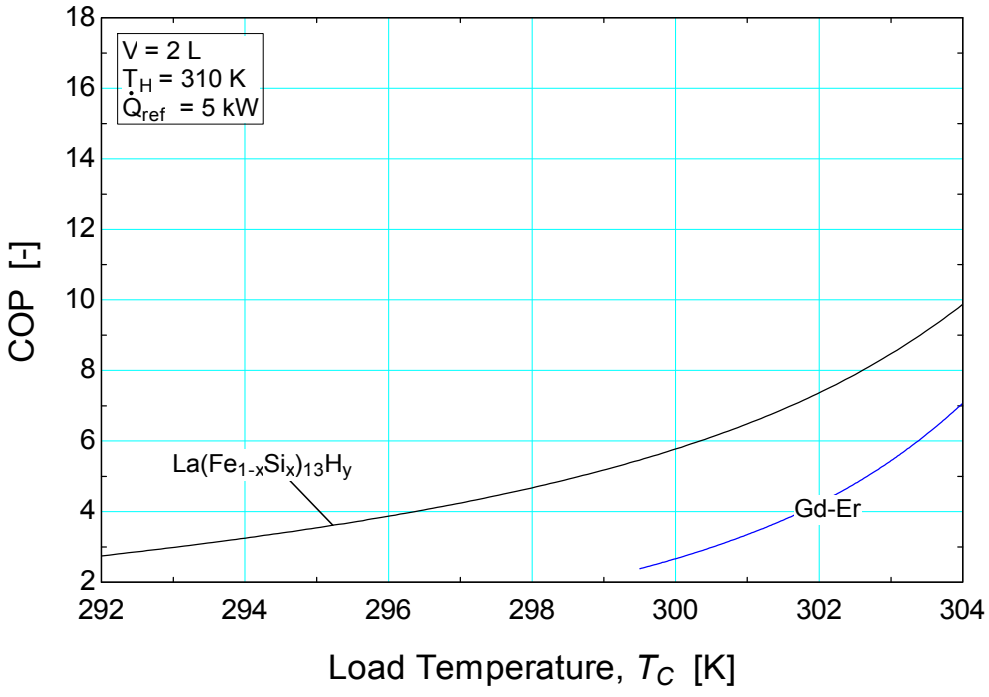

Figure 5-10. *COP* as a function of load temperature (T_C) at the optimal aspect ratio for an infinitely layered regenerator bed with a volume of 2 liters.

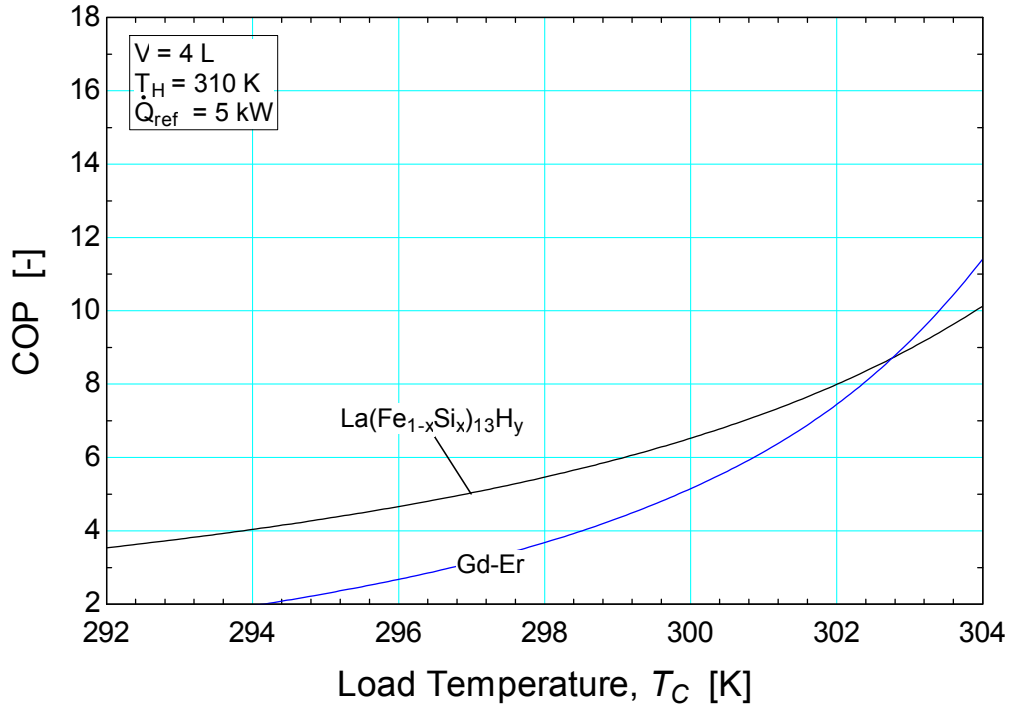

Figure 5-11. ***COP*** **as a function of load temperature (**T_C**) at the optimal aspect ratio for an infinitely layered regenerator bed with a volume of 4 liters.**

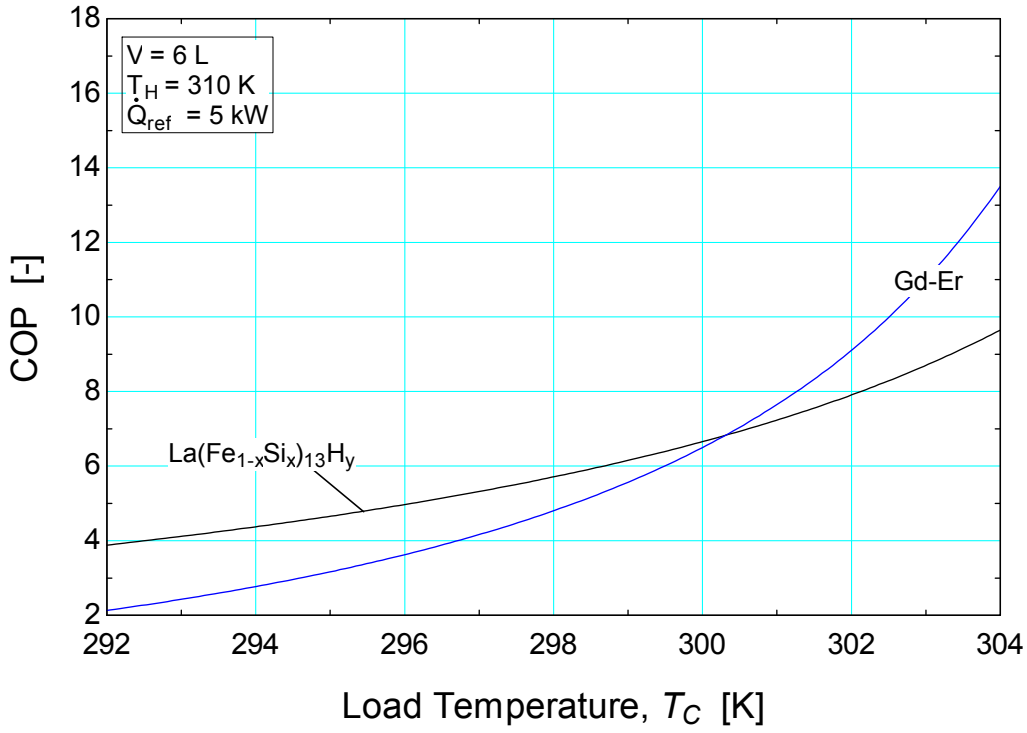

Figure 5-12. ***COP*** **as a function of load temperature (**T_C**) at the optimal aspect ratio for an infinitely layered regenerator bed with a volume of 6 liters.**

In order to compare the performance of the AMR cycle with each refrigerant, the *COP* of Gd-Er can be used as a baseline for comparison. The percent deviation (*%dev*) of the *COP* of $La(Fe_{1-x}Si_x)_{13}H_y$ from the *COP* of Gd-Er can be represented as:

$$\%dev = \frac{COP_{LaFeSiH} - COP_{GdEr}}{COP_{GdEr}} \cdot (100\%) \tag{5-3}$$

where $COP_{LaFeSiH}$ is the coefficient of performance of the AMR cycle with $La(Fe_{1-x}Si_x)_{13}H_y$ as the refrigerant and COP_{GdEr} is the coefficient of performance of the AMR cycle with Gd-Er as the refrigerant. In this study, the *COP* of each material will be evaluated at their respective optimal aspect ratios.

Figure 5-13 presents the *COP* percent deviation as a function of load temperature for various values of regenerator volume. Lines are only drawn for operation points (load temperatures and volumes) where both refrigerants are physically capable of producing 5 kW of refrigeration capacity. Positive percent deviation indicates a performance advantage for $La(Fe_{1-x}Si_x)_{13}H_y$ whereas a negative percent deviation indicates a performance advantage for Gd-Er. For regenerator volumes below 8 liters, the plot indicates that a cycle with $La(Fe_{1-x}Si_x)_{13}H_y$ runs more efficiently than one with Gd-Er for load temperatures below 297 K.

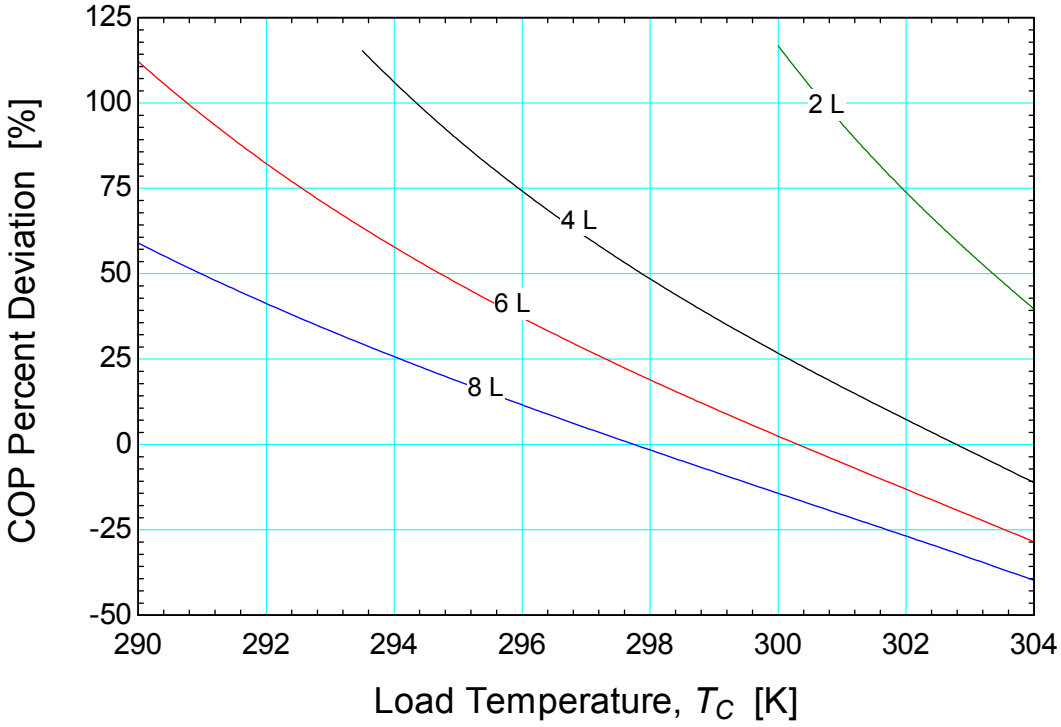

Figure 5-13. *COP* percent deviation as a function of load temperature for various values of regenerator volume for a 5 kW cooling application.

Bed Layering

In the studies presented in the previous sections, the number of layers across each bed was assumed constant at $N_L = 60$. In each regenerator bed, the Curie temperature of each layer varies linearly between the load and heat rejection temperatures. In this study, the effect of the number of layers on cycle performance is evaluated at a specified refrigeration capacity of 5 kW, a regenerator volume of 8 liters, and a heat rejection temperature of 310 K for various load temperatures. Other pertinent model inputs are listed in Table 5-2. The equation used to model the spatial distribution of the Curie temperature is:

$$T_{Curie,i} = T_H - (T_H - T_C)\frac{\left\lceil (i-0.5)\frac{N_L}{Nx} \right\rceil - 0.5}{N_L} \tag{5-4}$$

where i is the spatial node number, Nx is the number of spatial nodes, and N_L is the number of layers. The argument of the $\lceil\ \rceil$ operator indicates rounding up to the nearest integer.

Figure 5-14 shows the coefficient of performance as a function of the number of layers in each regenerator bed for various values of load temperature at their optimal aspect ratio with $Gd_{1-x}Er_x$ as the working refrigerant. For all load temperatures, the *COP* is negligibly affected by an increase in the number of layers above approximately 10 layers. Thus, for applications in this range of load temperatures, a bed with 10 layers is sufficient.

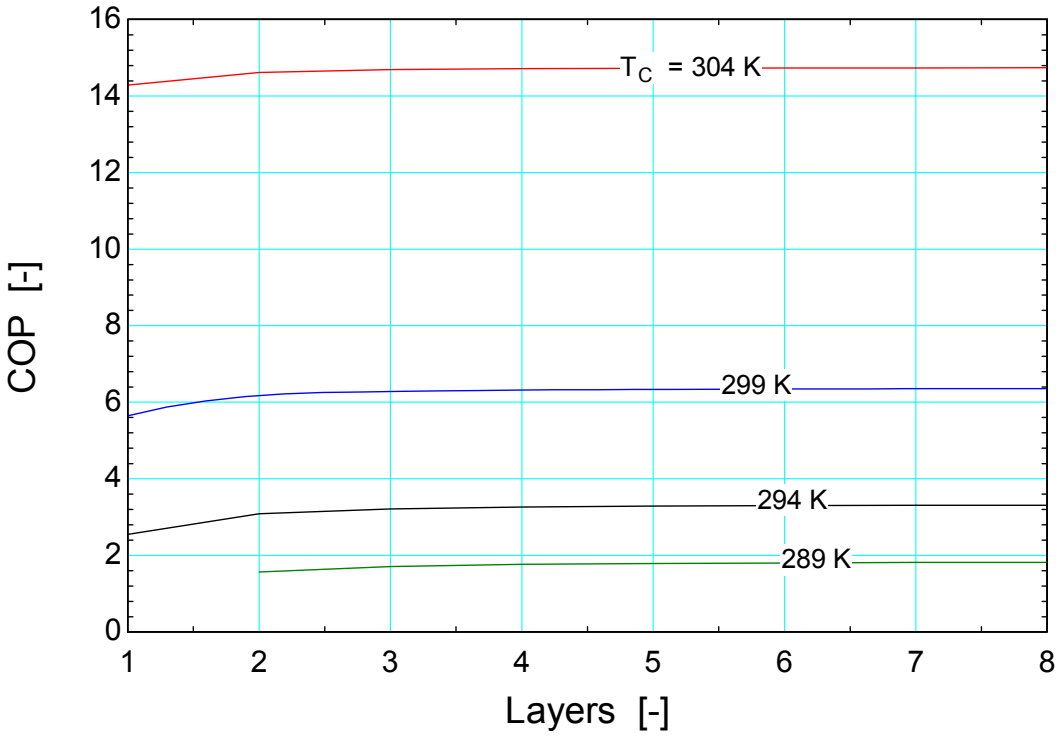

Figure 5-14. *COP* as a function of the number of layers in each regenerator bed for various load temperatures at their respective optimal aspect ratios with $Gd_{1-x}Er_x$ as the refrigerant.

Figure 5-15 shows the *COP* as a function of the number of layers in each regenerator bed for various load temperatures at their respective optimal aspect ratios with $La(Fe_{1-x}Si_x)_{13}H_y$ as the active refrigerant. For each temperature span, there exists a number of layers below which the cycle cannot produce the specified refrigeration capacity of 5 kW. As the temperature span increases, the minimum number of layers required to achieve the desired refrigeration capacity also increases; larger temperature spans require more layers to operate properly. Figure 5-16 shows the minimum number of layers required by an AMRR cycle running with regenerator beds layered with Gd-Er and $La(Fe_{1-x}Si_x)_{13}H_y$ to achieve a

refrigeration capacity of 5 kW at the optimal aspect ratio. The minimum number of layers for a load temperature of 294 K is N_L = 19, as illustrated by Figure 5-16. Thus, in general, a FOMT refrigerant requires more bed layers than a SOMT refrigerant to operate properly at the same refrigeration capacity.

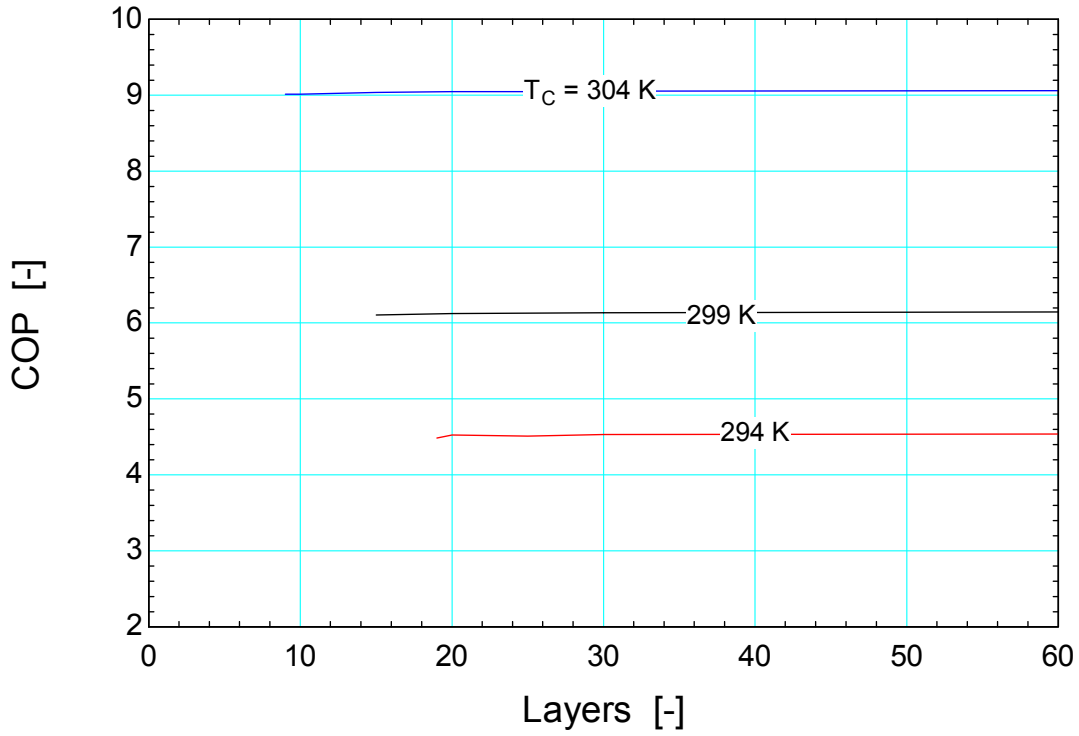

Figure 5-15. *COP* as a function of the number of layers in each regenerator bed for various load temperatures at their respective optimal aspect ratios with $La(Fe_{1-x}Si_x)_{13}H_y$ as the refrigerant.

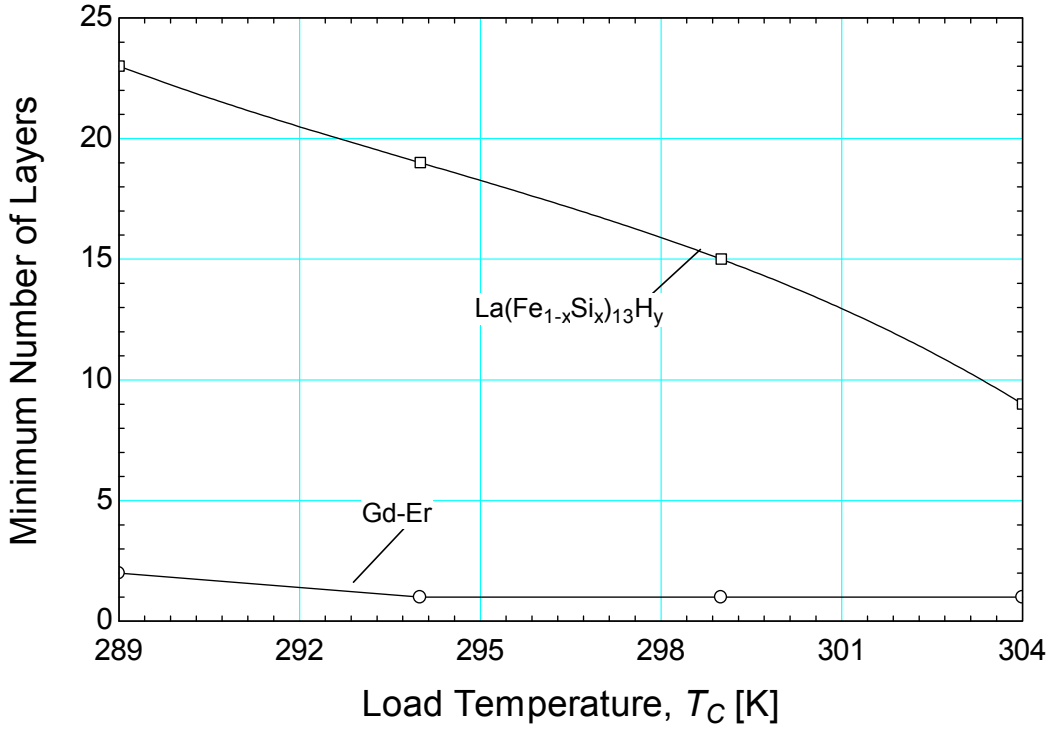

Figure 5-16. Minimum number of layers required each regenerator bed to achieve a refrigeration capacity of 5 kW for AMRR cycle running with Gd-Er and La(Fe$_{1-x}$Si$_x$)$_{13}$H$_y$.

Hysteresis Scaling

In this study, the load temperature, the heat rejection temperature, volume and other model inputs listed in Table 5-2 are held constant, while the hysteresis scaling factor (C_h) is varied from 0 to 6 (0 to 600%). La(Fe$_{1-x}$Si$_x$)$_{13}$H$_y$ is used as the refrigerant in this study and the number of layers is fixed at N_L = 60. A hysteresis scaling factor of 0 indicates no hysteresis in the model while a factor of 1 indicates the amount of hysteresis that La(Fe$_{1-x}$Si$_x$)$_{13}$H$_y$ would normally exhibit under these conditions. Figure 5-17 shows the *COP* at the optimal aspect ratio as a function of percent hysteresis for La(Fe$_{1-x}$Si$_x$)$_{13}$H$_y$ for various regenerator volumes. Percent hysteresis is defined as the hysteresis scaling factor multiplied by 100%.

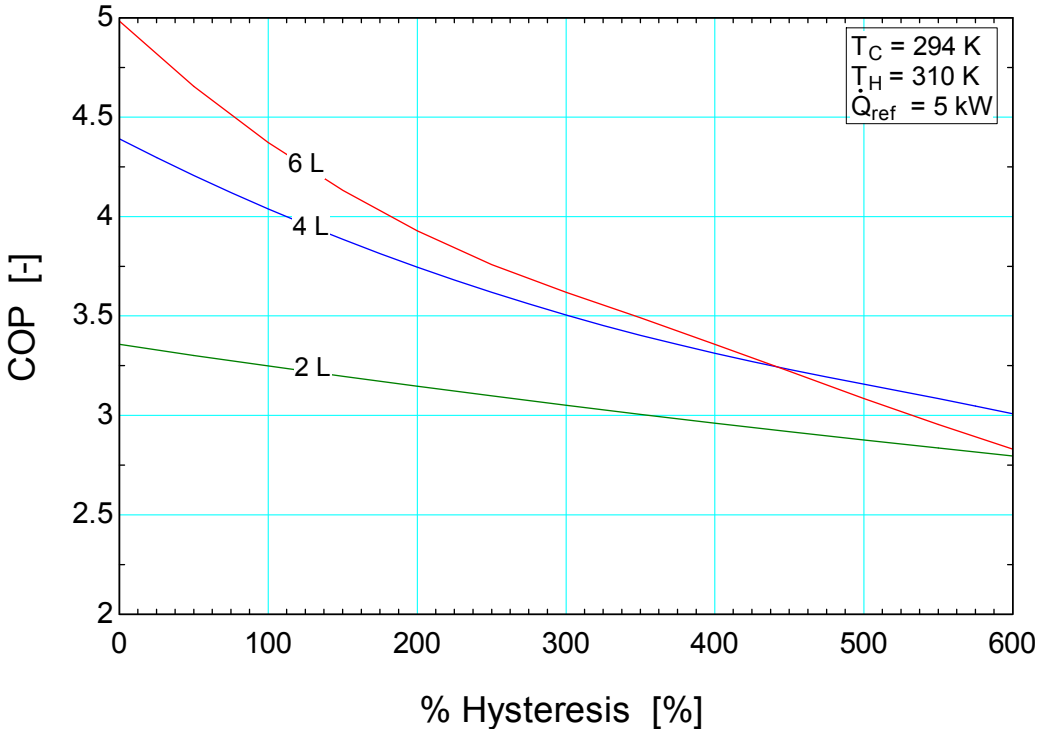

Figure 5-17. COP at the optimal aspect ratio as a function of percent hysteresis for $La(Fe_{1-x}Si_x)_{13}H_y$ for various regenerator volumes. 100% hysteresis indicates normal hysteresis losses for $La(Fe_{1-x}Si_x)_{13}H_y$ under specified conditions.

As shown by Figure 5-17, increasing the hysteresis is detrimental to the *COP* of the cycle for all regenerator volumes. However, for smaller volumes, increasing the percent hysteresis has less effect on cycle performance than it does for larger volumes. This behavior is due to hysteresis being a volumetric loss, which therefore becomes more substantial at larger regenerator volumes. Thus, a well-designed regenerator with a FOMT refrigerant should be small enough to negate hysteretic losses but large enough to provide the required cooling power at an acceptable *COP*.

5.3 Magnetocaloric Property Modulation

There are two parameters that are often used in the literature to characterize magnetocaloric materials: the adiabatic temperature change (ΔT_{ad}) and the isothermal entropy change (Δs_M). These values are expressed for a given change in magnetic field ($\Delta \mu_0 H$), generally from 0 Tesla to a specified value. The specific isothermal entropy change is determined from a material's partial derivative of entropy with respect to magnetic field at constant temperature according to:

$$\Delta s_M\left(T,\mu_0 H,\mu_0 H_1,\mu_0 H_2\right)=\int_{\mu_0 H_1}^{\mu_0 H_2}\left(\frac{\partial s_r}{\partial \mu_0 H}\right)_T d\mu_0 H \tag{5-5}$$

which, by use of the Maxwell relation shown as Eq. (2-4) can be rewritten as:

$$\Delta s_M\left(T,\mu_0 H,\mu_0 H_1,\mu_0 H_2\right)=\int_{\mu_0 H_1}^{\mu_0 H_2}\left(\frac{\partial v_r M_{an}}{\partial T}\right)_{\mu_0 H} d\mu_0 H \tag{5-6}$$

where $\left(\frac{\partial v_r M_{an}}{\partial T}\right)_{\mu_0 H}$ is the partial derivative of the mass specific anhysteretic magnetization with respect to temperature at constant applied field. The parameters $\mu_0 H_1$ and $\mu_0 H_2$ are the initial and final applied magnetic field of integration.

The adiabatic temperature change can be written as:

$$\Delta T_{ad}\left(T,\mu_0 H,\mu_0 H_1,\mu_0 H_2\right)=\int_{\mu_0 H_1}^{\mu_0 H_2}\frac{T}{c_{\mu_0 H}}\left(\frac{\partial v_r M_{an}}{\partial T}\right)_{\mu_0 H} d\mu_0 H \tag{5-7}$$

where $c_{\mu_0 H}$ is the magnetic material mass specific heat capacity at a constant magnetic field. By inspection of Eq. (5-6), the isothermal entropy change is proportional to the partial derivative of the mass specific anhysteretic magnetization with respect to temperature at constant applied field. From Eq. (5-7), the adiabatic temperature change is also proportional to the partial derivative of the mass specific anhysteretic magnetization with respect to temperature at constant applied field and is inversely proportional to the constant applied field specific heat capacity.

Using a set of property data or an equation of state, the adiabatic temperature and isothermal entropy changes can be computed. These values can then be artificially modulated using scaling factors. Changing these parameters with scaling factors allows parametric studies on the mutual effect of ΔT_{ad} and Δs_M on AMRR system performance. The scaling factor C_M is chosen to modify partial derivative of the mass specific anhysteretic magnetization with respect to temperature at constant applied field and the

scaling factor C_c is chosen to modify the mass specific heat at constant applied field. The entropy derivative is written as:

$$ds = C_M \frac{c_{\mu_0 H}}{C_c} dT + C_M \left(\frac{\partial v_r M_{an}}{\partial T} \right)_{\mu_0 H} d\mu_0 H \tag{5-8}$$

In a similar fashion, Eqs. (5-6) and (5-7) can be written to include the scaling factors:

$$\Delta s_M \left(T, \mu_0 H, \mu_0 H_1, \mu_0 H_2, C_M \right) = \int_{\mu_0 H_1}^{\mu_0 H_2} C_M \left(\frac{\partial v_r M_{an}}{\partial T} \right)_{\mu_0 H} d\mu_0 H \tag{5-9}$$

$$\Delta T_{ad} \left(T, \mu_0 H, \mu_0 H_1, \mu_0 H_2, C_c \right) = \int_{\mu_0 H_1}^{\mu_0 H_2} C_c \frac{T}{c_{\mu_0 H}} \left(\frac{\partial v_r M_{an}}{\partial T} \right)_{\mu_0 H} d\mu_0 H \tag{5-10}$$

Note that now the isothermal entropy change and adiabatic temperature change are functions of C_M and C_c, respectively.

Utilizing the scaling factors, a parametric study is conducted to examine the effect of the adiabatic temperature and isothermal entropy changes on AMRR cycle performance. The inputs for the UW AMRR model are listed in Table 5-3. The mass flow and magnetic field profiles are same as described in Section 5.2 .

Table 5-3. Inputs to AMRR model for magnetocaloric parameter study

Parameter	Value	Parameter	Value
cycle time	0.2 s	dwell ratio	1/2
max magnetic field	1.5 T	regenerator type	packed sphere
heat transfer fluid	water	particle diameter	0.0002 m
porosity	0.36	motor efficiency	0.9
heat rejection temperature	310 K	pump efficiency	0.7
load temperature	299 K	number of beds	6

Figure 5-18 shows the *COP* at the optimal aspect ratio of layered bed with a Gd-Er compound as a function of adiabatic temperature and (negative) isothermal entropy change. The field change is from 0 to

1.5 Tesla. The base properties of the SOMT Gd-Er compound were modified according to Eqs. (5-8), (5-9), and (5-10). The volume-specific refrigeration capacity ($\dot{Q}_{ref}/V$) is held constant at 1.25 kW/L. By examination of Figure 5-18, the *COP* of this system is not a strong function of adiabatic temperature change for values above $\Delta T_{ad} = 4$ K, below this value of ΔT_{ad} the *COP* begins to decrease rapidly.

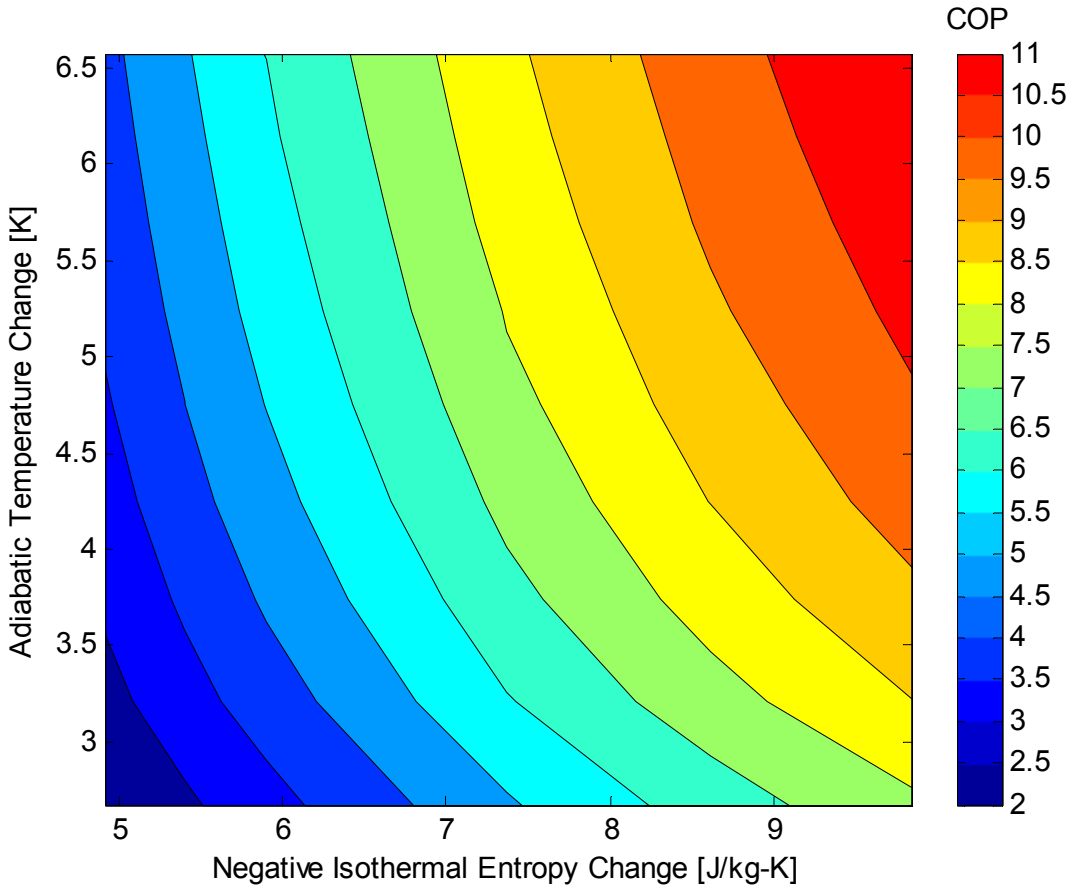

Figure 5-18. *COP* at the optimal aspect ratio as a function of negative isothermal entropy change and adiabatic entropy change for Gd-Er layered bed with a volume specific refrigeration capacity of 1.25 kW/L.

Figure 5-19 shows the regenerator volume specific refrigeration capacity as a function of adiabatic temperature change and isothermal entropy change for a infinitely layered regenerator bed of Gd-Er with a specified *COP* = 4. As the figure shows, the volume specific refrigeration capacity is not a strong

function of adiabatic temperature change above $\Delta T_{ad} = 4$ K for negative isothermal entropy changes below $\Delta s_M = 20 \frac{\text{J}}{\text{kg-K}}$.

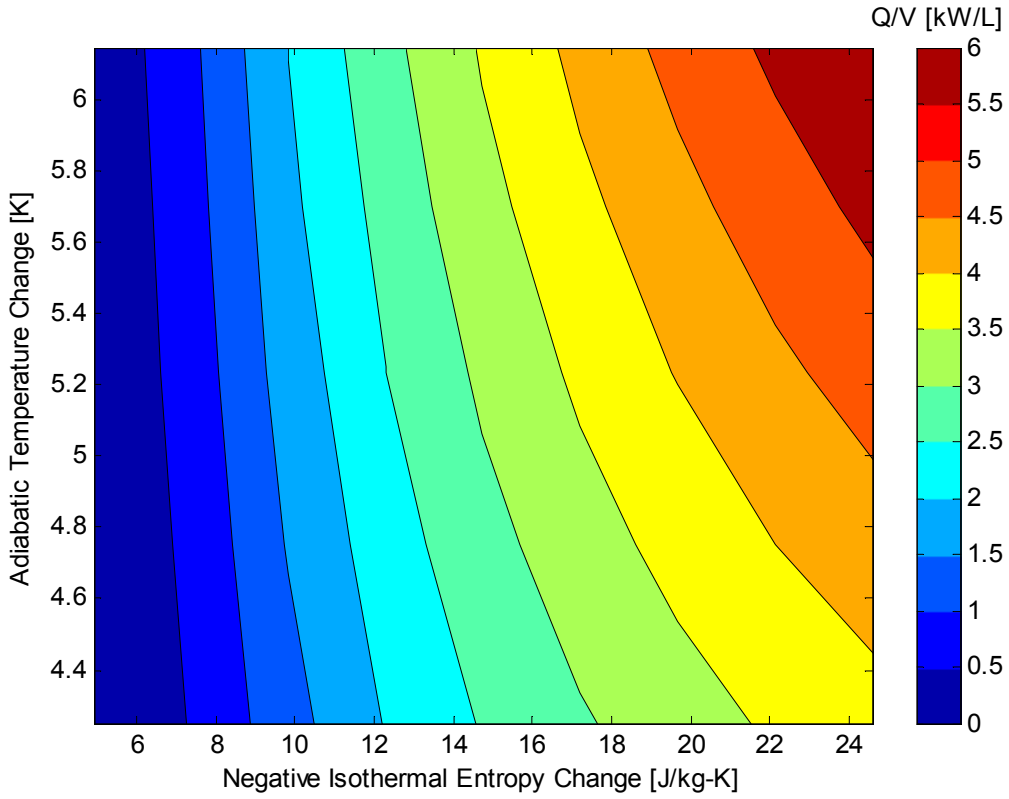

Figure 5-19. Volume Specific refrigeration capacity at the optimal aspect ratio as a function of negative isothermal entropy change and adiabatic entropy change for Gd-Er layered bed with a specified *COP* of 4.

Figure 5-20 is the *COP* at the optimal aspect ratio of a layered bed with modified $La(Fe_{1-x}Si_x)_{13}H_y$ as a function of adiabatic temperature and (negative) isothermal entropy change. The field change is from 0 to 1.5 Tesla and the hysteresis is set to zero. Adiabatic temperature changes below 4 K are shown. In this range, the *COP* becomes a strong function of ΔT_{ad} and only weakly depends on Δs_M.

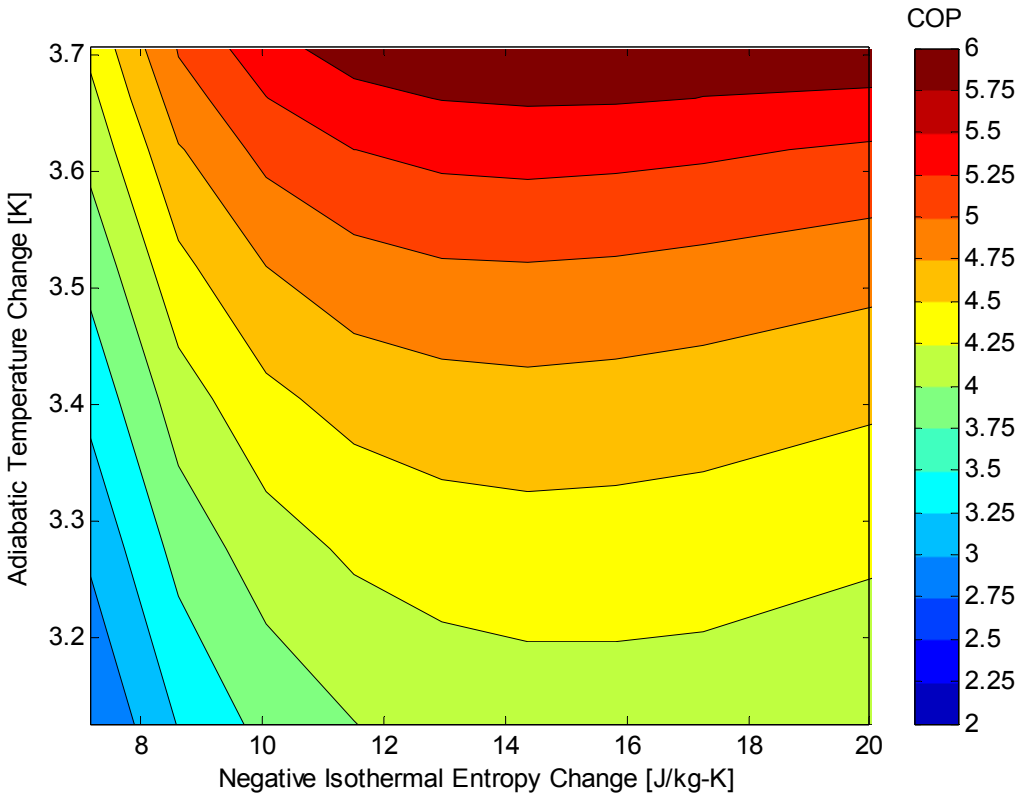

Figure 5-20. *COP* at the optimal aspect ratio as a function of negative isothermal entropy change and adiabatic entropy change for $La(Fe_{1-x}Si_x)_{13}H_y$ layered bed with a volume specific refrigeration capacity of 1.25 kW/L. Hysteresis is set to zero.

Figure 5-21 is the *COP* at the optimal aspect ratio of a layered bed with modified $La(Fe_{1-x}Si_x)_{13}H_y$ as a function of adiabatic temperature and (negative) isothermal entropy change with hysteresis set to unity for a volume of 4 liters. The field change is from 0 to 1.5. Adiabatic temperature changes below 4 K are shown. By comparison to Figure 5-20, the *COP* is slightly less for a hysteretic material. The detriment to hysteresis is relatively small since it was used for a relatively small bed of 4 liters. Again, because hysteresis is a volumetric loss, increasing the bed size increases the hysteretic losses.

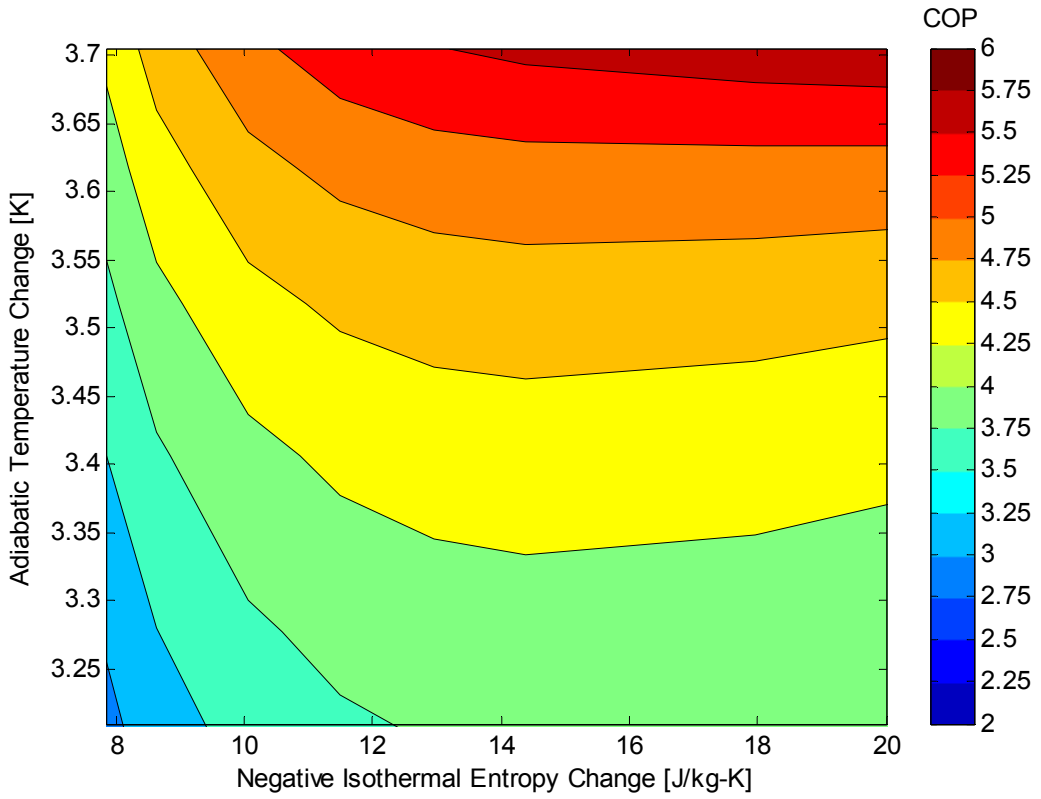

Figure 5-21. ***COP*** **at the optimal aspect ratio as a function of negative isothermal entropy change and adiabatic entropy change for $La(Fe_{1-x}Si_x)_{13}H_y$ layered bed with a volume specific refrigeration capacity of 1.25 kW/L. Hysteresis is set to unity for a volume of 4 L.**

For an infinitely layered regenerator bed in an AMRR cycle for a field change from 0 to 1.5 Tesla, an ideal material would have an adiabatic temperature change above 4 Kelvin and large isothermal entropy change near room temperature, with minimal hysteresis. However, hysteretic losses can be mitigated by designing for a minimal regenerator volume for a particular application.

Chapter 6 CONCLUSIONS

Room temperature magnetic refrigeration is a promising alternative to vapor compression refrigeration because it has a high theoretical efficiency, uses non-ozone depleting refrigerants, and exhibits relatively quiet operation. However, magnetic cooling system design presents numerous challenges that must be overcome before becoming a practical alternative to vapor compression systems. The most encouraging thermodynamic cycle for magnetic refrigeration is the active magnetic regenerative refrigeration (AMRR) cycle using a layered magnetocaloric refrigerant. By the nature of the solid state refrigerant, magnetic coolers require a separate heat transfer fluid to physically transport heat from one location to another, which requires complex pumping systems. These systems also require large magnets and high magnetic fields to operate properly. Additionally, there is currently difficulty understanding the thermodynamics of these systems since detailed magnetocaloric equations of state are not readily available for exotic refrigerants that exhibit the most promise for use in magnetic coolers.

Pure gadolinium is considered the baseline magnetic refrigerant for use in magnetic coolers because its magnetocaloric properties near room temperature have been measured and modeled most precisely. Gadolinium exhibits a modest magnetocaloric effect and has been successfully used in prototype magnetic coolers. In 1997, Pecharsky and Gschneidner announced the discovery of the giant magnetocaloric effect (GMCE) in $Gd_5(Si_{1-x}Ge_x)_4$ type compounds. Due to the nature of their phase transition near room temperature, these compounds exhibit a large magnetocaloric effect but also exhibit magnetic hysteresis. Since the discovery of the GMCE, several promising hysteretic compounds that exhibit a GMCE under magnetic field changes have been discovered, including $La(Fe_{1-x}Si_x)_{13}H_y$ compounds. These materials have a tunable Curie temperature, making them ideal for use in a layered regenerator bed. Extensive property data of these materials are not publically available, and the effects of magnetic hysteresis on AMRR performance are not well understood.

This thesis presents a thermodynamic model of magnetic hysteresis that treats the phenomenon as a form of internal entropy generation. This model of magnetic hysteresis is based on the Jiles-Atherton model of magnetic hysteresis. The proposed model defines the magnetization induced in the material in terms of reversible, anhysteretic magnetization and irreversible, hysteretic magnetization components. For an incompressible substance, the anhysteretic magnetization (M_{an}) is a function of applied magnetic field and temperature only. However, for the same incompressible substance (assuming no thermal hysteresis), the irreversible magnetization (M_{irr}) is a complex function of instantaneous applied magnetic field ($\mu_0 H$), temperature (T), maximum applied magnetic field ($\mu_0 H_{max}$), minimum applied magnetic field ($\mu_0 H_{min}$), and the rate of change of applied magnetic field in time ($\frac{\partial \mu_o H}{\partial t}$). Since there are limited property data for hysteretic materials, the irreversible magnetization is treated as being independent of the rate of change of applied field in this thesis.

The proposed thermodynamic model of irreversible magnetization was tested for its effect on the performance of a magnetic Carnot cycle. The irreversible magnetization was defined as a sinusoidal function that is zero at the minimum and maximum applied magnetic fields. The area enclosed by the hysteretic *H-M* curve was shown to be equivalent to the integral of the irreversible magnetization function over 1 cycle, and is representative of the exergy destroyed per cycle due to hysteresis. At a given load and rejection temperature, as the irreversible magnetization function was increased in magnitude, the *COP* of the cycle was shown to decrease. This simple model verified the thermodynamic treatment of hysteresis as a source of internal entropy generation in the ideal limit of a Carnot cycle.

The model of entropy generation that was implemented in the Carnot cycle model was subsequently implemented into the governing regenerator equations used in the the one-dimensional University of Wisconsin numerical model developed by Engelbrecht (2005, 2008). By combining the first and second laws of thermodynamics, the internal energy of the regenerator material is resolved in terms of the temperature and magnetic field driven components, the latter of which includes the entropy generated due to hysteresis. The entropy generation rate can be further resolved in terms of the irreversible

magnetization according to Eq. (2-8). The equations are subsequently discretized and can be solved for steady state operating conditions.

Chapter 4 discussed magnetic equations of state for ferromagnetic, paramagnetic, and metamagnetic phase transition materials. These equations of state are all based on the Brillouin function. For first order magnetic transition type materials, the magnetic equation of state model proposed by Von Ranke et al. (2004) may be appropriate. The anhysteretic magnetization as a function of applied field and temperature can be estimated from raw magnetization data. One method is to estimate it as the arithmetic mean of the induced magnetization while the applied field is increasing and magnetization wiled the field is for a given temperature and applied magnetic field. For a given temperature and applied field, the irreversible magnetization is thus the absolute value of the difference between the anhysteretic magnetization and actual magnetization (field increasing or decreasing). These data can, along with data for a constant field specific heat, be used to create a map of the magnetocaloric material entropy as a function of temperature and applied field to be used by the 1D UW model.

The effect of magnetic hysteresis of AMRR systems was quantified through parametric studies with the hysteresis-modified 1D UW model. For a specified refrigeration capacity and load temperature, a bed layered with $La(Fe_{1-x}Si_x)_{13}H_y$ showed a higher *COP* at relatively small volumes when compared to a bed layered with Gd-Er. Furthermore, for a specified refrigeration capacity and regenerator volume, a bed layered with $La(Fe_{1-x}Si_x)_{13}H_y$ was shown to outperform a bed layered with Gd-Er at large temperature spans. As regenerator volume increases, hysteretic losses outweigh the capacity gains associated with adding more refrigerant. Parametric studies also implied that the adiabatic temperature change may not have a significant effect on the performance of a layered bed for $\Delta T_{ad} > 4$ K.

6.1 Recommendations for Future Work

There are several areas for future work to improve upon the accuracy of the model:

- Implementation of an accurate equation of state for a hysteretic material, which includes the irreversible magnetization.
- Investigate the dependence of irreversible magnetization for a given material on the minimum and maximum applied magnetic fields and the rate at which the applied field is ramped.
- Experimental validation of the magnetic hysteresis model.
- Investigate the effect of hysteresis on an AMRR heat pump cycle.
- Model the thermal interaction between the regenerator bed and the regenerator housing.

Appendix A SINGLE SHOT MATLAB MODEL

```
clear;
muH_max=2;          %maximum applied magnetic field in Tesla
vdM_max=0.1;        %mass specific irreversible magnetization in A-m^2/kg
cmu0H=0.5;          %specific heat in J/kg-k
rho=1;              %density of fictional material in kg/m^3
tau=4;              %period of magnetic field oscillation in s
c=273;              %Curie constant in K-A/T-m
h=0.008;            %time step in s
t=0:h:12;
n=length(t)-1;
T(1)=293;           %initial temperature in K
vM(1)=0;
muH=muH_max*(1-cos(2*pi*t/tau))/2;  %sinusoidal function for magnetic field

for i=1:n
    dmuHdt=muH_max*pi*sin(2*pi*t(i)/tau)/tau; %derivative of magnetic field
w.r.t. time
    dsdT=cmu0H/T(i);    %partial derivative of entropy w.r.t. temperature
    dvMandT=-c*muH(i)/(rho*(T(i)^2));   %partial derivative of entropy w.r.t.
magnetic field
    vM_irr(i)=vdM_max*sin(muH(i)*pi/muH_max);   %irreversible magnetization

    dTdt=((vM_irr(i)/T(i))*abs(dmuHdt)-dvMandT*dmuHdt)/dsdT;
    T(i+1)=T(i)+h*dTdt;
    vM(i)=c*muH(i)/T(i)-vM_irr(i)*sign(dmuHdt); %magnetization
    muHi(i)=muH(i);
    S_gen_dot(i)=vM_irr(i)*abs(dmuHdt)/T(i);    %entropy generation rate
    ti(i)=t(i);         %new time vector for plotting
end
Tiso=(290:15/(n):305)';

for i=1:n+1       %entropy calculation - analytical
    s(i)=cmu0H*log(T(i))-c*((muH(i)/T(i))^2)/(2*rho);
    s_min(i)=cmu0H*log(Tiso(i));
    s_max(i)=cmu0H*log(Tiso(i))-c*((muH_max/Tiso(i))^2)/(2*rho);
end

for i=1:n-1
    dmuHdt=muH_max*pi*sin(2*pi*t(i)/tau)/tau;
    dS_gen(i)=((vM_irr(i+1)+vM_irr(i))/(T(i+1)+T(i)))*abs(dmuHdt)*(t(i+1)-
t(i));    %integrate S_gen function numerically; trapezoidal rule
end

%compare area of curve to area of irreversible curve
A_mag=trapz(vM,muHi)                %evaluate @ t=tau
A_magirr=2*trapz(vM_irr,muHi)       %evaluate @ t=tau/2

%calculate total entropy generated
S_gen=sum(dS_gen)   %result of integrating S_gen_dot function
S_gen2=max(s)-min(s)    %result of subtracting the final entropy from the
initial entropy, should be equal.
```

Appendix B CARNOT CYCLE MATLAB MODEL

```
clear all;
muH_max=2;                %maximum applied magnetic field in Tesla
rho=7900;                 %Desnity in kg/m^3
cmu0H0=0.5;               %constant field specific heat in J/kg-K
C=20;                     %Curie constant in K
mu0=4*pi*10^-7;           %Permeability of free space in T-m/A
c=C/mu0;                  %adjusted curie constant A-K/T-m
tau=4;                    %cycle duration in seconds
dM_max=5*rho;             %maximum irreversible magnetization in A/m
T_H=280.00;               %hot reservoir temperature in K
h=0.001;                  %applied magnetic field step size in Tesla
muH=0:h:muH_max;          %ramp up magnetic field
n=length(muH)-1;          %number of iterations
m=1;

%preallocate space for matricies
T=zeros(n,m);
s_pos=zeros(n,m);
T1=zeros(n,m);
s_neg=zeros(n,m);

for k=1:m
    T_C=273;              %cold reservoir temperature in K
    T(1,k)=T_C(k);        %Initial condition for magnetizatiom
    T1(n+1,k)=T_H;        %initial condition for demagnetization
    s_pos(1,k)=cmu0H0*log(T_C(k)); %Initial entropy w/ref @ 0 applied field
and T=1 K
    %dM_max=linspace(0,rho*5,m)';  %various maximum irreversible
magnetization constants in A/m
    k
for i=1:n   %increment magnetic field from minimum to maximum
     if (T(i,k)<T_H)  %adiabatic magnetization
            Mirr=dM_max*sin(pi*muH(i)/muH_max); %irreversible magnetization
function
            dvMdT=-(c*muH(i))/(rho*(T(i,k))^2);   %maxwell relation for
dsdmuH
            cmu0H=cmu0H0+c*muH(i)^2/(rho*T(i,k)^2); %function for constant
field specific heat
            dsdT=cmu0H/T(i,k); %partial derivative of entropy wrt temperature
            dTdmuH=((Mirr/(rho*T(i,k)))-dvMdT)/dsdT;  %eliminate time
derivatives and rearrange entropy balance

            %calculate midpoint values
            T_mid=T(i,k)+h*dTdmuH/2;
            dvMdT_mid=-(c*(muH(i)+h/2))/(rho*(T_mid)^2);
            cmu0Hmid=cmu0H0+c*(muH(i)+h/2)^2/(rho*T_mid^2);
            dsdT_mid=cmu0Hmid/T_mid;
            Mirr_mid=dM_max*sin(pi*(muH(i)+h/2)/muH_max);
            dTdmuH_mid=((Mirr_mid/(rho*T_mid))-dvMdT_mid)/dsdT_mid;

            %calculate properties
            s_pos(i+1,k)=s_pos(i,k)+h*(Mirr_mid/(rho*T_mid)); %entropy vector
            T(i+1,k)=T(i,k)+h*dTdmuH_mid;   %temperature
```

```
     else   %isothermal heat rejection
            Mirr=dM_max*sin(pi*(muH(i)+h/2)/muH_max);
            dvMdT=-(c*muH(i))/(rho*(T_H)^2);    %only derivative for dsdmuH
exists since T=constant
            dvMdT_mid=-(c*(muH(i)+h/2))/(rho*(T_H)^2);
            s_pos(i+1,k)=s_pos(i,k)+h*dvMdT_mid;

            %calculate entriopy and heat rejection
            dq_o(i+1,k)=h*T_H*(dvMdT_mid-(Mirr/(rho*T_H)));
            T(i+1)=T_H; %temperature is constant
     end
end
q_out=sum(dq_o)';    %total amount of heat rejection
s_min=cmu0H0*log(T_H)-c*((muH_max/T_H)^2)/(2*rho); %initial condition for
demag @ T=T_H & muH=muH_max
s_max=cmu0H0*log(T_C(k));
s_neg(n+1,k)=s_min; %IC
for i=n+1:(-1):2    %decrement magnetic field from maximum to minimum
    if (T1(i)>T_C) %adiabatic demagnetization
            Mirr=dM_max*sin(pi*muH(i)/muH_max);  %irreversible magnetization
function
            dvMdT=-(c*muH(i))/(2*rho*(T1(i,k))^2);
            cmu0H=cmu0H0+c*muH(i)^2/(rho*T1(i,k)^2);
            dsdT=cmu0H/T1(i,k);
            dTdmuH=((-Mirr/(rho*T1(i,k)))-dvMdT)/dsdT;

            %calculate midpoint values
            T1_mid=T1(i,k)+h*dTdmuH/2;
            dvMdT_mid=-(c*(muH(i)-h/2))/(rho*(T1_mid)^2);
            cmu0Hmid=cmu0H0+c*(muH(i)+h/2)^2/(rho*T1_mid^2);
            dsdT_mid=cmu0Hmid/T1_mid;
            Mirr_mid=dM_max*sin(pi*(muH(i)-h/2)/muH_max);
            dTdmuH_mid=((-Mirr_mid/(rho*T1_mid))-dvMdT_mid)/dsdT_mid;

            %calculate temperature and entropy
            T1(i-1,k)=T1(i,k)-h*dTdmuH_mid; %temperature; steps are negative
since field is decreasing
            s_neg(i-1,k)=s_neg(i,k)-h*dvMdT_mid-h*dTdmuH_mid*dsdT_mid;

    else    %isothermal heat addition from cold reservoir
            Mirr=dM_max*sin(pi*(muH(i)-h/2)/muH_max);
            dvMdT=-(c*muH(i))/(rho*(T_C(k))^2);
            dvMdT_mid=-(c*(muH(i)-h/2))/(rho*(T_C(k))^2);

            %calculate entropy and heat absorption
            s_neg(i-1,k)=s_neg(i,k)-h*dvMdT_mid;
            dq_i(i-1,k)=-h*T_C(k)*(dvMdT_mid+(Mirr/(rho*T_C(k))));
            T1(i-1,k)=T_C(k);
    end
end
q_in=sum(dq_i)'; %total amount of heat absorption

for i=1:n+1
```

```
     s_pos_ana(i,k)=cmu0H0*log(T(i,k))-c*((muH(i)/T(i,k))^2)/(2*rho);
%analytical calculation of entropy for magnetization
end
for i=1:n+1
    s_neg_ana(i)=cmu0H0*log(T1(i,k))-c*((muH(i)^2)/T1(i,k)^2)/(2*rho);
%analytical calculation of entropy for demagnetization
end

COP(1,k)=q_in(k)/abs(q_in(k)+q_out(k))  %coefficient of performance for cycle
COP_carnot=T_C(k)/(T_H-T_C(k))    %COP for an ideal carnot cycle
end
```

Appendix C MATLAB AMRR REGENERATOR BED MODEL CODE

```
%% This is the main regenerator model developed at UW.  This function takes
%% inputs that define the system and forcing functions, such as mass flow
%% profile, and calculates the regenerator performance.  This model does
%% not account for heat exchangers.  The main outputs of the model are the
%% cyclical steady state temperatures of the fluid and solid over an entire
%% cycle and the heat rejection, cooling power, and pumping power of the
%% system.

%% This model has been modified to include the effects of hysteresis

function[mdot,muoH,heat_rej,ref_load,ref_cap,COP,COP_h,Wmag,Wpump,mdot_amp,Ql
oss,Qent,Qentt,DS_iso,DT_ad]=AMR_pl_imp(TC,TH,TCurie,mdot_amp,Vol,AR,n,Ch,Cx,
Cy,tau)
%%Bed paramters
fluid='eg50';
n_beds=6;
bed_vol=Vol/n_beds;
D=(4*bed_vol/(AR*pi))^(1/3);
L=AR*D;
muoH_max=1.5; %Tesla
dwell=1/2;
delay=(1-dwell)*.45*tau;
unbal=0.0;
flow_ramp=0.25;
dh=0.0002; %m
Ac=pi*D^2/4; %m^2
eps=0.36;
as=6*(1-eps)/dh; %m^2/m^3
L_flow=1*L; %ratio of bed length to bed length in which there is flow
n_motor=.9; %electric motor efficiency
n_pump=.7; %pump efficiency

massflowinputs=[dwell,delay,flow_ramp,unbal];

m=120;
% n=60;
reltol=0.0002;
wt=1;
N=2*m*n+m+n;
A=spalloc(N,N,4*N);
B=spalloc(N,1,N);
%modelcheck=0; %1=show T-s and enthalpy flux graphs 0=don't show them

i=0:n;
xf=L*i'/n;
j=1:m;
tf=(j'-0.5)*tau/m;
i=1:n;
xr=(i'-0.5)*L/n';
j=0:m;
tr=j'*tau/m;
```

```
mdot=mdotsmoothunbal_delay(tf,tau,mdot_amp,massflowinputs);
muoH=muoH_ramp(xr,tr,tau,muoH_max);

for j=0:m
    Trg(:,j+1)=TH-xr*(TH-TC)/L;
end
for j=1:m
    Tfg(:,j)=TH-xf*(TH-TC)/L;
end

%Calculate lumped cap correction factor
if(strcmp(fluid,'water'))
    [muf,kf,cf,rhof,hf,sf]=props_water(Tfg);
elseif(strcmp(fluid,'air'))
    [muf,kf,cf,rhof,hf,sf]=props_air(Tfg);
elseif(strcmp(fluid,'water_const'))
    [muf,kf,cf,rhof,cfunc,T_ref]=fluidprops(Tfg);
elseif(strcmp(fluid,'eg50'))
    [muf,kf,cf,rhof,hf,sf]=props_ethgly50_3(Tfg);
end

[cmuoH,dsdmuoH,rhor,kr,sr,hr,vM_irr,DS_iso,DT_ad]=JF1142A(Trg,TCurie,muoH,Cx,
Cy);
cf_av=mean(mean(cf));
cmuoH_av=mean(mean(cmuoH));

done=0;
while(done==0)
   if(strcmp(fluid,'water'))
       [muf,kf,cf,rhof,hf,sf]=props_water(Tfg);
   elseif(strcmp(fluid,'air'))
       [muf,kf,cf,rhof,hf,sf]=props_air(Tfg);
   elseif(strcmp(fluid,'water_const'))
       [muf,kf,cf,rhof,cfunc,T_ref]=fluidprops(Tfg);
   elseif(strcmp(fluid,'eg50'))
       [muf,kf,cf,rhof,hf,sf]=props_ethgly50_3(Tfg);
   end
   for i=1:n
      mufn(i,:)=(muf(i,:)+muf(i+1,:))/2;
      cfn(i,:)=(cf(i,:)+cf(i+1,:))/2;
      kfn(i,:)=(kf(i,:)+kf(i+1,:))/2;
   end
   Prf=cfn.*mufn./(kfn);
   Ref=ones(n,1)*abs(mdot')*dh./(Ac*mufn);

[cmuoH,dsdmuoH,rhor,kr,sr,hr,vM_irr,DS_iso,DT_ad]=JF1142A(Trg,TCurie,muoH,Cx,
Cy); %JF1142A_nh Gd94Er6
   cf_av=mean(mean(cf));
   cmuoH_av=mean(mean(cmuoH));
   R=(rhof*eps*cf_av)/(rhor*(1-eps)*cmuoH_av);
   AF=1+1.764*R+1.0064*R^2; %correction factor
   v=mdot/(Ac*rhof);
   [Nuf,dP,keff]=sph_part_1(Ref,Prf,eps, kfn, kr,v,dh,mufn,rhof,1,1,1);
%cNu,cff,cnk
   for j=1:m
       ff(:,j)=dP(:,j)*2*dh./(rhof*v(j)^2);
```

```
   end
   Bi=(Nuf.*kfn)/(2*kr);
   Fo=kfn*tau./(rhof*cfn*(dh/2)^2);
   Fo_av=mean(mean(Fo));
   Bi_av=mean(mean(Bi));
   chi=Fo_av*exp(0.246196-0.84878*log(Fo_av)-0.05639*(log(Fo_av))^2);
   DFFc=1/(1+Bi_av*chi/5);
   eta_c=1/(1+(2*pi/(3*Bi_av*Fo_av)*(1/DFFc))^2)^(1/2);
   rhor=eta_c*rhor;

   for j=1:m
    cmuoH(:,j)=(cmuoH(:,j)+cmuoH(:,j+1))/2;
    dsdmuoH(:,j)=(dsdmuoH(:,j)+dsdmuoH(:,j+1))/2;
    vM_irr(:,j)=(vM_irr(:,j)+vM_irr(:,j+1))/2;
   end
%Fill matrices used to solved temperature profile
   for j=1:m
      if(mdot(j)>=0)
         %hot-to-cold flow
         i=1:n;
         A(((n+1)*(j-1)+i+1-1)*N+(n+1)*(j-
1)+i+1)=Nuf(:,j).*kfn(:,j)*as*Ac./((1+chi(:,j).*Bi(:,j)/5)*(2*dh))+n*mdot(j)*
cfn(:,j)/L;
         A(((n+1)*(j-1)+i-1+1-1)*N+(n+1)*(j-
1)+i+1)=Nuf(:,j).*kfn(:,j)*as*Ac./((1+chi(:,j).*Bi(:,j)/5)*(2*dh))-
n*mdot(j)*cfn(:,j)/L;
         A(((n+1)*m+n*j+i-1)*N+(n+1)*(j-1)+i+1)=-
Nuf(:,j).*kfn(:,j)*as*Ac./((1+chi(:,j).*Bi(:,j)/5)*(2*dh));
         A(((n+1)*m+n*(j-1)+i-1)*N+(n+1)*(j-1)+i+1)=-
Nuf(:,j).*kfn(:,j)*as*Ac./((1+chi(:,j).*Bi(:,j)/5)*(2*dh));
        B((n+1)*(j-1)+i+1,1)=abs(ff(:,j).*mdot(j)^3/(2*rhof^2*Ac^2*dh));
%Viscous dissipation
         i=0;
         A((n+1)*(j-1)+i+1,(n+1)*(j-1)+i+1)=1;
         B((n+1)*(j-1)+i+1,1)=TH;

      else
         if(mdot(j)<0)
            %cold-to-hot flow
             i=0:(n-1);
             A(((n+1)*(j-1)+i+1-1)*N+(n+1)*(j-
1)+i+1)=Nuf(:,j).*kfn(:,j)*as*Ac./((1+chi(:,j).*Bi(:,j)/5)*(2*dh))-
mdot(j)*cfn(:,j)*n/L;
             A(((n+1)*(j-1)+i+1+1-1)*N+(n+1)*(j-
1)+i+1)=Nuf(:,j).*kfn(:,j)*as*Ac./((1+chi(:,j).*Bi(:,j)/5)*(2*dh))+mdot(j)*cf
n(:,j)*n/L;
             A(((n+1)*m+n*j+i+1-1)*N+(n+1)*(j-1)+i+1)=-
Nuf(:,j).*kfn(:,j)*as*Ac./((1+chi(:,j).*Bi(:,j)/5)*(2*dh));
             A(((n+1)*m+n*(j-1)+i+1-1)*N+(n+1)*(j-1)+i+1)=-
Nuf(:,j).*kfn(:,j)*as*Ac./((1+chi(:,j).*Bi(:,j)/5)*(2*dh));
                B((n+1)*(j-
1)+i+1,1)=abs(ff(:,j).*mdot(j)^3/(2*rhof^2*Ac^2*dh)); %viscous dissipation
             i=n;
             A((n+1)*(j-1)+i+1,(n+1)*(j-1)+i+1)=1;
             B((n+1)*(j-1)+i+1,1)=TC;
         else
```

```
            %no flow

          end
        end
    end
    for j=1:m
        i=1:n;
        A(((n+1)*(j-1)+i+1-1)*N+(n+1)*m+n*j+i)=-
Nuf(:,j).*kfn(:,j)*as*Ac./((1+chi(:,j).*Bi(:,j)/5)*(2*dh));
        A(((n+1)*(j-1)+i-1+1-1)*N+(n+1)*m+n*j+i)=-
Nuf(:,j).*kfn(:,j)*as*Ac./((1+chi(:,j).*Bi(:,j)/5)*(2*dh));
        B((n+1)*m+n*j+i,1)=-Ac*(1-
eps)*rhor*((Trg(:,j+1)+Trg(:,j))/2).*dsdmuoH(:,j).*(muoH(:,j+1)-
muoH(:,j))*m/tau...
          +Ch*Ac*(1-eps)*rhor.*vM_irr(:,j).*abs(muoH(:,j+1)-muoH(:,j))*m/tau;
        i=2:(n-1);
        A(((n+1)*m+n*j+i-
1)*N+(n+1)*m+n*j+i)=Nuf(i',j).*kfn(i',j)*as*Ac./((1+chi(i',j).*Bi(i',j)/5)*(2
*dh))+Ac*(rhof*eps*cfn(i',j)+(1-
eps)*rhor*cmuoH(i',j))*m/tau+n^2*keff(i',j)*Ac/L^2;
        A(((n+1)*m+n*(j-1)+i-
1)*N+(n+1)*m+n*j+i)=Nuf(i',j).*kfn(i',j)*as*Ac./((1+chi(i',j).*Bi(i',j)/5)*(2
*dh))-Ac*(rhof*eps*cfn(i',j)+(1-
eps)*rhor*cmuoH(i',j))*m/tau+n^2*keff(i',j)*Ac/L^2;
        A(((n+1)*m+n*(j-1)+(i-1)-1)*N+(n+1)*m+n*j+i)=-
n^2*keff(i',j)*Ac/(2*L^2);
        A(((n+1)*m+n*(j)+(i-1)-1)*N+(n+1)*m+n*j+i)=-n^2*keff(i',j)*Ac/(2*L^2);
        A(((n+1)*m+n*(j-1)+(i+1)-1)*N+(n+1)*m+n*j+i)=-
n^2*keff(i',j)*Ac/(2*L^2);
        A(((n+1)*m+n*(j)+(i+1)-1)*N+(n+1)*m+n*j+i)=-n^2*keff(i',j)*Ac/(2*L^2);
        i=1;
        A(((n+1)*m+n*j+i-
1)*N+(n+1)*m+n*j+i)=Nuf(i',j).*kfn(i',j)*as*Ac./((1+chi(i',j).*Bi(i',j)/5)*(2
*dh))+Ac*(rhof*eps*cfn(i',j)+(1-
eps)*rhor*cmuoH(i',j))*m/tau+n^2*keff(i',j)*Ac/(2*L^2);;
        A(((n+1)*m+n*(j-1)+i-
1)*N+(n+1)*m+n*j+i)=Nuf(i',j).*kfn(i',j)*as*Ac./((1+chi(i',j).*Bi(i',j)/5)*(2
*dh))-Ac*(rhof*eps*cfn(i',j)+(1-
eps)*rhor*cmuoH(i',j))*m/tau+n^2*keff(i',j)*Ac/(2*L^2);
        A(((n+1)*m+n*(j-1)+(i+1)-1)*N+(n+1)*m+n*j+i)=-
n^2*keff(i',j)*Ac./(2*L^2);
        A(((n+1)*m+n*(j)+(i+1)-1)*N+(n+1)*m+n*j+i)=-n^2*keff(i',j)*Ac./(2*L^2);
        i=n;
        A(((n+1)*m+n*j+i-
1)*N+(n+1)*m+n*j+i)=Nuf(i',j).*kfn(i',j)*as*Ac./((1+chi(i',j).*Bi(i',j)/5)*(2
*dh))+Ac*(rhof*eps*cfn(i',j)+(1-
eps)*rhor*cmuoH(i',j))*m/tau+n^2*keff(i',j)*Ac/(2*L^2);;
        A(((n+1)*m+n*(j-1)+i-
1)*N+(n+1)*m+n*j+i)=Nuf(i',j).*kfn(i',j)*as*Ac./((1+chi(i',j).*Bi(i',j)/5)*(2
*dh))-Ac*(rhof*eps*cfn(i',j)+(1-
eps)*rhor*cmuoH(i',j))*m/tau+n^2*keff(i',j)*Ac/(2*L^2);
        A(((n+1)*m+n*(j-1)+(i-1)-1)*N+(n+1)*m+n*j+i)=-
n^2*keff(i',j)*Ac./(2*L^2);
        A(((n+1)*m+n*(j)+(i-1)-1)*N+(n+1)*m+n*j+i)=-n^2*keff(i',j)*Ac./(2*L^2);
    end
    j=0;
    i=1:n;
```

```
   A(((n+1)*m+n*j+i-1)*N+(n+1)*m+n*j+i)=1;
   A(((n+1)*m+n*m+i-1)*N+(n+1)*m+n*j+i)=-1;
   X=A\B;
   for j=1:m
      i=0:n;
      Tf(:,j)=full(X((n+1)*(j-1)+i+1));
   end
   for j=0:m
      i=1:n;
        Tr(:,j+1)=full(X((n+1)*m+n*j+i));
   end
   err=max(max(max(abs(Tf-Tfg))),max(max(abs(Tr-Trg))))
   if(err<reltol)
       if(strcmp(fluid,'water'))
           [muf,kf,cf,rhof,hf,sf]=props_water(Tf);
       elseif(strcmp(fluid,'air'))
           [muf,kf,cf,rhof,hf,sf]=props_air(Tf);
       elseif(strcmp(fluid,'water_const'))
           [muf,kf,cf,rhof,hf,sf]=fluidprops(Tf);
       elseif(strcmp(fluid,'eg50'))
           [muf,kf,cf,rhof,hf,sf]=props_ethgly50_3(Tf);
       end

[cmuoH,dsdmuoH,rhor,kr,sr,hr,vM_irr,DS_iso,DT_ad]=JF1142A(Trg,TCurie,muoH,Cx,
Cy); %JF1142A_nh Gd94Er6
      done=1;%Relaxation process complete
   else
      Tfg=Tf*wt+Tfg*(1-wt);
      Trg=Tr*wt+Trg*(1-wt);
   end %Update guess temp values
end
for i=1:n
   for j=1:m
      Tfn(i,j)=(Tf(i,j)+Tf(i+1,j))/2;
      Trn(i,j)=(Tf(i,j)+Tr(i,j+1))/2;
   end
end
for i=1:m
    if abs(mdot(i))<mdot_amp
        Tfa(:,i)=Tfn(:,i);
    else
        Tfa(:,i)=Tfn(:,i);
    end
end

Tout_avg=trapz(tf(1:m/2),Tf(n+1,1:m/2)')/(tf(m/2,1)-tf(1,1));
eff=(TH-Tout_avg)/(TH-TC);
U=mdot_amp*cf(1,1)*tau/(2*Ac*L*(1-eps)*rhor*cmuoH(1,1));
Crat=Ac*L*(1-eps)*rhor*cmuoH(1,1)/(mdot_amp*cf(1,1)*tau/2);

%Calculate regenerator bed capacity
for i=1:n
    dcapr(i)=trapz(tr,cmuoH(i,:))/tau;
end
capr=sum(dcapr)*rhor*Ac*L/n;
```

```
%Calculate parameters for lumped heat capacitance corrections
V=Ac*L;
crtot=mean(mean(cmuoH));
cftot=mean(mean(cf));
Cr=rhor*V*(1-eps)*crtot;
Cf=rhof*V*(eps)*cftot;
R=Cf/Cr;
lambda=tau*L_flow/(L*n_beds);
U=mdot_amp*cftot*lambda/(Cr+Cf);
NTU=Nuf(1,19)*kf(1,19)*Ac*L*as/(dh*mdot_amp*cf(1,19));

for i=1:(n+1)
   hflux(i,1)=sum(mdot.*hf(i,:)')*tau/m;
   sflux(i,1)=sum(mdot.*sf(i,:)')*tau/m;
end
%Calculate energy loss due to pressure drop across the bed and pumping
%power
v=mdot/(Ac*rhof);
alpha=(1-eps)^2/eps^3;
beta=(1-eps)/eps^3;
A=180; %for Ergun model from Fand et al
B=1.8; %for Ergun model from Fand et al
for j=1:m
    dP(:,j)=abs(ff(:,j).*mdot(j)^2/(2*rhof*Ac^2)*L/(n*dh)); %delta P in Pa
    dWpump(:,j)=abs(mdot(j)/rhof*dP(:,j)); %W

dP_ergun(:,j)=(A*alpha*muf(:,j)/dh^2*abs(v(j))+B*beta*rhof/dh*v(j)^2)*L/n;
%Pa
end
deltaP=sum(dP,1);
deltaP_ergun=sum(dP_ergun,1);
Wpump=sum(sum(dWpump,1),2)*tau/m; %J
%Calculate Energy Change due to Thermal Entropy Change per cycle
for j=1:m
    dQentt(:,j)=(Tr(:,j+1)-Tr(:,j)).*L/n*Ac*(1-eps)*rhor.*cmuoH(:,j);
end
Qentt=sum(sum(dQentt,1),2);

%Calculate Energy Change due to Magnetic Entropy Change per cycle
for j=1:m
    dQent(:,j)=Ac*(1-
eps)*rhor*((Tr(:,j+1)+Tr(:,j))/2).*dsdmuoH(:,j).*(muoH(:,j+1)-muoH(:,j))*L/n;
end
Qent=sum(sum(dQent,1),2);

%Calculate Heat Loss Per Cycle Due to Hysteresis
for j=1:m
    dQloss(:,j)=-Ch*Ac*(1-eps)*rhor.*vM_irr(:,j).*abs(muoH(:,j+1)-
muoH(:,j))*L/n;
end
Qloss=sum(sum(dQloss,1),2);

%calculate total cooling in the cycle (J) and cooling rate (W)
ref_load=-hflux(n+1); %J
ref_cap=ref_load/tau/1000*n_beds %kW
```

```
%calculate heat rejection in the cycle (J) and heat rejection rate (W)
heat_load=-hflux(1); %J
heat_rej=heat_load*n_beds/tau/1000 %kW
Wmag=heat_load-ref_load-Wpump;%hflux(n+1)-hflux(1);
Wmotor=(Wmag)/n_motor;

%Calculate COP from cooling power, magnetic work and pump work
COP=ref_load/(Wmotor+Wpump/n_pump)
COP_h=heat_load/(Wmotor+Wpump/n_pump)
COP_Carnot=(TC)/(TH-TC);
```